To the Graduate Council:

I am submitting herewith a thesis written by Rebecca Anne Lind entitled "Design and Analysis of Steel Plate Shear Walls." I have examined the final electronic copy of this thesis for form and content and recommend that it be accepted in partial fulfillment of the requirements for the degree of Master of Science, with a major in Civil Engineering.

Qiuhong Zhao, Major Professor

We have read this thesis
and recommend its acceptance:

Richard M. Bennett

Edwin G. Burdette

Accepted for the Council:

Carolyn R. Hodges, Vice Provost and
Dean of the Graduate School

(Original signatures are on file with official student records.)

DESIGN AND ANALYSIS OF STEEL PLATE SHEAR WALLS

A THESIS
PRESENTED FOR THE
MASTER'S OF SCIENCE DEGREE
THE UNIVERSITY OF TENNESSEE, KNOXVILLE

REBECCA Anne LIND
MAY 2008

ACKNOWLEDGEMENTS

I wish to thank my committee members for their guidance throughout my academic career. I would like to thank my advisor, Dr. Qiuhong Zhao, for her efforts toward furthering my understanding for steel plate shear walls and for supplying data from her past test specimens. I would also like to thank Dr. Edwin Burdette and Dr. Richard Bennett for their technical assistance.

I would also like to thank my mother and father for their constant love and support without which this would not have been possible.

ABSTRACT

Steel plate shear walls are investigated as a lateral load resisting system with particular interest towards seismic loads. Past physical testing is studied in order to determine trends in failure modes and design considerations. Analysis is conducted on data from two, large scale, steel plate shear walls that were tested under quasi-static loading. The investigation includes energy dissipation, axial forces in members, bending moment, curvature, infill stresses, and shear distribution. Recommendations are made for future projects.

PART 1: INTRODUCTION **1**

1.1 INTRODUCTION 2

PART 2: LITERATURE REVIEW **4**

2.1 ABSTRACT 5
2.2 SUMMARY OF PHYSICAL TESTS 6
2.2.1 Takahashi et al *6*
2.2.2 Timler and Kulak *7*
2.2.3 Tromposch and Kulak *8*
2.2.4 Roberts and Sabouri-Ghomi *9*
2.2.5 Elgaaly and Caccese *10*
2.2.6 Driver et al *12*
2.2.7 Lubell and Rezai et al *14*
2.2.8 Schumacher et al *17*
2.2.9 Behbahanifard et al *18*
2.2.10 Zhao and Astaneh-Asl *19*
2.2.11 Berman and Bruneau *20*
2.2.12 Park et al *22*
2.3 MODELING 23
2.4 RECOMMENDATIONS 28
2.4.1 Failure Modes *28*
2.4.2 Boundary Elements *29*
2.4.3 Connections *30*
2.4.4 Panels *31*
2.5 SUMMARY 32
APPENDIX 35

PART 3: ANALYSIS OF STEEL PLATE SHEAR WALL SPECIMENS **59**

3.1 ABSTRACT 60
3.2 BACKGROUND 60
3.3 ENERGY DISSIPATION 62
3.4 AXIAL LOADS AND BENDING MOMENTS 63
3.5 ANGLE OF INCLINATION IN INFILL PANELS 65
3.6 MOMENT VERSUS CURVATURE 67
3.7 COMPARISON OF TEST RESULTS AND CODE CALCULATIONS 69
3.7.1 Test Results *69*
3.7.2 AISC Code *71*
3.8 CONCLUSION 74
APPENDICES 76
APPENDIX A: FIGURES AND TABLES 77
APPENDIX B: SAMPLE CALCULATIONS AND EQUATIONS 138

PART 4: CONCLUSION **144**

4.1 CONCLUSIONS 145

WORKS CITED **147**

WORKS REFERENCED **152**

VITA **158**

LIST OF FIGURES

FIGURE 2.1: SCHEMATIC OF SPECIMEN BY TIMLER AND KULAK (1983) 36
FIGURE 2.2: STRIP MODEL PRESENTED BY THORBURN *ET AL* (1983) 36
FIGURE 2.3: ANGLE OF PRINCIPAL STRAINS FOR COMPARISON WITH CALCULATED ANGLE OF INCLINATION BY TIMLER AND KULAK (1983) 37
FIGURE 2.4: SCHEMATIC OF SPECIMEN BY TROMPOSCH AND KULAK (1987) 38
FIGURE 2.5: HYSTERESIS LOOPS PRODUCED BY SPECIMEN TESTED BY TROMPOSCH AND KULAK (1987) 38
FIGURE 2.6: SCHEMATIC OF SPECIMEN BY ROBERTS AND SABOURI-GHOMI (1992) 39
FIGURE 2.7: HYSTERESIS LOOPS FOR SPECIMENS (ABOVE: SOLID PANEL; BELOW: PANEL WITH OPENING)TESTED BY ROBERTS AND SABOURI-GHOMI (1992) 39
FIGURE 2.8: TEST SPECIMEN BY ELGAALY AND CACCESE, 1993 40
FIGURE 2.9: MODEL USED BY ELGAALY, 1998 40
FIGURE 2.10: FOUR-STORY SPECIMEN TESTED BY DRIVER ET AL (1997) 41
FIGURE 2.11: HYSTERESIS BEHAVIOR OF FOUR-STORY SPECIMEN TESTED BY DRIVER *ET AL* (1997) 42
FIGURE 2.12: SINGLE-STORY SPECIMEN TESTED BY REZAI (1999) 42
FIGURE 2.13: HYSTERESIS BEHAVIOR OF SINGLE-STORY SPECIMENS (ABOVE: FIRST SPECIMEN; BELOW: SECOND SPECIMEN) TESTED BY REZAI (1999) 43
FIGURE 2.14: FOUR-STORY SPECIMEN TESTED WITH SHAKE TABLE BY REZAI (1999) 44
FIGURE 2.15: MODIFIED STRIP MODEL PROPOSED BY REZAI (1999) 45
FIGURE 2.16: COMPARISON OF SINGLE-STORY EXPERIMENTAL RESULTS TO THE RESULTS USING MODEL PROPOSED BY REZAI (1999) 45
FIGURE 2.17: CORNER DETAILS TESTED BY SCHUMACHER *ET AL* (1999) 46
FIGURE 2.18: TEST SET-UP FOR EXPERIMENTAL INVESTIGATION BY SCHUMACHER *ET AL* (1999) 46
FIGURE 2.19: TEST SPECIMEN TESTED BY BEHBAHANIFARD *ET AL* (2001) 47
FIGURE 2.20: HYSTERESIS BEHAVIOR OF SPECIMEN TESTED BY BEHBAHANIFARD *ET AL* (2001) 47
FIGURE 2.21: SPECIMENS TESTED BY ASTANEH-ASL AND ZHAO (2001) 48
FIGURE 2.22: HYSTERESIS BEHAVIOR OF SPECIMENS (ABOVE: SINGLE-STORY; BELOW: TWO-STORY) TESTED BY ASTANEH-ASL AND ZHAO (2001) 48
FIGURE 2.23: SPECIMEN WITH CORRUGATED METAL DECKING TESTED BY BERMAN AND BRUNEAU (2005) 49
FIGURE 2.24: HYSTERESIS LOOPS FOR SPECIMENS (ABOVE: CORRUGATED INFILL; BELOW: FLAT INFILL WITH WELDS) TESTED BY BERMAN AND BRUNEAU (2005) 49

Figure 2.25: Specimen Tested by Park *et al* (2007) 50
Figure 2.26: Comparison of Plastic Deformations for Shear and Flexure Dominated Behavior as Described by Park, Kwack, Jeon, Kim, and Choi (2007) 50
Figure 2.27: Hysteresis Behavior of Specimens (W-denotes 'weak' column; 51
Figure 2.28: Plate Girder Analogy as described by Astaneh-Asl (2001) 52
Figure 2.29: Strip Model Introduced by Thorburn *et al* (1983) paired with the Modified Strip Model Introduced by Rezai (2000) as described by Astaneh-Asl (2001) 52
Figure 3.1: Components of Lateral Load Resisting System Studied (Zhao and Astaneh-Asl, 2004) 78
Figure 3.2: Structural Details for Specimen One (Zhao, 2004) 79
Figure 3.3: Structural Details for Specimen Two (Zhao, 2004) 79
Figure 3.4: Testing Set-Up (Zhao and Astaneh-Asl, 2004) 80
Figure 3.5: Loading History Applied to Both Specimens (Zhao and Astaneh-Asl, 2004) 80
Figure 3.6: Global Displacement Transducers on Specimen One (Zhao, 2004) 81
Figure 3.7: Local Displacement Transducers on Specimen One (Zhao, 2004) 81
Figure 3.8: Strain Gage Locations on Specimen One (Zhao, 2004) 82
Figure 3.9: Global Displacement Transducers on Specimen Two (Zhao, 2004) 82
Figure 3.10: Local Displacement Transducers on Specimen Two (Zhao, 2004) 83
Figure 3.11: Strain Gage Locations on Specimen Two (Zhao, 2004) 83
Figure 3.12: Energy Dissipation for Specimen One 84
Figure 3.13: Energy Dissipation for Specimen Two 84
Figure 3.14: Elastic-Perfectly Plastic Material Model 86
Figure 3.15: Cyclic Material Model Accounting for Permanent Deformations 86
Figure 3.16: Sample Cases for Bending Moment and Axial Force Calculations 87
Figure 3.17: Specimen One Cross Sections Analyzed using Strain Gages 88
Figure 3.18: Specimen Two Cross Sections Analyzed using Strain Gages 88
Figure 3.19: Specimen One Axial Forces in WF Column at Section One 89
Figure 3.20: Specimen One Axial Forces in WF Column at Section Two 89
Figure 3.21: Specimen One Axial Forces in WF Column at Section Three 90
Figure 3.22: Specimen One Axial Forces in Coupling Beam at Section Four 90
Figure 3.23: Specimen One Axial Forces in Coupling Beam at Section Five 91
Figure 3.24: Specimen One Axial Distribution along WF Column (Drift = 0.004) 91
Figure 3.25: Specimen One Axial Distribution along WF Column (Drift = 0.006) 92
Figure 3.26: Specimen One Axial Distribution along WF Column (Drift = 0.02) 92

Figure 3.27: Specimen Two Axial Forces in WF Column at Section One 93
Figure 3.28: Specimen Two Axial Forces in WF Column at Section Two 93
Figure 3.29: Specimen Two Axial Forces in WF Column at Section Three 94
Figure 3.30: Specimen Two Axial Forces in Coupling Beam at Section Four 94
Figure 3.31: Specimen Two Axial Distribution along WF Column (Drift = 0.004) 95
Figure 3.32: Specimen Two Axial Distribution along WF Column (Drift = 0.006) 95
Figure 3.33: Specimen Two Axial Distribution along WF Column (Drift = 0.02) 96
Figure 3.34: Specimen One Moment in WF Column at Section One 96
Figure 3.35: Specimen One Moment in WF Column at Section Two 97
Figure 3.36: Specimen One Moment in WF Column at Section Three 97
Figure 3.37: Specimen One Moment in Coupling Beam at Section Four 98
Figure 3.38: Specimen One Moment in Coupling Beam at Section Five........................ 98
Figure 3.39: Specimen One Moment Distribution along WF Column (Drift = 0.004).. 99
Figure 3.40: Specimen One Moment Distribution along WF Column (Drift = 0.006).. 99
Figure 3.41: Specimen One Moment Distribution along WF Column (Drift = 0.02).. 100
Figure 3.42: Specimen Two Moment in WF Column at Section One 100
Figure 3.43: Specimen Two Moment in WF Column at Section Two........................... 101
Figure 3.44: Specimen Two Moment in WF Column at Section Three........................ 101
Figure 3.45: Specimen Two Moment in Coupling Beam at Section Four.................... 102
Figure 3.46: Specimen Two Moment Distribution along WF Column (Drift = 0.004)102
Figure 3.47: Specimen Two Moment Distribution along WF Column (Drift = 0.006)103
Figure 3.48: Specimen Two Moment Distribution along WF Column (Drift = 0.02) . 103
Figure 3.49: Specimen One Strain Gage Placement for Infill Panel 104
Figure 3.50: Specimen One Angles of Major and Minor Principal Stresses of Infill Panels during Elastic Range of Loading 106
Figure 3.51: Specimen One Angles of Major and Minor Principal Stresses of Infill Panels during Yield Range of Loading 107
Figure 3.52: Specimen One Angles of Major and Minor Principal Stresses of Infill Panels during Inelastic Range of Loading.. 108
Figure 3.53: Specimen Two Strain Gage Placement of Infill Panel.......................... 109
Figure 3.54: Specimen Two Angles of Major and Minor Principal Stresses of Infill Panels during Elastic Range of Loading 111
Figure 3.55: Specimen Two Angles of Major and Minor Principal Stresses of Infill Panels during Yield Range of Loading 112
Figure 3.56: Specimen Two Angles of Major and Minor Principal Stresses of Infill Panels during Inelastic Range of Loading.. 113

FIGURE 3.57: ELASTIC BEHAVIOR FROM STRAIN GAGES SHOWING DIFFERENT STIFFNESS FOR PUSHING AND PULLING 114
FIGURE 3.58: MOMENT VERSUS CURVATURE USING STRAIN GAGE DATA 114
FIGURE 3.59: STRAIN GAGE DATA SHOWING DIFFERENT STIFFNESS AT LOW LOADING 115
FIGURE 3.60: EVIDENCE OF YIELDING 115
FIGURE 3.61: MOMENT CURVATURE USING TRANSDUCER READINGS 116
FIGURE 3.62: MOMENT CURVATURE USING TRANSDUCER READINGS 116
FIGURE 3.63: MOMENT CURVATURE USING STRAIN GAGE DATA 117
FIGURE 3.64: MOMENT VERSUS CURVATURE USING TRANSDUCER READINGS 117
FIGURE 3.65: MOMENT VERSUS CURVATURE USING TRANSDUCER READINGS 118
FIGURE 3.66: MOMENT VERSUS CURVATURE FOR TRANSDUCER READINGS 118
FIGURE 3.67: SPECIMEN ONE CROSS SECTIONS WHERE SHEAR DISTRIBUTION IS ANALYZED 119
FIGURE 3.68: SPECIMEN TWO CROSS SECTIONS WHERE SHEAR DISTRIBUTION IS ANALYZED 119
FIGURE 3.69: SPECIMEN ONE SHEAR STRESS DISTRIBUTION IN 120
FIGURE 3.70: SPECIMEN ONE SHEAR STRESS DISTRIBUTION IN 120
FIGURE 3.71: SPECIMEN ONE SHEAR STRESS DISTRIBUTION IN 121
FIGURE 3.72: SPECIMEN ONE SHEAR STRESS DISTRIBUTION IN 121
FIGURE 3.73: SPECIMEN ONE SHEAR STRESS DISTRIBUTION IN 122
FIGURE 3.74: SPECIMEN ONE SHEAR STRESS DISTRIBUTION IN 122
FIGURE 3.75: SPECIMEN TWO SHEAR STRESS DISTRIBUTION IN 123
FIGURE 3.76: SPECIMEN TWO SHEAR STRESS DISTRIBUTION IN 123
FIGURE 3.77: SPECIMEN TWO SHEAR STRESS DISTRIBUTION IN 124
FIGURE 3.78: SPECIMEN TWO SHEAR STRESS DISTRIBUTION IN 124
FIGURE 3.79: SPECIMEN TWO SHEAR STRESS DISTRIBUTION IN 125
FIGURE 3.80: SPECIMEN TWO SHEAR STRESS DISTRIBUTION IN 125
FIGURE 3.81: SPECIMEN ONE SHEAR DISTRIBUTION FOR TOP CROSS-SECTION WHEN 130
FIGURE 3.82: SPECIMEN ONE SHEAR DISTRIBUTION FOR BOTTOM CROSS-SECTION WHEN ACTUATOR MOVES TO RIGHT 130
FIGURE 3.83: SPECIMEN ONE SHEAR DISTRIBUTION FOR TOP CROSS-SECTION WHEN ACTUATOR MOVES TO LEFT 131
FIGURE 3.84: SPECIMEN ONE SHEAR DISTRIBUTION FOR BOTTOM CROSS-SECTION WHEN ACTUATOR MOVES TO LEFT 131
FIGURE 3.85: SPECIMEN ONE INFILL COMPARISON WHEN ACTUATOR MOVES TO RIGHT 132
FIGURE 3.86: SPECIMEN ONE INFILL COMPARISON WHEN ACTUATOR MOVES TO LEFT 132
FIGURE 3.87: SPECIMEN TWO SHEAR DISTRIBUTION FOR SECOND STORY WHEN 133
FIGURE 3.88: SPECIMEN TWO SHEAR DISTRIBUTION FOR FIRST STORY WHEN 133

FIGURE 3.89: SPECIMEN TWO SHEAR DISTRIBUTION FOR SECOND STORY WHEN 134
FIGURE 3.90: SPECIMEN TWO SHEAR DISTRIBUTION FOR FIRST STORY WHEN 134
FIGURE 3.91: SPECIMEN TWO INFILL COMPARISON WHEN ACTUATOR MOVES TO RIGHT 135
FIGURE 3.92: SPECIMEN TWO INFILL COMPARISON WHEN ACTUATOR MOVES TO LEFT 135
FIGURE 3.93: SPECIMEN ONE CFT COMPARISON 136
FIGURE 3.94: SPECIMEN TWO CFT COMPARISON... 136

List of Tables

Table 2.1: Summary of Physical Tests 53
Table 3.1: Section Properties for Test Specimens (Zhao and Astaneh-Asl, 2004) ... 78
Table 3.2: Specimen One Energy Dissipation 85
Table 3.3: Specimen Two Energy Dissipation 85
Table 3.4: Tabulated Principal Stresses and Angles for Specimen One Infills 105
Table 3.5: Tabulated Principal Stresses and Angles for Specimen Two Infills 110
Table 3.6: Specimen One Shear Forces and Percentages taken by Components when Actuator moves to Right 126
Table 3.7: Specimen One Shear Forces and Percentages taken by Components when Actuator moves to Left 127
Table 3.8: Specimen Two Shear Forces and Percentages taken by Components when Actuator Moves to Right 128
Table 3.9: Specimen Two Shear Forces and Percentages taken by Components when Actuator Moves to Left 129
Table 3.10: Comparison of Experimental vs. Analytical Shear Wall Capacity 137

List of Symbols

a .... Distance between Transverse Stiffeners

b .... Width of Cross-Section where Shear Stress is Determined

b_f .... Width of Flange

d .... Depth of Member

h .... Distance between HBE Centerlines

h .... Height of Infill

t_f .... Thickness of Flange

t_w .... Thickness of Web

w .... Infill Panel Thickness

A .... Cross-Sectional Area

A_b .... Cross-Sectional Area of HBE

A_c .... Cross-Sectional Area of VBE

A_f .... Area of Flange

A_w .... Area of Web

E .... Modulus of Elasticity

F_y .... Yield Stress

G .... Shear Modulus

HBE .... Horizontal Boundary Element

I .... Moment of Inertia

I_c .... Moment of Inertia of VBE taken Perpendicular to Web Plate Line

I_h .... Moment of Inertia of HBE taken Perpendicular to Web Plate Line

L .... Distance between VBE Centerlines

L .... Length of Infill

L_{cf} .... Distance between HBE flanges

M .... Bending Moment

P .... Axial Force

Q ---- First Moment of Cross-Sectional Area above Centroid

V ---- Shear Force

VBE ---- Vertical Boundary Element

V_n ---- Nominal Shear Strength

α ---- Angle of Inclination of Tension Field

β_3 ---- Column Flexibility Parameter (Behbahanifard, Grondin, and Elwi, 2003)

γ_{xy} ---- Shear Strain

δ_y ---- Yield Displacement

ε_1 ---- Major Principal Strain

ε_2 ---- Minor Principal Strain

ε_{bottom} ---- Average of Strain Readings on Bottom Flange

ε_D ---- Strain Reading in at Diagonal Direction

ε_L ---- Strain Reading in Lateral Direction

ε_T ---- Strain Reading in Transverse Direction

ε_{top} ---- Average of Strain Readings on Top Flange

ε_x ---- Strain in x Direction

ε_y ---- Strain in y Direction

λ ---- Effective Panel Width

υ ---- Poisson's Ratio

σ_1 ---- Major Principal Stress

σ_2 ---- Minor Principal Stress

σ_y ---- Yielding Stress of Material

τ_{sy} ---- Yielding Stress for Shear Theory (Takahashi, 1973)

τ_{xy} ---- Shear Stress

ϕ ---- Curvature

θ ---- Angle of Major Principal Stress

Δ_{energy} ---- Change in Energy Dissipated between Data Points

PART 1: INTRODUCTION

1.1 INTRODUCTION

Shear walls are a common lateral load resisting system. They are used to counteract in-plane forces applied along the height of a building produced by both wind and seismic loads. This is achieved by constructing a stiff section vertically spanning the height of a particular building. Currently, reinforced concrete is widely used to construct shear walls in buildings. An alternative to reinforced concrete is the use of a thin steel plate. Generally steel plate shear walls span one bay and the entire height of a building, welded or bolted to the surrounding boundary elements.

The use of steel plates compared to reinforced concrete has many benefits. Structural characteristics of steel plate shear walls include high initial stiffness, high ductility, high dissipation of energy, and good resistance to degradation when subjected to cyclic loading. These are all positive traits for a lateral load resisting system for seismic design. The use of thin steel plates also increases the amount of usable floor space. Since the amount of steel needed to resist design forces weighs considerably less than that of reinforced concrete, dead loads are decreased as well, leading to a decrease in foundation costs and seismic loads. Construction time is also reduced due to the elimination of the curing period involved with reinforced concrete. When constructing a steel structure, using steel plate shear walls can be beneficial, as well, since there is only a need for one trade on site. This form of lateral load resisting system is also easily applied to the seismic retrofit of older buildings or the repair of damaged structures.

Although there are many advantages to the application of steel plate shear walls, research has shown that there are some drawbacks. Installation often involves a large amount of welding, which can lead to high residual stresses. Formation of tension field action, which is a fundamental concept to the performance of steel plate shear walls, increases the demands on the beams and columns and often leads to premature failure in the boundary elements. Tension field action is the theory that steel plates form diagonal tension forces when subjected to shear in the horizontal direction. This concept is adopted in the American Institute of Steel Construction manual for the design of plate girders.

An extensive summary of past experiments covering the effectiveness and behavior of steel plate shear walls as a lateral load resisting system follows. Trends in behavior and failure are also discussed along with design considerations. An in depth investigation of experimental data collected for two specimens tested at the University of California, Berkley is also included. Analysis was completed from these specimens to examine the innovative design tested.

PART 2: LITERATURE REVIEW

2.1 ABSTRACT

Research on steel shear walls has been conducted in Taiwan and Japan covering the use of stiffeners, perforations, and low yield steel (Takahashi, Takeda, Takemoto, and Takagi, 1973; Nakashima, 1995; Yamaguchi, Takeuchi, Nagao, Suzuki, Nakata, Ikebe, and Minami, 1998; Hitaka and Matsui, 2003; Chen and Jhang, 2006), while the research in the US, Canada, and England have focused mainly on the performance of unstiffened steel plates. Past research conducted at the University of Alberta in Canada (Timler and Kulak, 1983; Tromposch and Kulak, 1987; Driver, Kulak, Kennedy, and Elwi, 1997; Schumacher, Grondin, and Kulak, 1997; Behbahanifard, 2003), University of Wales in England (Roberts and Sabouri-Ghomi, 1992), University of Maine (Elgaaly, Caccese, and Du, 1993; Elgaaly, 1998), University of British Columbia (Rezai, Ventura, Prion and Lubell, 1998; Lubell, Prion, Ventura, and Rezai, 2000), University of California at Berkley (Zhao and Astaneh-Asl, 2004), and the University of Buffalo (Berman and Bruneau, 2005) will be summarized. Analytical research (Thorburn, Kulak, and Montgomery, 1983; Xue and Lu, 1994; Shishkin, Driver, and Grondin, 2005) has also been conducted; however, only physical tests will be discussed. The majority of the tests to be discussed have been conducted in the US, Canada, or England, but several significant studies have been conducted in other countries. These will also be included to provide a complete sample of experimental results.

2.2 Summary of Physical Tests

2.2.1 Takahashi *et al*

Takahashi, et al, conducted the first steel plate shear wall tests in Japan in the early 1970's. Twelve small scale, single story specimens were subjected to 4 to 6 complete cycles of loading. Specimens measured 2100 by 900 mm. Takahashi et al's testing varied stiffener configurations and plate thickness. Three stiffened configurations were paired with plate thicknesses from 2.3, 3.2, or 4.5 mm. One control specimen was tested as an unstiffened steel panel. The specimens consisted of a stiff frame and pinned joints (Takahashi, 1973). The single-story specimens all behaved in a ductile manner, while the stiffened plates dissipated significantly more energy. As a result of their findings, they suggested limiting buckling in the panels to local buckling between stiffeners and prohibiting plate buckling in the elastic region (Takahashi, 1973).

Two full scale, two-story specimens were also tested to determine the effect of openings on steel plate shear walls. Thicker plate material was used in the specimen with openings to provide the same stiffness and strength in the plate without openings. Testing terminated due to entire buckling caused by poor lateral bracing at the second floor. Researchers concluded that the yielding stress of the wall could be determined using the equation below.

$$\tau_{sy} = \sigma_y / \sqrt{3}$$

τ_{xy} = Shear stress

σ_y = Stress in y direction

Both specimens performed in a ductile manner and produced stable hysteresis loops. The research showed that by increasing plate thickness, steel plate shear walls with holes perform similar to those without (Takahashi, 1973).

2.2.2 TIMLER AND KULAK

Timler and Kulak conducted the first test exploring the post buckling strength of a thin steel plate at the University of Alberta in Canada (Timler and Kulak, 1983). As with plate girders, it was recognized that steel infill plates are capable of considerable post buckling strength due to the formation of tension field action. Based on this theory, an unstiffened panel, meant to act as the web in a plate girder, was designed to resist shear forces. One large scale specimen was subjected to a cyclic load. Boundary elements were built up sections approximately the size of W 310 x 129 for columns and W 460 x 144 for beams. These sections were designed to represent typical construction; however, anchoring tension field action forces required large members. By orienting the columns horizontally and the beams vertically, one specimen was capable of producing results for two single-story specimens as shown in Figure 2.1. Corner connections were simply pinned. The middle beam-to-column connections were continuously welded with stiffeners added to the interior beam. Infill panels, 5 mm thick, were connected to the boundary frame using fish plates as shown in detail of Figure 2.1.

The specimen resembled a simply supported beam with a concentrated load at center span. Loading was applied up to three times the serviceability drift limit with a monotonic pushover applied to failure. Failure mode of Timler and Kulak's specimen occurred in a corner connection. Due to the failure at the corner, Timler and Kulak suggest that a continuous stiff boundary is required to anchor the tension field action forces (Timler and Kulak, 1983).

Results were compared to the analytical method suggested by Thorburn *et al* where the infill plate is represented by diagonal struts as shown in Figure 2.2. Because the angle of inclination is an important factor, the theoretical and experimental results were compared. Figure 2.3 shows the angle of principal stresses acting during the formation of tension field action. Researchers determined that the strip model was an acceptable method for analytical analysis (Timler and Kulak, 1983).

2.2.3 TROMPOSCH AND KULAK

A test similar to Timler and Kulak's was conducted by Tromposch and Kulak. The test was conducted at the University of Alberta in Canada on a single full scale, double panel specimen (Tromposch and Kulak, 1987). Similar to the earlier work with Kulak, this specimen consisted of vertical beams of W 610 x 241, horizontal columns of W310 x 129, and fish plates connecting the infill plate to boundary elements as shown in Figure 2.4. Infill plates consisted of 3.25 mm thick hot-rolled steel. Differing from the earlier test, bolted shear beam to column connections were used, gravity loads of 500 kN were applied to the columns and larger beam sections were used to anchor the tension field action.

Quasi-static loading was applied at center span to produce results for two single-story specimens as done with the previous research. Twenty-eight fully reversed cycles were completed. After which, a monotonic load was applied until ultimate capacity was reached. The specimen failed due to a tear in a fillet weld at the web plate to fish plate connection possibly caused by "robust beam-column joint rotation", instability at the pinned joint where the flange was coped, and slippage of bolts (Tromposch and Kulak, 1987).

Tromposch and Kulak found that unstiffened steel plate walls produce the same "S" shaped hysteretic loops typical for steel bracing or reinforced concrete shear walls shown in Figure 2.5. They suggested that the use of thin steel plate is comparable to these conventional systems already widely used. It was also recommended to design welds for the tensile capacity of the plate and consider the additional stress added by welding (Tromposch and Kulak, 1987).

The analytical model presented by Thorburn *et al* was used for an analytical analysis of the test specimen. It was found that measured internal forces in the boundary frame validate the strip model. Measured infill stresses also were in good agreement with the calculated values. It was determined that the inclined tension bar model will be conservative with good agreement (Tromposch and Kulak, 1987).

2.2.4 Roberts and Sabouri-Ghomi

A series of 16 small scale, single-story specimens were tested at the University of Wales in England by Roberts and Sabouri-Ghomi. Researchers examined effects of openings on steel plate shear walls due to their necessity in practice (Roberts and Sabouri-Ghomi, 1992). The diameter of the centrally placed openings varied from 0 mm, 60 mm, 105 mm, to 150 mm. This experiment also investigated the effects of plate thickness and aspect ratio (Roberts and Sabouri-Ghomi, 1992). Infill plates varied from 0.83 mm to 1.23

mm, and aspect ratios of 300/300 and 450/300 were tested. Two rows of high strength bolts connected the infill plate to the boundary frame. The boundary frame consisted of rigid frame members pinned together at corners as shown in Figure 2.6. Loading equipment was placed on diagonally opposite corners in order to apply shear forces. Each specimen was subjected to at least four displacement controlled cycles of quasi-static loading.

All specimens displayed ductile behavior, and the amount of energy dissipated increased per cycle. Sample hysteresis loops showing the specimens stable behavior are shown in Figure 2.7. As the diameter of opening increased the load carrying capacity decreased because they interfered with the development of tension field action (Roberts and Sabouri-Ghomi, 1992).

2.2.5 Elgaaly and Caccese

Eight, quarter scale, three-story specimens were tested at the University of Maine by Elgaaly and Caccese. Beam to column connection type was varied from shear to moment resisting, along with panel thickness (Elgaaly, 1998). Shear connections were accomplished by welding the beam web to the column flange, while moment connections required a continuous fillet weld of the entire beam section to the column flange. Infill panels were continuously welded to beam and column flanges. A stiff 9 in panel was used at the top of each specimen to anchor the tension field action as shown in Figure 2.8. Lateral bracing was supplied to support the boundary frame for out of plane deformations (Caccese, Elgaaly, and Chen, 1993).

A single horizontal force applied by an actuator at the top of the wall was used to complete 24 fully reversed, displacement controlled cycles. These 24 cycles were repeated and a monotonic load was applied reaching the actuator limit (Caccese, Elgaaly, and Chen, 1993). Specimens with moment connections failed due to tension failure at column base weld, yielding of the column base, and excessive deformations of the infill. Failure in the specimens with shear type connections was caused by plate yielding, followed by column yielding (Elgaaly and Caccese, 1990).

Elgaaly and Caccese concluded that the use of shear or moment connections had little effect on the overall performance. Specimens with thicker plates also mimicked the performance of a beam rather than a truss, which can lead to an excessive transfer of forces to columns (Elgaaly and Caccese, 1990). Designs that neglect the post-buckling strength of the plate result in thicker plates. Elgaaly and Caccese recommended accounting for this added strength to prevent premature failures in columns.

Phase II of the research conducted at the University of Maine included seven ⅓ scale, two-story specimens. Infill panels for each were 0.0897” thick. A gravity load equal to 50% of the column capacity was applied to all but one. Six of the seven specimens had fish plates welded to the boundary then varied bolt spacing attaching the infill to the fish plates. Along with these characteristics, column section and the configuration of stiffened openings were studied. A stiff, deep top beam was used to anchor tension field action in the top story panel (Elgaaly, 1998). Each specimen was subjected to fully reversed, displacement controlled, cyclic loading. Loading included eight displacement levels and three cycles for each level. Out of plane buckling was prohibited by lateral bracing provided at mid-floor level and top (Elgaaly, 1998).

Failures included local buckling of column, rupture of weld between column and base plate, and shearing of bolts connecting infill panel to mid-floor beam. Due to a high number of column failures, larger column sections were used and full post-buckling strength was reached in plates (Elgaaly, 1998). It is then suggested that column sections allow panels to develop tension field action and yield prior to column failure. Results also showed that the bolt spacing was not a factor determining failure mode, however the specimen using only welded connections showed higher stiffness and load at yield (Elgaaly, 1998).

An analytical analysis was completed for these test specimens by replacing the infill panels with truss members placed at 45° in both directions as shown in Figure 2.9. These truss members were modeled with elastic, elastic-plastic, perfectly plastic behavior in the computer program ANSR-III. When subjected to monotonic and displacement controlled cyclic loading, the test and model produced results in good agreement (Elgaaly, 1998).

2.2.6 DRIVER *ET AL*

The first large scale multi-story specimen was tested by Driver *et al* at the University of Alberta in Canada. A four-story, ½ scale specimen was designed according to typical steel plate shear wall construction (Driver, Kulak, Kennedy, and Elwi, 1998). The plate thickness and grade of steel varied over the height of the structure. The boundary frame consisted of W310 x 118 columns and W310 x 60 beams as shown in Figure 2.10. Welded moment resisting connections were used to tie the beam and columns together. Fish plates were welded to beam and column flanges and the infill welded to fish plates. All welds were designed to reach the ultimate strength of the infill panel.

Before performing the final experiment, a test was run on the proposed corner detail. The detail tested included a beam section, column section, and portion of the infill. The manner of connecting the infill to its boundary elements was to weld fish plates to both frame and panel with a strap plate used for continuity between fish plates. Cyclic loading was applied by actuators simulating the opening and closing action that occurs due to the application of shear forces, and a tensile force was applied in order to simulate the formation of tension field action (Driver, 1997). The connection was found to be suitable for the experiment because failures occurring in the welds were not expected to affect the overall strength of wall. The specimen described above was tested according to ATC-24 with four equal lateral loads applied at each level for a total of 30 cycles. Gravity loads representing dead loads present in the lowest story of a typical building were also applied to the columns through testing.

The four-story test preformed in a stable and ductile manner as expected. After reaching the ultimate load of 3080 kN, the wall strength gradually decreased. Hysteresis loops for the specimen are shown in Figure 2.11. There was not a sudden change in the wall's behavior because the infill panel is capable of redistributing forces after damage has occurred (Driver, 1997). Failure of the specimen was caused by a fracture in the column base. This fracture started at the welded connection of the flange and continued through the column web. Research suggests that failure could be prevented by adding stiffeners to the columns near each level (Driver, Kulak, Kennedy, and Elwi, 1998).

Driver conducted both a finite element analysis using ABAQUS along with an analysis using Thorburn *et al's* strip model in the computer program S-FRAME. The finite element model was subjected to monotonic and cyclic loadings, Driver concluded that the ultimate load is accurately predicted; however, the stiffness at higher levels is overestimated due to geometric nonlinearities (Driver, 1997). The strip model analysis produced results in good agreement with the experimental findings. The specimen stiffness was underestimated using this model (Driver, 1997). Since finite element modeling software is not readily available, the strip model presents a simplified approach which can be performed in common modeling software.

2.2.7 LUBELL AND REZAI *ET AL*

A series of dynamic tests were done at the University of British Columbia, one of which was the first shake table test conducted on a steel plate shear wall specimen. The specimens tested included two single-story, ¼ scale and two four-story, ⅓ scale. All beam-to-column connections were full moment resisting, accomplished by welding the entire beam section to column flange. Fish plates cut at 45 degrees weld connected the infill panels to boundary frame. Lateral bracing was provided to restrict out of plane buckling (Lubell, Prion, Ventura, and Rezai, 2000).

The single-story specimens varied by the depth of the top beam, method of loading, and fabrication techniques. These single-story specimens were designed to represent the bottom level of the four-story specimens later tested. Both specimens included triangular stiffeners welded at column bases as shown in Figure 2.12. A second beam was welded to the top of the second specimen in order to anchor the tension field forces. Precautions were also taken to prevent deformations due to welding in the second specimen. Specimen one was tested with 1-2 cycles per loading displacement up to $4\delta_y$, with monotonic loading applied to $7\delta_y$. In contrast, the second specimen was loaded according to ATC-24 (Lubell, Prion, Ventura, and Rezai, 2000). The infill panel in the first single-story specimen exhibited severe tearing and fractures at welds. Testing was terminated due to distress in the lateral bracing. The second wall failure mode was column fracture at base (Rezai, 1999). Hysteresis behavior of both specimens, shown in Figure 2.13, demonstrates the significant improvement of the behavior of the specimen by adding a stiff top beam.

The first of the four-story specimens to be discussed was tested using hydraulic actuators at each level. The specimen was designing to mimic a steel framed office building and steel masses were attached at each floor level to simulate gravity loads. Infill panel was constructed using the thinnest available hot rolled steel plate. Loading was applied according to ATC-24. Testing was terminated due to global, out-of-plane buckling in the first-story column (Rezai, 1999).

The second four-story specimen was tested using a shake table setup. The specimen was constructed similarly to the previous four-story specimen and is shown in Figure 2.14. The column section and beam flange welded to base plate and two parallel frames were used to brace the specimen against out of plane buckling. Records for several different earthquakes were used in testing, including Landers from 1992, Petrolia from 1992, and Northridge 1994. The specimen remained basically elastic during testing, so failure mode could not be determined (Rezai, 1999).

Through comparing the two single-story specimens, research suggest that the use of a stiff top beam is necessary to anchor the additional forces created by the formation of tension field action. The formation of a plastic hinge in the first specimen supports this theory. Stiff, ductile behavior with good energy dissipation was present in both single-story specimens when compared to the behavior of a frame (Rezai, 1999). The four-story specimen was more flexible when subjected to quasi-static loading due to the increased effect of the overturning moment. Researchers observed that the column in the lowest story was subjected to combined shear and bending moment forces, while the upper levels moved as a rigid body. This observation proves the added demand at the column base. Premature failure in this specimen prohibited examination of the ductility and degradation of the wall (Rezai, 1999).

Several analytical studies were carried out for comparison. Two types of models were created in SAP90: a strip model and a model applying shell elements for the infill member. A third type of model was created in CANNY-E program which included shell elements and accounted for material nonlinearities. There were several models created to represent the four-story specimen using SAP90. The angle of inclination varied from a single strut, 22.5°, 37°, 45°, to 55°. The strip model overestimated the specimen's stiffness, and the sensitivity study confirmed that the angle of inclination used for models significantly affects the ultimate capacity and stiffness. As a result, the modified strip model shown in Figure 2.15 was suggested for time history analysis of steel plate shear walls (Rezai, 1999). In order to validate the proposed model, results were compared to experimental findings. This comparison is shown in Figure 2.16.

2.2.8 SCHUMACHER *ET AL*

An examination into steel plate shear wall connections continued at the University of Alberta by Schumacher *et al.* Four corner details were studied with different configurations for fish plate attachment as shown in Figure 2.17. In the first detail the infill panel was welded directly to the boundary frame. The second connection included two fish plates that were first welded to the boundary frame. The infill panel was then welded to the two fish plates excluding a strap plate. The third detail is a combination of the other two, only one fish plate was used to connect the infill panel. An alternate arrangement for two fish plates was tested as the fourth specimen. The fish plates met each other at a 45 degree angle and the corner was removed in hopes of reducing a high stress area (Schumacher, Grondin, and Kulak, 1999).

Cyclic testing was accomplished as in Driver's test. Forces were applied to boundary elements and infill plates. Forces on the beams and columns represented the opening and closing forces present in connections when a steel plate shear wall system is subject to shear. The force applied to the infill represented the tensile forces that form after buckling occurs. The test set-up is shown in Figure 2.18 along with locations of applied forces. Cycles were determined by ACT-24 and approximately 42 were completed per specimen.

Yielding in the welds and along the tensile force at a 45 occurred in the first specimen. Tearing along welded connections occurred in all other corner specimens. Researchers concluded that the damage to the infill connections would not affect the overall performance to the system (Schumacher, Grondin, and Kulak, 1999).

2.2.9 BEHBAHANIFARD *ET AL*

Damage to the four-story specimen tested by Driver was concentrated in the first level. After altering the specimen, another series of dynamic loadings were applied to a three-story section by Behbahanifard *et al*. Beam-to-column connections remained welded moment resisting. The columns were welded to base plates. Infill panels connected using fish plates and strap plates as with Driver's specimen (Behbahanifard and Grondin, 2001). The modified three-story wall is shown in Figure 2.19.

Fully reversed cyclic loading was accomplished by applying equal forces at each story level according to ATC-24. Yield displacement for this procedure was estimated using finite element analysis. A reasonable dead load value for a typical building was applied using a distributing beam at the top of the specimen. Hysteresis behavior of the specimen is shown in Figure 2.20. A large crack in the middle panel was caused in cycle 21 due to a fracture in the beam flange to column flange connection. This connection failure was repaired so that testing could continue. The test concluded because of severe local buckling in the column flange at the base. After failure, the lower story panel contained tears in the bottom corner (Behbahanifard and Grondin, 2001).

The finite element model was created in ABAQUS and validated with experimental results. The method of analysis proved more accurate for monotonic and cyclic loadings than simplified methods used by other researchers. A parametric study was then run testing aspect ratio, ratio of infill stiffness to column stiffness, column flexibility, and initial imperfections. The study showed that aspect ratios from 1 to 2 and increased infill stiffness to column stiffness have insignificant effect on the system capacity (Behbahanifard, Grondin, and Elwi, 2003). As the flexibility parameter, β_3, increased the columns are subject to more bending deformations resulting in a decrease in system capacity. This numerical investigation also showed that initial imperfections have little effect on shear capacity when under $\sqrt{L/h}$ (Behbahanifard, Grondin, and Elwi, 2003).

2.2.10 Zhao and Astaneh-Asl

Two steel shear wall specimens were tested at the University of California at Berkley by Zhao and Astaneh-Asl. This innovative design included a boundary CFT column to carry the gravity loads. Two- and three-story, ½ scale specimens were tested as shown in Figure 2.21. Each level consisted of two infill panels welded on three sides to a beam and both columns, then connected using a bolted spice plate. Specimen one consisted of a ¼" infill, while specimen two had a ⅜" infill plate. Beam and column sections were W 18 x 86, with a 24 in diameter CFT 8 mm thick for gravity loads. Full moment resisting connections created a moment frame for redundancy. The specimens were developed to represent an innovative design by Magnusson Klemencic Associates where two bays with steel infills are connected using coupling beams. Since the modeled system is symmetrical, rollers at the coupling beams simulated the boundary conditions. This allowed the system to be simplified; each specimen consisted of half of the constructed system (Zhao and Astaneh-Asl, 2004).

Displacement controlled, fully reversed, cyclic loading was applied to a deep top beam. SAC Joint Venture protocol for seismic loading was used to design the loading history. Gravity load was applied to CFT columns by prestressing eight DYWIDAG W/FPU bars inside the tubes before casting the concrete. Loading reached 79 cycles with an overall drift of 0.032 (Zhao and Astaneh-Asl, 2004). Hysteresis behavior of specimens are shown in Figure 2.22. Failure mode occurred when plastic hinges formed in top coupling beams and eventually fractured at column face. Several bolts slipped in the splice plates; however, the performance of the infill panels was not thought to be disrupted. This method may be beneficial due to the high amount of shop welding and field bolting (Zhao and Astaneh-Asl, 2004). Results of this experimental study are continued in Part 3.

2.2.11 Berman and Bruneau

At the University of Buffalo several tests have been conducted exploring boundary conditions and the use of corrugated decking as an infill material. Berman and Bruneau tested three large scale specimens. The purpose was to study the proposed retrofit design for a demonstration hospital. Flat infill plates were inserted in the boundary frame using two different techniques. One used an industrial strength epoxy which could be helpful for retrofitting. The other was welded. Both flat infills were connected to intermediate WT 18 x 39.5's which were in turn bolted to the boundary elements. The third specimen applied the epoxy connection with four sheets of corrugated metal riveted together with the indentions oriented at a 45 as shown in Figure 2.23 (Berman and Bruneau, 2005). All specimens had an aspect ratio or 2:1 (width: height). Boundary frames were all designed to remain elastic with a safely factor of 2.5.

All three specimens were subjected to quasi-static loading in accordance with ATC-24. Pushover analysis was used to estimate the yield displacement for the loading history. An actuator applied force at the top of each wall. The flat infill using epoxy only sustained seven cycles before the epoxy connection failed due to poor coverage. Flat infill specimen using welded/bolted connections failed during cycle 31 because the welded connections in the corners of the panel fractured. The corrugated specimen completed 19 cycles before failure occurred due to fractures of the infill in areas of repeated local buckling (Berman and Bruneau, 2005).

In order to determine the amount of shear carried by the infill panels, the empty frame was modeled using MATLAB. The results from this analysis were then subtracted from experimental results to show the behavior of only the infills. Hysteresis loops for infill panels are shown in Figure 2.24. Research found that the amount of energy dissipated was ⅔ for the flat infill with welded connections and ½ for the corrugated infill material. Berman and Bruneau also showed that the bolted connections implemented in there specimens have desired characteristics of ductility, energy dissipation and stiffness. These results demonstrate a good method for retrofitting. Tests demonstrate that the flat infill welded to the intermediate WT shapes had the best behavior. The epoxy method of attaching the infill to the boundary elements was sufficient for the corrugated specimen (Berman and Bruneau, 2005).

2.2.12 PARK *ET AL*

Most recently steel plate shear wall tests were conducted in South Korea. Five, ⅓ scale, three-story specimen were tested in order to explore the effects of plate thickness and column strength. Park et al used built-up sections for columns and beams of the specimens. Two classifications of columns were used: strong column (SC) and weak column (WC) with a noncompact section. Strong column sections were H-250 x 250 x 20 x 20, weak column sections were H-250 x 250 x 9 x12, and beams were H-200 x 200 x 16 x 16. Plate thickness varied from 2 mm, grade SS400, to 6 mm, grade SM490. Fish plates were used to attach the panels to the boundary frame. The specimen is shown in Figure 2.25(Park, Kwack, Jeon, Kim and Choi, 2007).

The yield displacement was determined using the finite element modeling program ABAQUS. Loading was applied in increasing increments of the yield displacement until failure was reached. Loading reached drift of 2.6% – 3.2% for the strong column specimens and 0.8% – 0.9% for the weak column sections. Failures included local buckling in column, fracture at column base, and fracture at beam to column connection. Some tearing in the plates and welded connections of plates occurred, but they were not considered detrimental to the strength of the wall. Behavior of the specimens determined using the finite element model underestimated the capacity of specimens with strong columns, but accurately estimated those with weak columns (Park, Kwack, Jeon, Kim and Choi, 2007).

From this research, Park *et al* stress the importance of designing a steel plate shear wall system to deform in a shear manner opposed to bending. Shear deformation allows plastic hinges to form in the beams after the infill has yielded. Flexure dominated behavior forms plastic hinges at the wall base due to the high concentration of plastic deformations as shown in Figure 2.26. This theory for design is contrary to reinforced concrete. Shear is an undesirable failure mode for reinforced concrete due to the brittle behavior. Ensuring shear dominated behavior forces deformations to spread throughout the structure and not concentrate at its base. Results prove that the specimens with weak columns or thick plates do not allow even distribution of plastic deformations (Park, Kwack, Jeon, Kim and Choi, 2007). Hysteresis loops for specimens are shown in Figure 2.27 and illustrate that the strong column specimens reach higher peak loads and dissipate more energy. Fractures of the infill panels do not strongly affect the response of the system, so Park suggests that properly designed steel plate shear walls will fail due to fractures in the column base or beam-to-column connections.

2.3 Modeling

For practical applications of steel plate shear walls, engineers must have a reliable method for design. Research and finite element models are not realistic for a design engineer. As a result, a simplified way to predict the behavior for steel plate shear walls is necessary. The research described previously has given insight into system, component, and connection behavior. This knowledge leads to the development of design requirements and modeling techniques. The strip model, developed at the University of Alberta in Canada, has been a popular method for design. It has been modified at the University of British Columbia for a more complex, but more accurate analysis. Other methods have also been developed over time, but these theories are most notable.

During the introduction of the concept of steel plate shear walls as a lateral load resisting system, it was thought that the infill should be restricted from buckling resulting in heavily stiffened walls. Post buckling strength has been accounted for in steel plates since the 1930's. Using the analogy of a plate girder, post-buckling strength can be accounted for in steel plate shear walls along with the development of tension field action. With the vertical boundary elements acting as flanges, infill panels as the web, and horizontal boundary elements as intermediate stiffeners, steel plate shear walls can be compared to a vertical, cantilevered plate girder as shown in Figure 2.28 (Thorburn, Kulak, and Montgomery, 1983; Elgaaly, 1998; Kulak, Kennedy, Driver, and Medhekar, 2000; Astaneh-Asl, 2006). There is much controversy concerning the accuracy of this relationship. When designing a steel plate shear wall system as a plate girder, results are very conservative (Thorburn, Kulak, and Montgomery, 1983). Berman and Bruneau comment that the vertical boundary elements are actually stiffer in bending than the plates generally used to create the flanges. Stiffness of the boundary elements are neglected in determining the angle of tension field forces in plate girder theory. Since the boundary elements add significant stiffness to the system, this theory underestimates the capacity for steel plate shear walls (Berman and Bruneau, 2004).

The analytical model developed at the University of Alberta, Canada is a simplified method to design a steel plate shear wall system. For this model, the infill panel is divided into strips of equal width at an inclination angle as shown in Figure 2.29. This inclination represents the angle of tensile forces that form in the plate postbuckling. Tensile strips have an area equal to the product of the width of the strip by the thickness of the infill. These tensile struts are then pin connected to the boundary elements. It is also suggested to use pin connections at beam ends with continuous columns to eliminate moment transfer to beams. This model can be implemented in common plane frame computer programs, which makes it a desirable option for design engineers. From the analysis, force distribution can be determined, leading to required member strengths and connection demands (Thorburn, Kulak, and Montgomery, 1983).

The AISC and Canadian code include design guidelines for steel plate shear walls based on the strip model concept developed at the University of Alberta, Canada by Thorburn *et al*. The infill panel is replaced by tensile struts at approximately a 45 degree angle. Using the equation below a more exact angle can be calculated for modeling (AISC, 2005; CAN/CSA S16-01, 2001). This equation was derived by Thorburn *et al* using the theory of least work and has since been adopted by several design codes (Thorburn, Kulak, and Montgomery, 1983).

$$\tan^4 \alpha = \frac{1 + \dfrac{t_w L}{2A_c}}{1 + t_w h\left(\dfrac{1}{A_b} + \dfrac{h^3}{360 I_c L}\right)}$$

α = Angle of inclination for tension field

h = Distance between HBE centerlines

A_b = Cross-sectional area of HBE

A_c = Cross-sectional area of VBE

I_c = Moment of inertia of VBE taken perpendicular to the direction of the web-plate line

L = Distance between VBE centerlines

t_w = Thickness of web plate

The strip model has been used since the 1980's to predict the behavior of steel plate shear walls. Modeling the infill panel as tensile struts allows for simplified design calculations, but it has been shown that this method of design tends to result in conservative designs (Driver, 1997).

Rezai studied the proposed strip model described above and suggests several adjustments for a more accurate analysis. When using the simplified approach, it is assumed that the infill behaves elastically, has uniform stress distribution, and has no shear resistance prior to buckling. Research has shown that the infill does not behave in such a uniform manner. Therefore, varying the angle of inclination is suggested. A tensile strut connects opposite corners and boundary elements as shown in Figure 2.29. Locations of struts and area of members are determined based on member interactions. The equation below determines the effective width of the panel, which can then be divided into the necessary tensile truss elements (Rezai, 1999).

$$\lambda = \frac{\dfrac{L}{wh\sin^3\phi}}{\dfrac{3}{wL} + \dfrac{h}{A_b L} + \dfrac{1}{2A_c} + \dfrac{0.001h^4}{I_c L^2} + \dfrac{0.001L^5}{I_b h^3}}$$

$$\phi = \tan^{-1}\frac{L}{h}$$

λ = Panel effective width

L = Width of shear wall panel

w = Infill panel thickness

h = Story height

I_b = Moment of inertia of HBE taken perpendicular to the direction of the web-plate line

This model was compared to experimental results and strip model analysis. In general it was in better agreement than the strip model results, except when compared to the four-story specimen tested by Driver. Through these comparisons, the modified strip model has been validated as a design model for steel plate shear walls (Rezai, 1999).

These models supply a simplified approach to designing a steel plate shear wall system when advanced finite element modeling software is unavailable or impractical. After forces are determined, individual members can be sized accordingly. However, in addition to determining the forces applied by the infill plate, there are special considerations for individual members due to the increased demands. Recommendations for system components are described in the following section.

2.4 RECOMMENDATIONS

After reviewing the experimental results outlined previously, the overall behavior of a steel plate shear wall system show a trend in failure modes. To ensure a ductile, stable failure there are special considerations for each element of a steel plate shear wall. The steel plate shear wall system has been divided into three components: boundary frame consisting of vertical and horizontal boundary elements, connections, and infill plates. Observations through experimentation are summarized.

2.4.1 FAILURE MODES

Failures in steel plate shear wall specimens vary from column fracture, beam fracture, plate tearing, and local buckling of boundary frame elements, to connection fractures. Through research it is shown that some have a more significant effect on the overall behavior. For instance, system capacity does not significantly decrease due to plate tearing (Driver, 1997; Schumacher, Grondin, and Kulak, 1999; Park, Kwack, Jeon, Kim, and Choi, 2007). Infill plates are capable of redistribution of forces, resulting in a gradual loss of strength as tearing increases. However, many tests have concluded due to a fracture at the column base (Elgaaly and Caccese, 1990; Driver, 1997; Elgaaly, 1998; Rezai, 1999; Behbahanifard and Grondin, 2001; Park, Kwack, Jeon, Kim and Choi, 2007). The addition of infill plates to a frame increase the demands on the columns due to the internal forces created by tension field action. This failure mode has been common in past research and is undesirable due to the abrupt loss of ductility. Shear dominated behavior results in area of yielding evenly distributing along the height of the specimen when compared to flexure dominated behavior where deformations are localized at the base (Park, Kwack, Jeon, Kim and Choi, 2007). Flexure dominated behavior may result in a premature column failure due to local buckling at the base of the shear wall (Park, Kwack, Jeon, Kim and Choi, 2007). Failure modes of the previously described research are summarized in Table 2.1.

2.4.2 Boundary Elements

Columns are a significant concern for the design of steel plate shear walls. They are subject to much higher forces due to the transfer of lateral load through tension field action. It was suggested by Bruneau that vertical boundary elements should have a minimum stiffness to withstand the tension field forces without excessive deformations (Bruneau, Berman, Lopez-Garcia, and Vian, 2007). This leads into the idea of “pull-in” which is present in columns when walls are subject to lateral loads due to the combination of axial, shear, and bending moment forces (Lubell, Prion, Ventura and Rezai, 2000). This inelastic action reduces the strength of the system, and it is recommended that limits should be designated for columns. This would ensure that the infill yields prior to inelastic deformations in columns effect the system capacity (Lubell, Prion, Ventura and Rezai, 2000).

Columns must be designed to resist the forces transferred by tension field action forming in all plates (Park, Kwack, Jeon, Kim, and Choi, 2007). It is clear there is a large emphasis on column strength, and some researchers have even suggested strengthening column bases or adding stiffeners between column flanges (Driver, Kulak, Kennedy, and Elwi, 1998). However, a practical design alternative could be to design a primary gravity resisting column similar to the specimens tested by Zhao and Astaneh-Asl. It is also desirable for vertical and horizontal boundary elements to remain elastic during lateral loading so that panels will yield before plastic hinges form (Bruneau, Berman, Lopez-Garcia, and Vian, 2007).

As with most of the experiments discussed, the horizontal boundary elements must be deep, strong members in order to anchor tension field forces. Due to the symmetry of tension field action, intermediate horizontal elements do not have as severe of an increase in demand. Tension field forces from the higher story will counteract those from the lower story. However, the top and bottom horizontal members will not have opposing forces, so these must be strong enough to internally counteract the tension field action.

2.4.3 CONNECTIONS

Beam-column connection failures result in an abrupt loss of strength, therefore design should ensure that the infill reaches full post-buckling prior to a connection failure resulting in a ductile failure. Connections should be designed to reach the capacity of the infill panel (Bruneau, Berman, Lopez-Garcia, and Vian, 2007). Using moment connections form a back-up moment frame that will help resist shear forces after the infill yields. Moment resisting connections create a redundant lateral load resisting system (Kulak, Kennedy, Driver, and Medhekar, 2001). However, results of the experimental study at the University of

Maine suggest that there is no noticeable difference in the use of shear or moment connections.

Connecting the infill panel is important to the integrity of the system. Past research has explored using welded, bolted, or epoxy connections. Bolts and epoxy are beneficial alternatives to welding because these techniques allow for seismic retrofitting steel plates into existing buildings (Berman and Bruneau, 2005). However, epoxy connections did not prove to be a comparable alternative to bolted or welded connections due to poor coverage in the experiment where the connection was tested. However, bolting or welding of infills to boundary frames shows little to no difference in system behavior. Different configurations of fish plates, with and without strap plates, have also been studied (Driver, 1997; Schumacher, Grondin, and Kulak, 1999). Research has shown that the fish plate configuration does not strongly affect the performance of the system. The important factor in connecting a steel panel is to ensure that it is stiffly fixed to all boundary elements.

2.4.4 PANELS

Steel plate infill panels are the most important component to the system. Research has shown that the infills are responsible for the majority of energy dissipation and ensure a ductile behavior. Infill panels may vary in thickness at different levels of a structure depending on the demand at each level (Bruneau, Berman, Lopez-Garcia, and Vian, 2007). Tall buildings will result in an increase in required panel thickness at lower levels (Sabelli and Bruneau, 2006). Available panel material may be thicker than required which will cause an increase in vertical and horizontal boundary elements size and foundations due to the high post-buckling strength of the material. The use of thick infill panels causes the column strength to govern the systems stability. Thin plates should be used so that inelastic deformations can first form in the infills (Caccese, Elgaaly, and Chen, 1993). To prevent premature failure, light gage steel, low yield steel or perforated panels could be used (Bruneau, Berman, Lopez-Garcia, and Vian, 2007). Research by Zhao and Astaneh-Asl also showed that for ease during fabrication and reduced construction time it is suitable to shop-weld steel plate to boundary elements and use a splice plate bolting panels together on site. The panels spliced together showed similar behavior as would be expected from a solid plate (Zhao and Astaneh-Asl, 2003).

2.5 SUMMARY

Research has proven that steel plate shear walls are an excellent lateral load resisting system. Test specimens subject to significant lateral loads have consistently performed in a ductile and stable manner. The system is also capable of dissipating large amounts of energy when subjected to high lateral loads. Experimental results show that this system is an exceptional consideration for seismic design. The review of experimental results shows that there are several considerations:

- System should be designed to ensure full post-buckling strength of the infill panels; therefore special attention is needed in the design of the columns. Column capacity needs to withstand the additional forces present during the formation of tension field to prevent a premature, brittle column failure.

- Design should ensure a shear dominated behavior at failure so that specimen yielding can be distributed throughout the stories. Flexure dominated behavior will result in premature failures at the column base since stresses are concentrated at the base of the steel shear wall.
- Both vertical and horizontal members should be designed to remain elastic, generally resulting in large cross-sections in order to anchor tension field forces.
- Moment connections may be used for redundancy; however, experimental results show no significant difference in capacity with shear or moment connections.
- Connection of infill panels to frame has been studied and no significant difference was found for various fish plate configurations or bolted connections. Steel plate shear walls are a reasonable option for seismic retrofitting due to the consistent behavior of bolted connections with welded connections. Epoxy was also studied as a method of connecting infills; however, due to poor coverage there is not sufficient evidence to suggest this method is adequate.
- Panel thickness may vary along the height of a buildings and material thickness may be greater than required. Thicker plates result in larger beam and column cross-sections or premature failure at the column base prior to reaching full post-buckling strength in the infills.

- Strip and modified strip model have been developed so this technique can be applied to practical design situations and implemented by consulting engineers with a reasonable level of accuracy.

APPENDIX

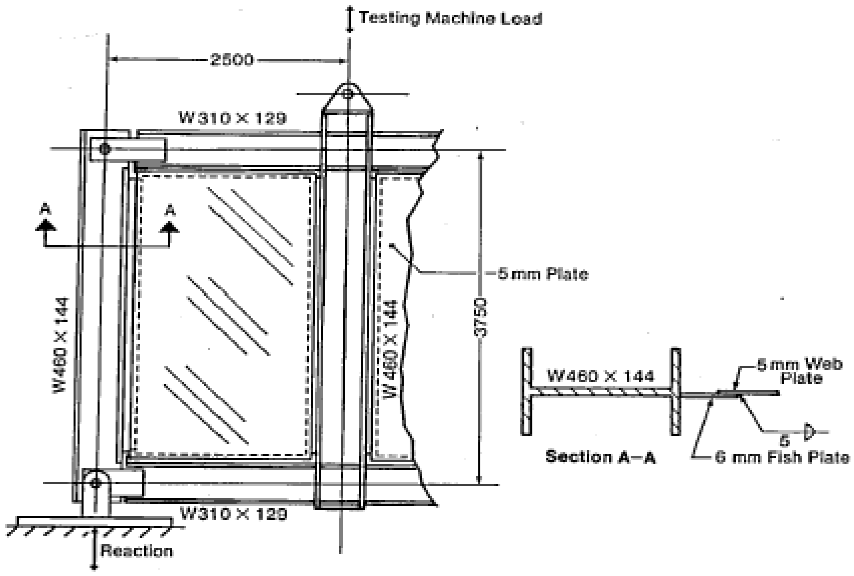

Figure 2.1: Schematic of Specimen by Timler and Kulak (1983)

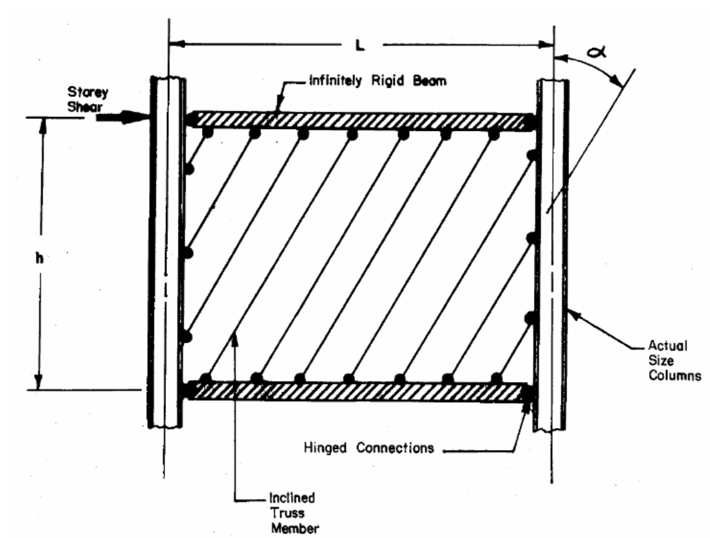

Figure 2.2: Strip Model Presented by Thorburn *et al* (1983)

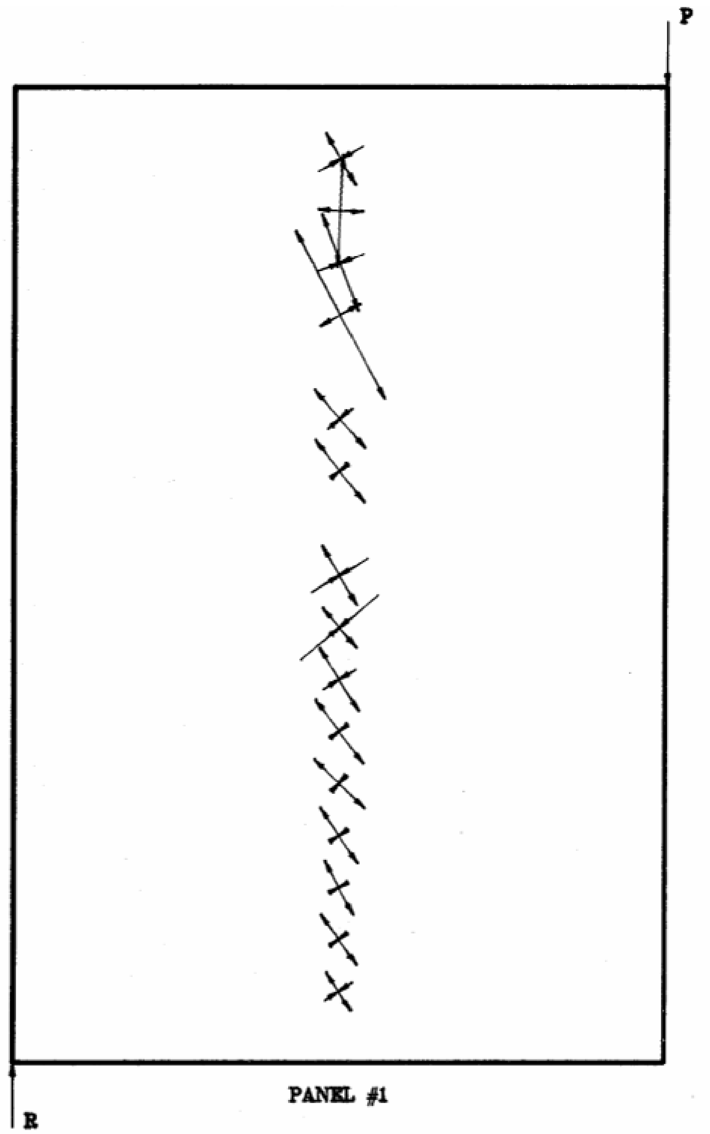

Figure 2.3: Angle of Principal Strains for Comparison with Calculated Angle of Inclination by Timler and Kulak (1983)

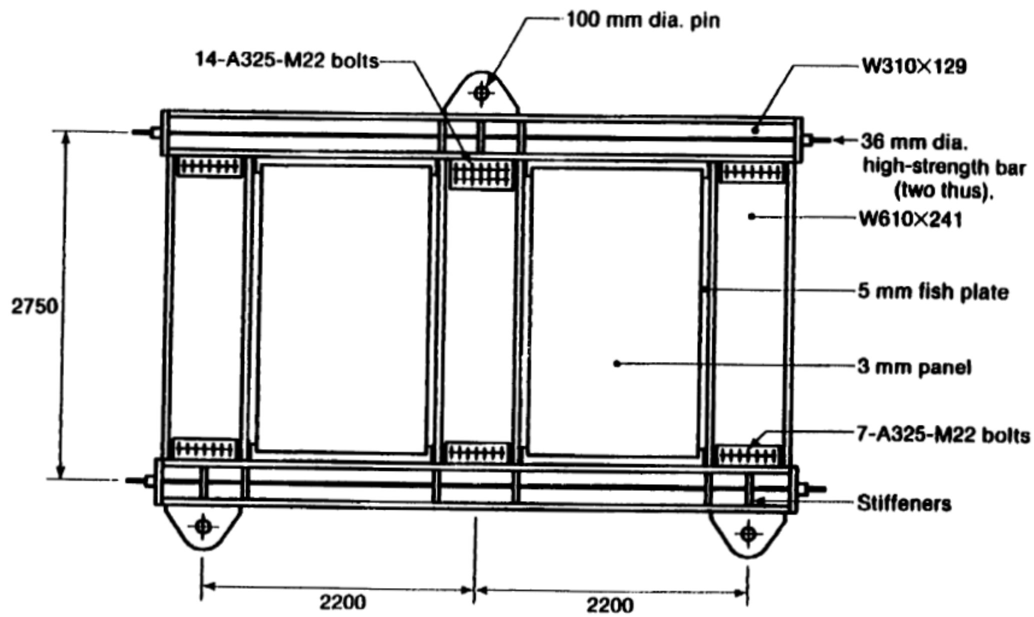

Figure 2.4: Schematic of Specimen by Tromposch and Kulak (1987)

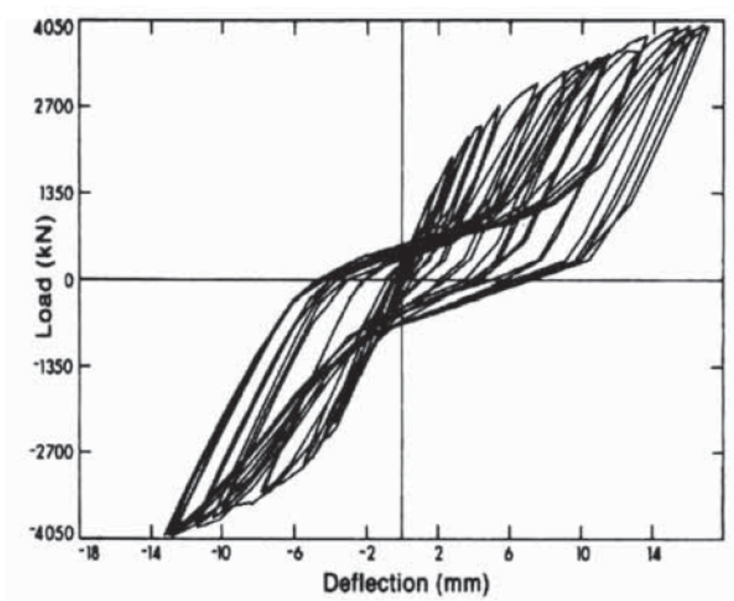

Figure 2.5: Hysteresis Loops Produced by Specimen Tested by Tromposch and Kulak (1987)

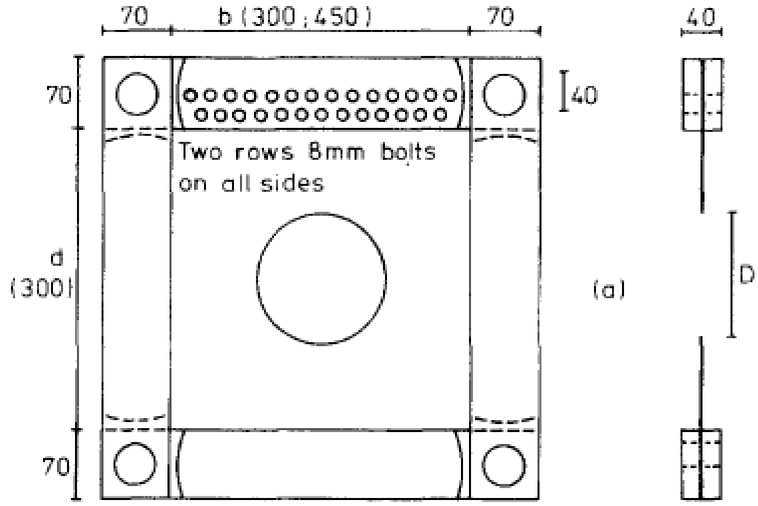

Figure 2.6: Schematic of Specimen by Roberts and Sabouri-Ghomi (1992)

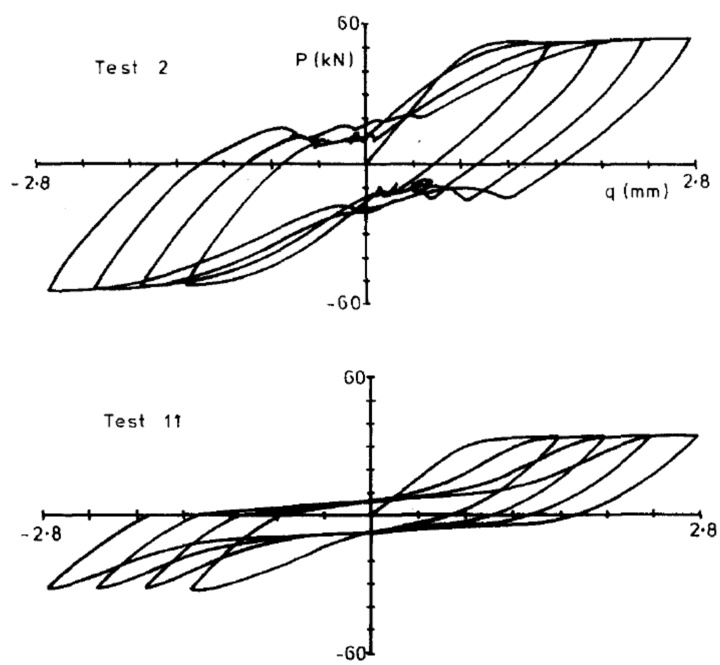

Figure 2.7: Hysteresis Loops for Specimens (Above: Solid Panel; Below: Panel with Opening)Tested by Roberts and Sabouri-Ghomi (1992)

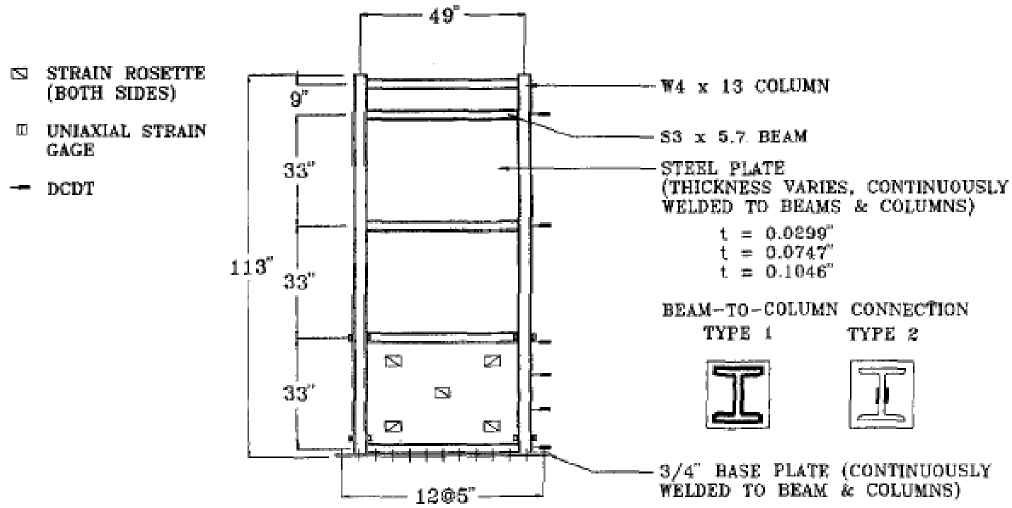

Figure 2.8: Test Specimen by Elgaaly and Caccese, 1993

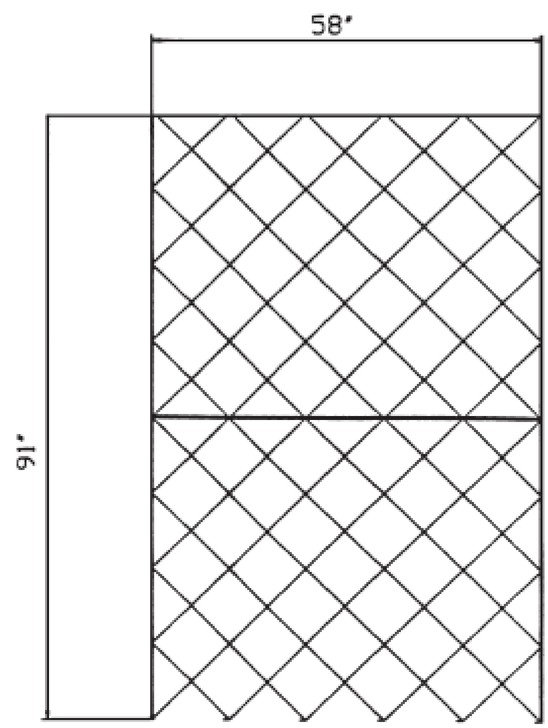

Figure 2.9: Model Used by Elgaaly, 1998

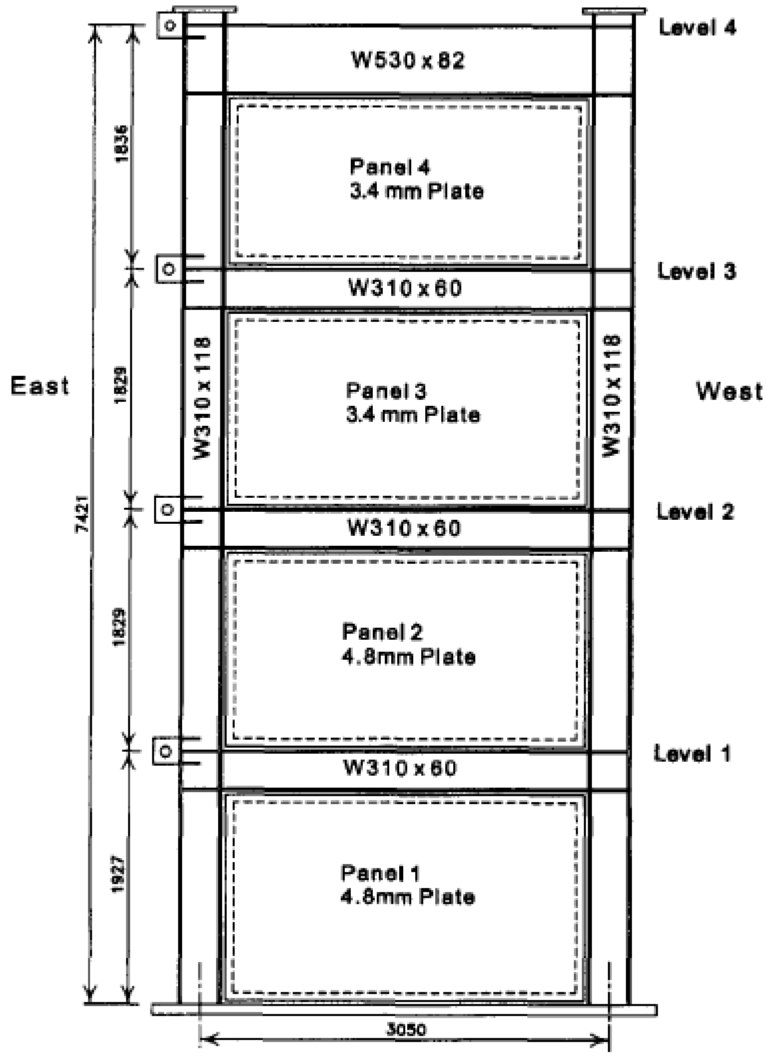

Figure 2.10: Four-Story Specimen Tested by Driver et al (1997)

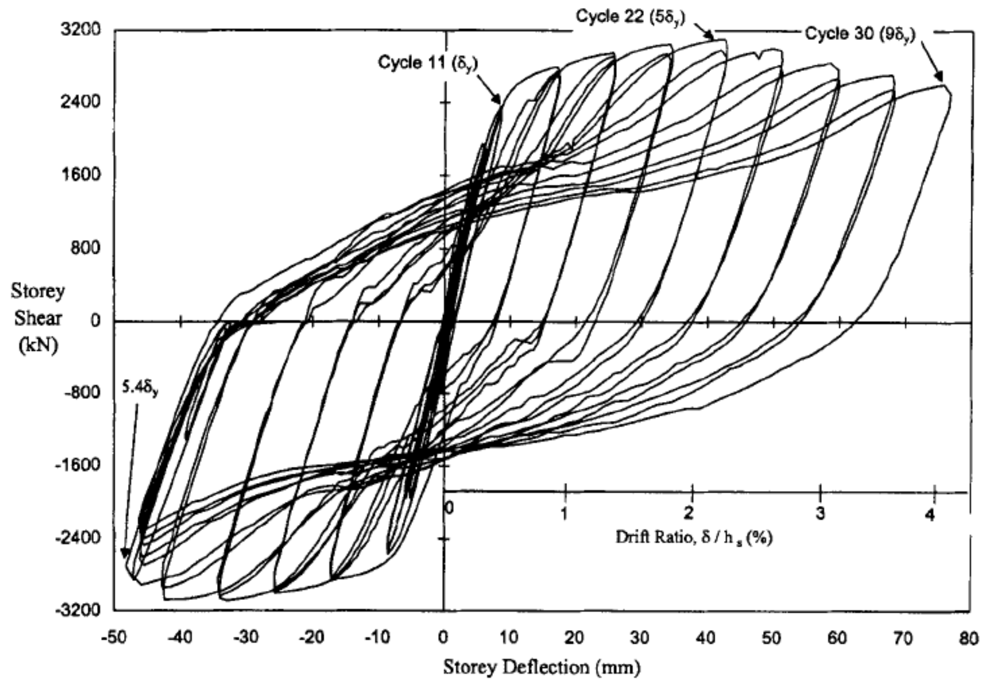

Figure 2.11: Hysteresis Behavior of Four-Story Specimen Tested by Driver *et al* (1997)

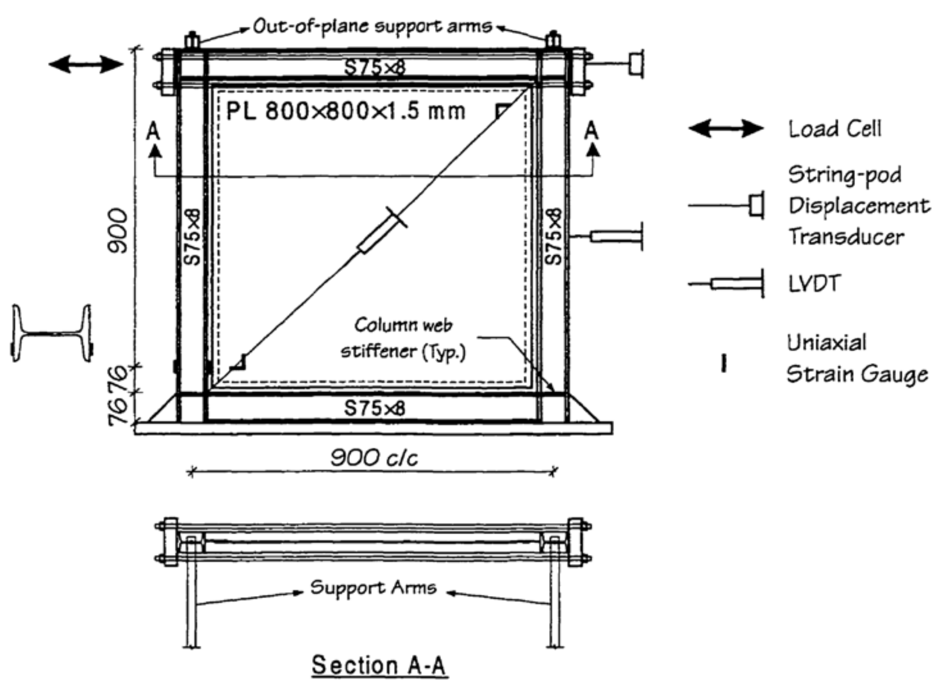

Figure 2.12: Single-Story Specimen Tested by Rezai (1999)

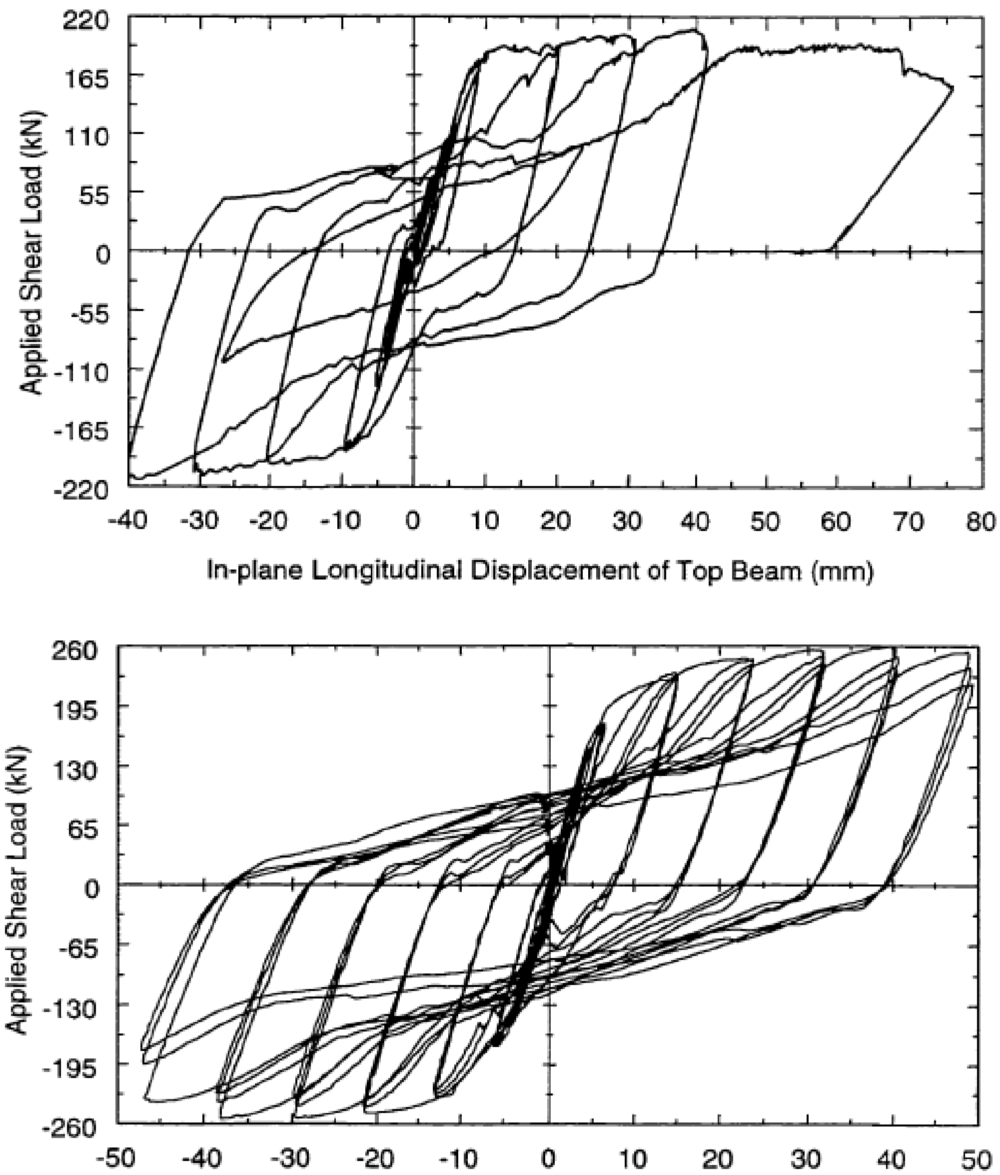

Figure 2.13: Hysteresis Behavior of Single-Story Specimens (Above: First Specimen; Below: Second Specimen) Tested by Rezai (1999)

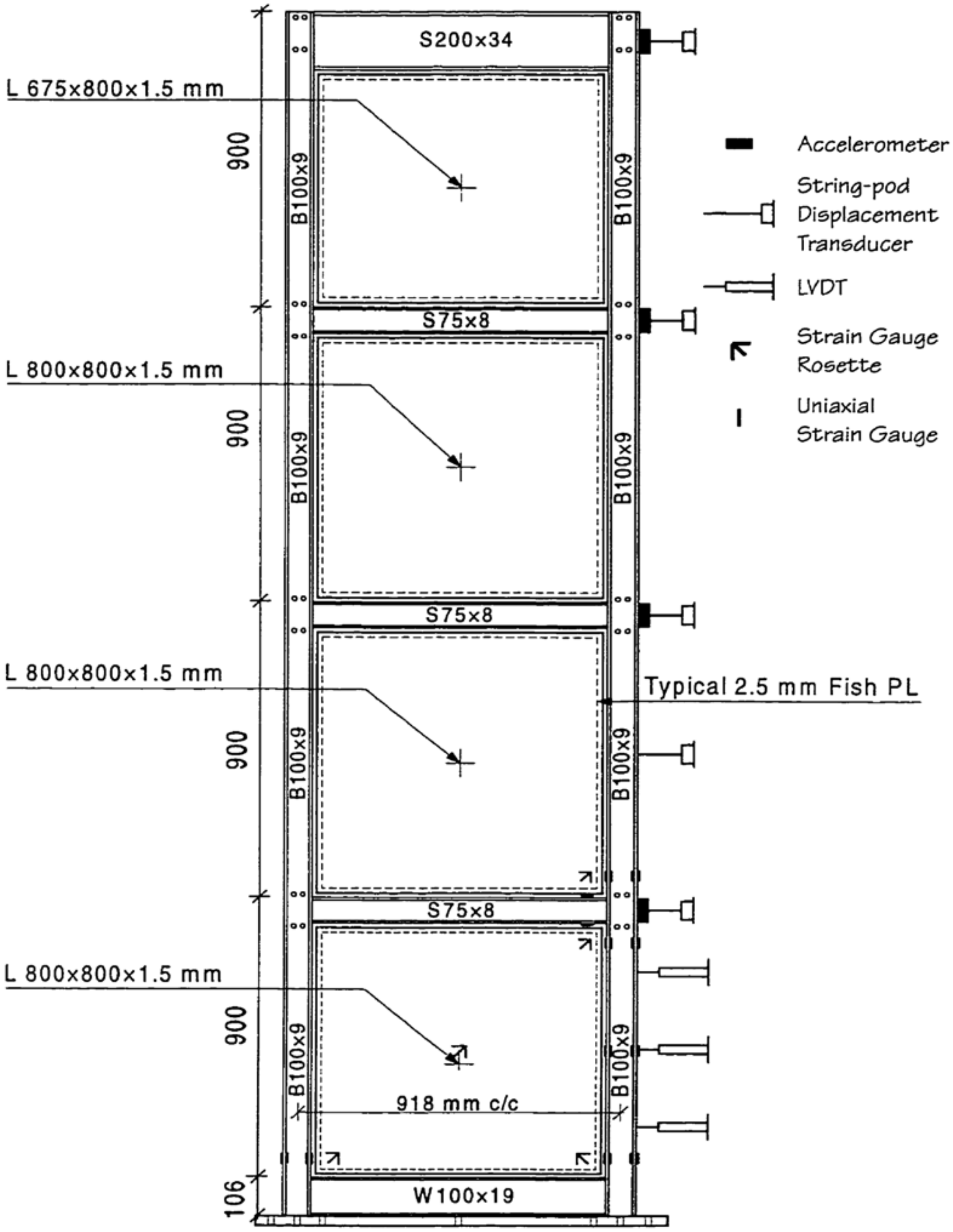

Figure 2.14: Four-Story Specimen Tested with Shake Table by Rezai (1999)

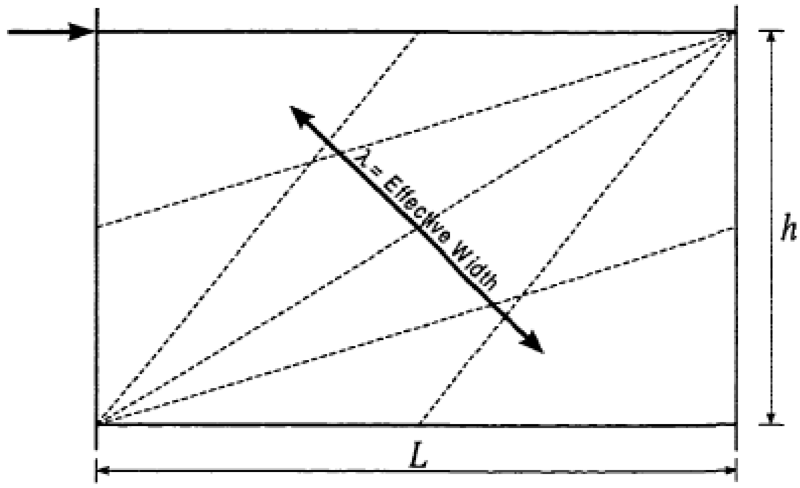

Figure 2.15: Modified Strip Model Proposed by Rezai (1999)

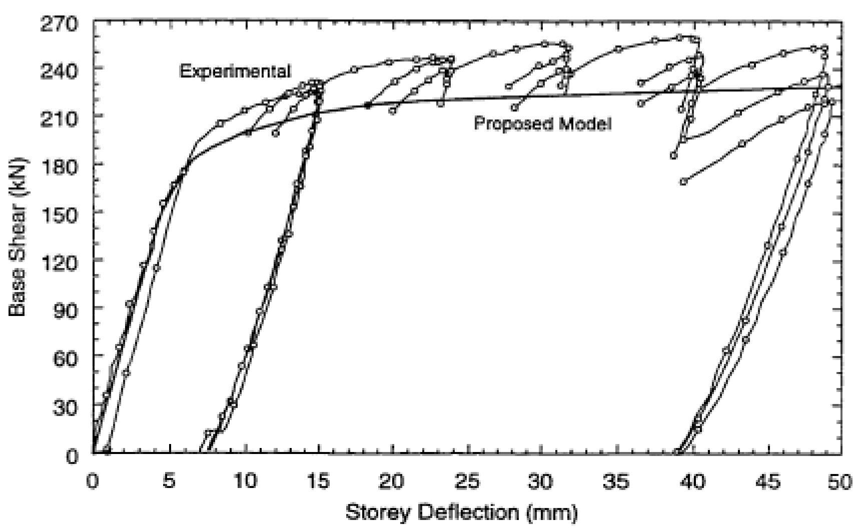

Figure 2.16: Comparison of Single-Story Experimental Results to the Results using Model Proposed by Rezai (1999)

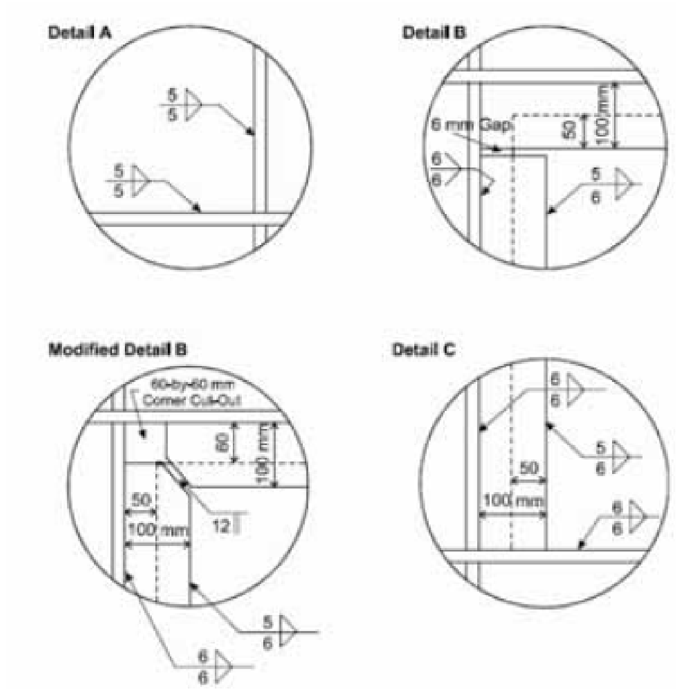

Figure 2.17: Corner Details Tested by Schumacher *et al* (1999)

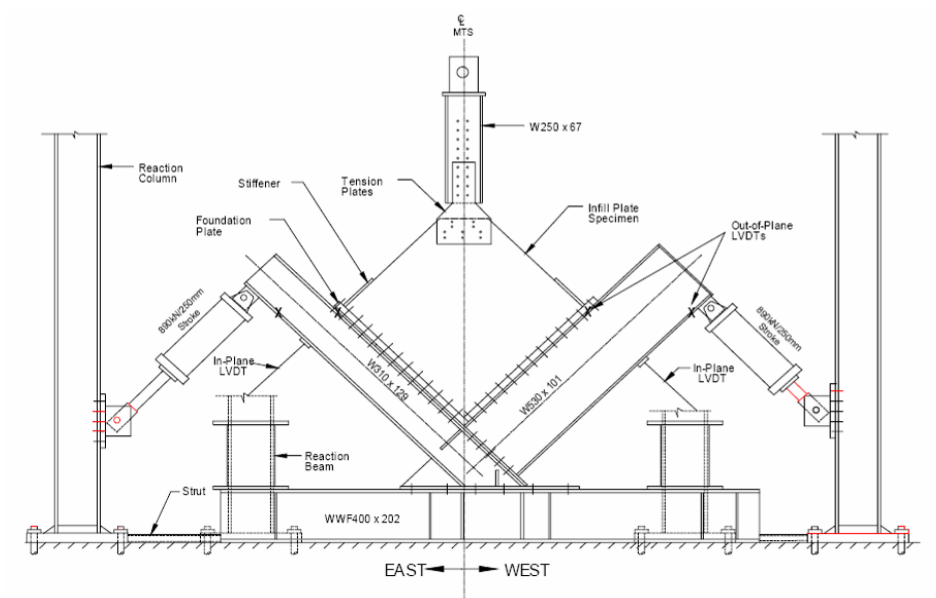

Figure 2.18: Test Set-up for Experimental Investigation by Schumacher *et al* (1999)

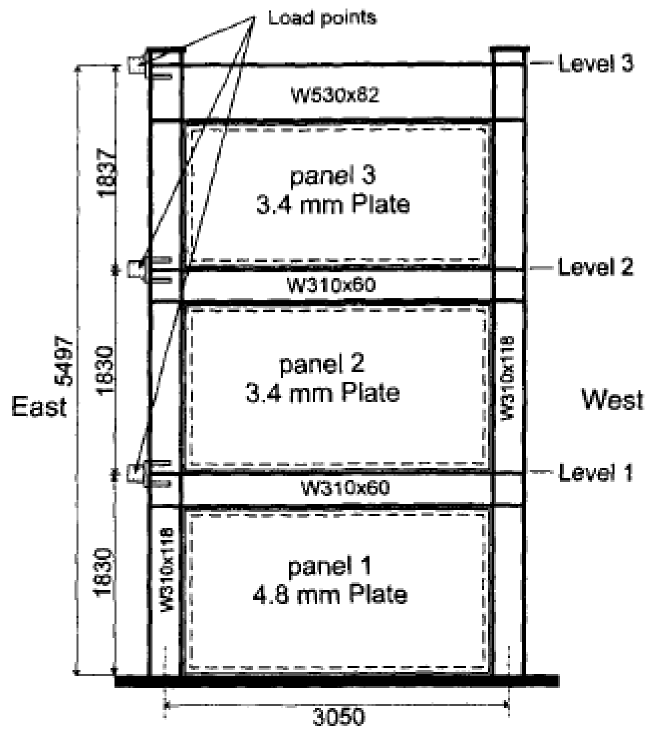

Figure 2.19: Test Specimen Tested by Behbahanifard *et al* (2001)

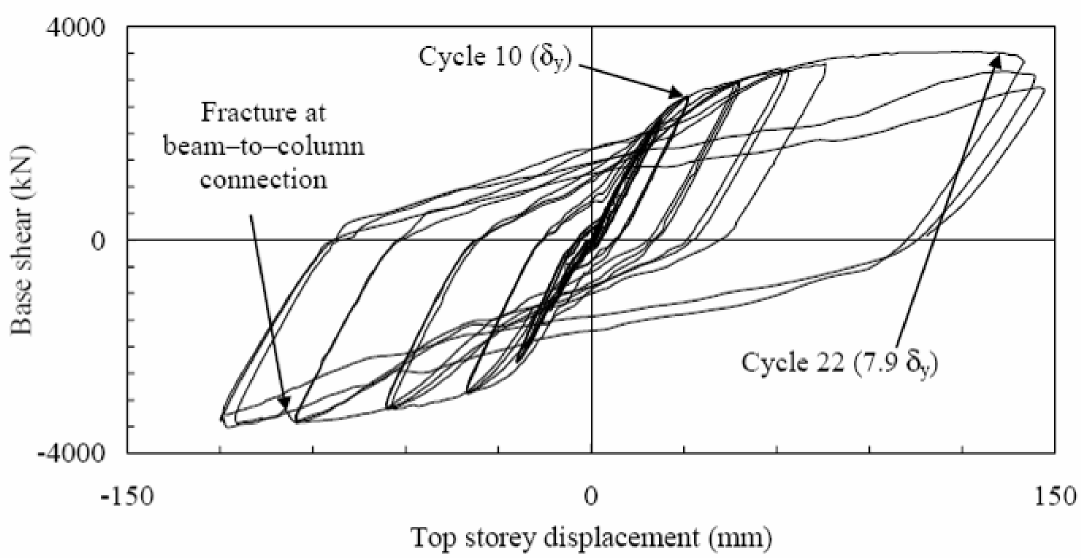

Figure 2.20: Hysteresis Behavior of Specimen Tested by Behbahanifard *et al* (2001)

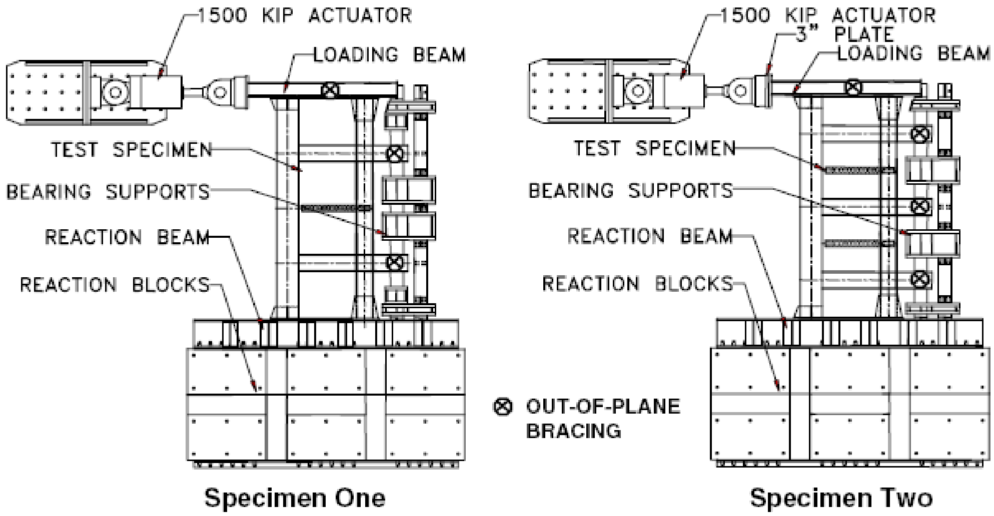

Figure 2.21: Specimens Tested by Astaneh-Asl and Zhao (2001)

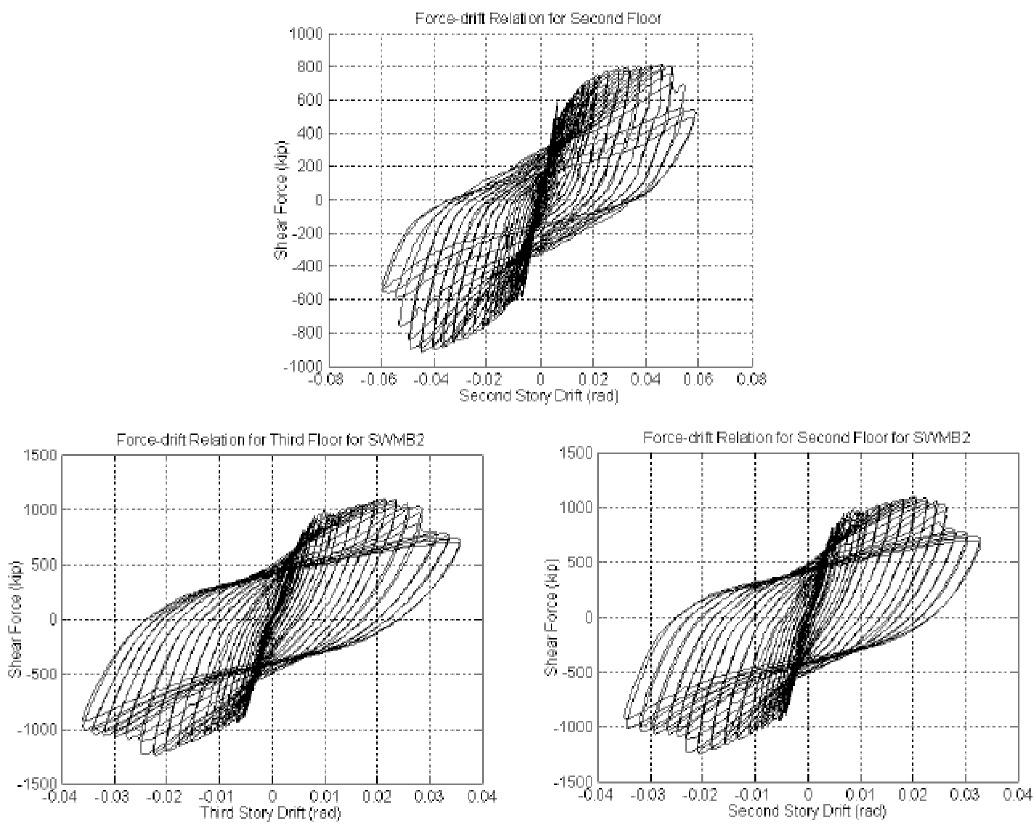

Figure 2.22: Hysteresis Behavior of Specimens (Above: Single-Story; Below: Two-Story) Tested by Astaneh-Asl and Zhao (2001)

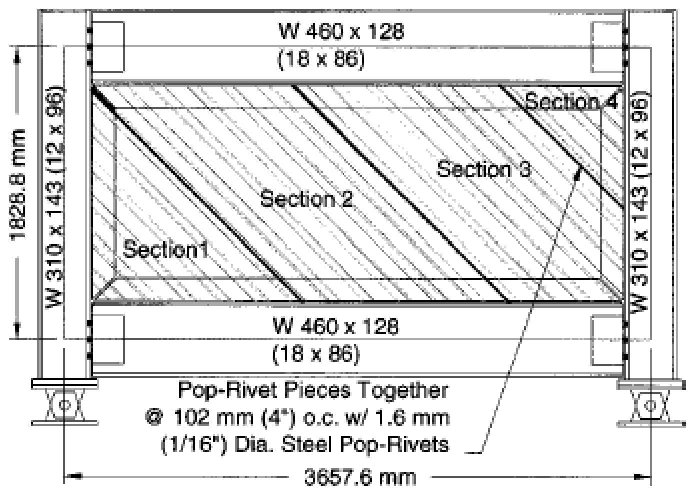

Figure 2.23: Specimen with Corrugated Metal Decking Tested by Berman and Bruneau (2005)

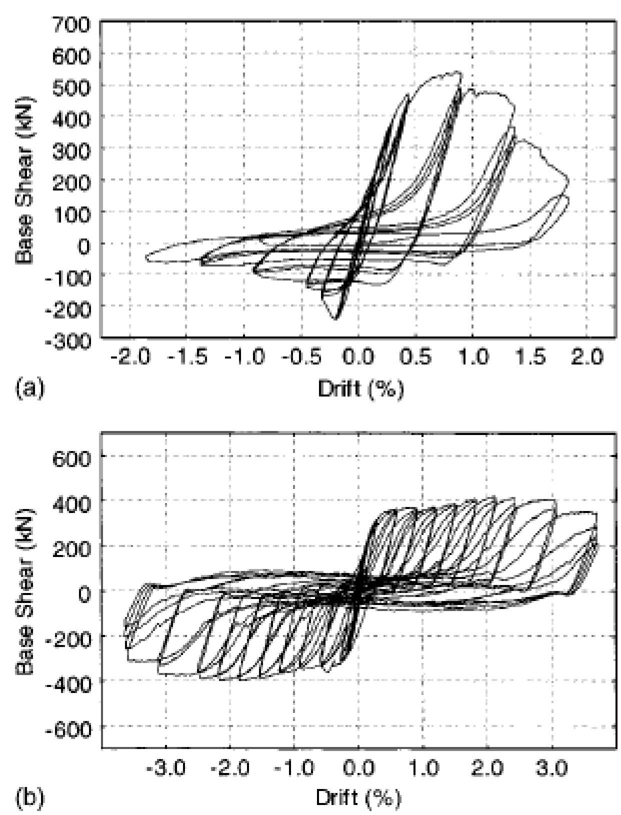

Figure 2.24: Hysteresis Loops for Specimens (Above: Corrugated Infill; Below: Flat Infill with Welds) Tested by Berman and Bruneau (2005)

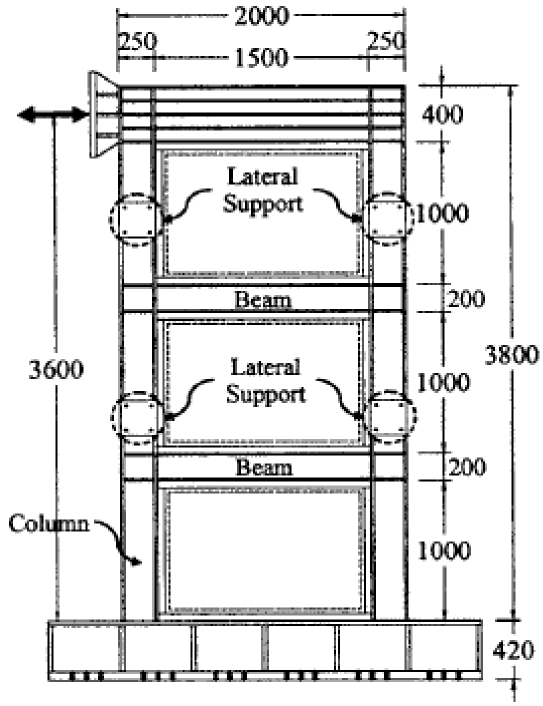

Figure 2.25: Specimen Tested by Park *et al* (2007)

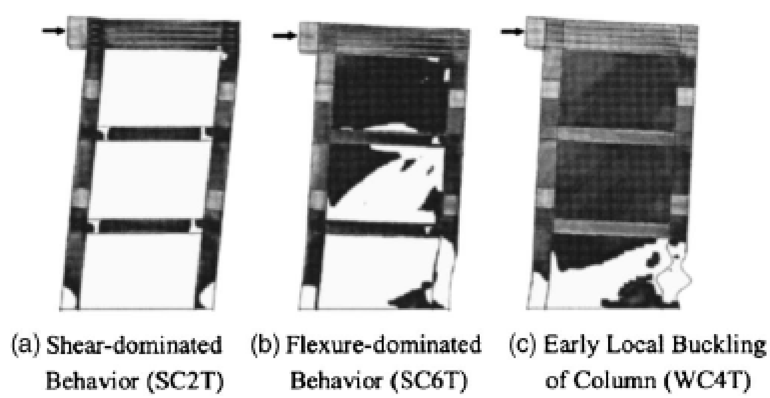

Figure 2.26: Comparison of Plastic Deformations for Shear and Flexure Dominated Behavior as Described by Park, Kwack, Jeon, Kim, and Choi (2007)

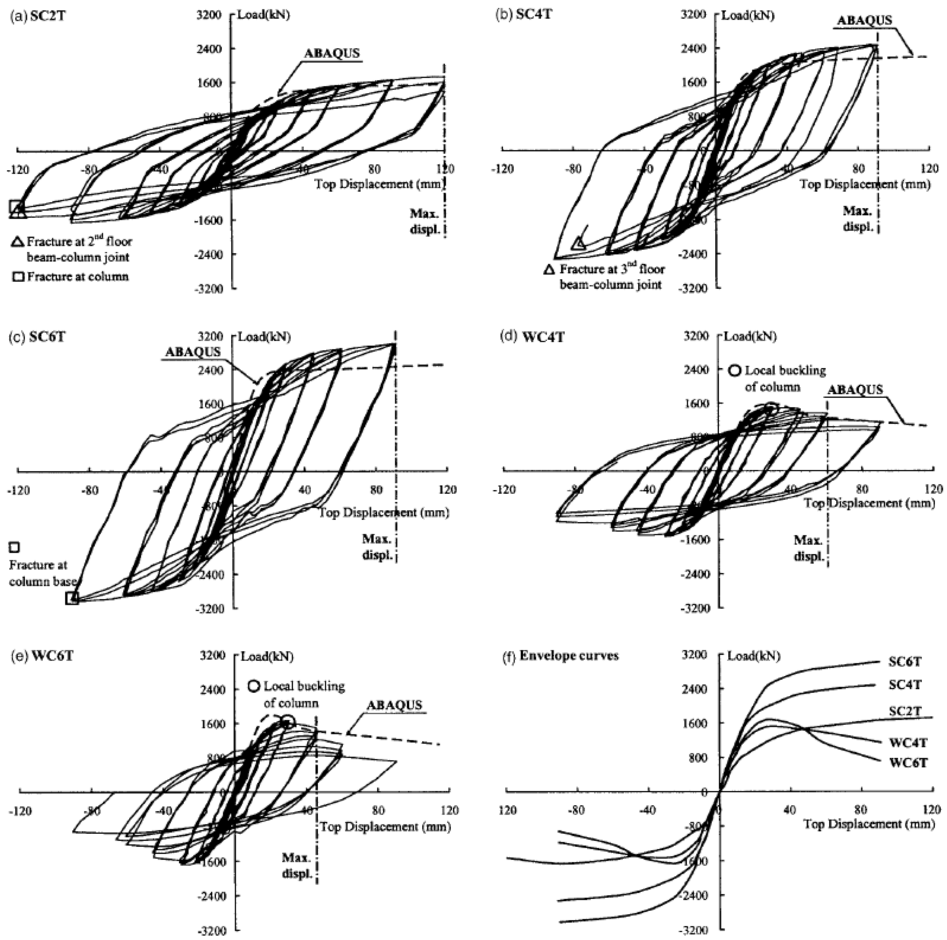

Figure 2.27: Hysteresis Behavior of Specimens (W-denotes 'weak' column; S-denotes 'strong' column) by Park, Kwack, Jeon, Kim, and Choi (2007)

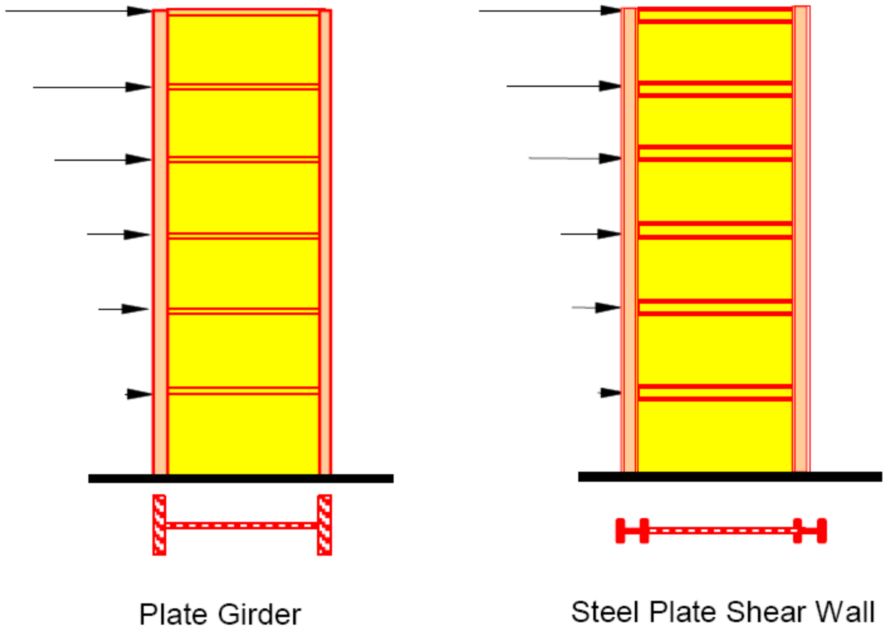

Figure 2.28: Plate Girder Analogy as described by Astaneh-Asl (2001)

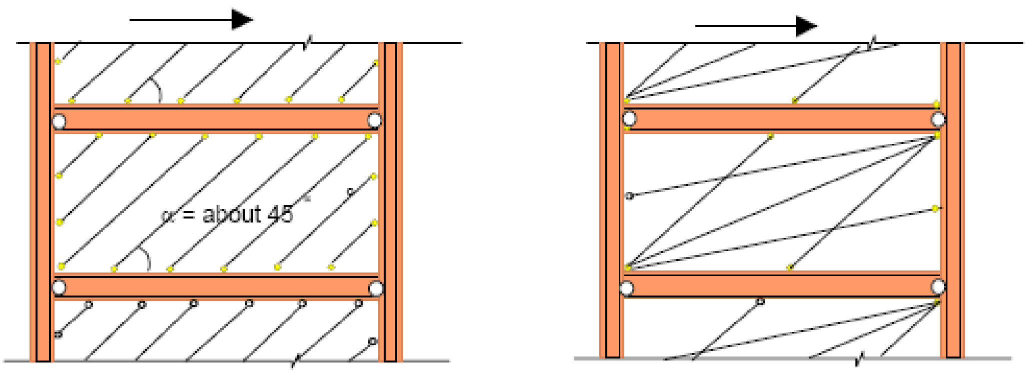

Figure 2.29: Strip Model Introduced by Thorburn *et al* (1983) paired with the Modified Strip Model Introduced by Rezai (2000) as described by Astaneh-Asl (2001)

Table 2.1: Summary of Physical Tests

Author	Year	Institute/ Country	Specimens	Stories	Parameters	Loading	Boundary Conditions	Failure Mode
Takahashi	1973	Japan	12 one-story; 900mm x 1200 mm	1	Stiffener configurations, plate thickness	Cyclic, 4-6 complete cycles	Stiff Frame, Pin-jointed, Panel-Frame connected by high-strength bolts	
Takahashi	1973	Japan	2 Full-Scale, single-bay, 2-story	2	Stiffened Openings vs. no openings	Cyclic, Loaded and unloaded in one direction, a few fully reversed cycles		Tearing at welds at the base of the columns
Timler and Kulak	1983	University of Alberta, Canada	2 Large scale, 1-story	1	Single two-story specimen tested as two single-story specimens	Cyclic static loading: 3 times to serviceability drift limit and pushover loading to failure. Loaded as a simply supported beam.	Vertical beams, horizontal columns, pinned corner joints. Built up column and beam sections. Infill to boundary fish plate connection. Beam to Column continuously welded with stiffeners.	Failure occurred in a corner connection.
Tromposch and Kulak	1987	University of Alberta, Canada	1 single-story, full scale, 2-panel	1	Single Specimen	Quasi Static, fully reversed cyclic loading, 28 cycles completed, Monotonic loading to ultimate, Axial load applied	Typical bolted shear beam-to-column connections, pin connections at column base, stiff vertical beam members	Fillet weld tear at web plate to fish plate connection due to robust beam-column joint rotation, local lateral instability around pin in region where flange had been cut back, and slip of the bolts
Roberts and Sabouri-Ghomi	1992	University of Wales, England	16 small scales	1	Plate thickness and Diameter of opening. Aspect ratios (b/d) of 300/300 and 450/300.	Quasi-Static cyclic, at least 4 cycles. Equal and opposite loads along one diagonal in order to reach a desired displacement.	Plate clamped to frame with 2 rows high-strength bolts, Pinned joints at corners of frame. Corners cut from plates to pins.	Only comments on ultimate load carrying capacity, not failure specific.

Table 2.1 continued: Summary of Physical Tests

Author	Year	Institute/ Country	Specimens	Stories	Parameters	Loading	Boundary Conditions	Failure Mode
Elgaaly and Caccese	1993	University of Maine	8 1/4 scale, 3-story, single bay	3	Panel slenderness ratio, beam-to-column connections. Moment connection: Continuous fillet weld of entire beam section to column. Shear connection: Fillet weld of beam web to column flange.	Cyclic loadings, single horizontal force applied at top of wall, 24 fully reversed cycles, 2 series, final loading was monotonic to failure. Displacement controlled cyclic loading. Each displacement repeated 3 times. Full 24 cycles repeated, then pulled monotonically to actuator limit.	Beam-to-column connections varied from shear to moment resisting connections in frame. Infill panels continuously welded to flanges of beams and columns. Stiff, 9 in panel at top to anchor TFA. Base plate continuously welded to beam and columns at base. Lateral bracing restricted out-of-plane movement.	Moment connection specimens failed due to weld at column base failing in tension, column base yielding, and excessive plate deformations. Shear connection specimens plate yielded first, followed by column yielding.
Sugii and Yamada	1996	Kansi University, Japan	14, 1/10 scale model, 2-story	2	H:L ratio, wall thickness, monotonic vs cyclic loading, with and without concrete covering	Both monotonic and cyclic shear loading	Rigid, composite frame with steel WF encased in rectangular RC sections	Steel shear walls more ductile. Walls with concrete covering had higher initial stiffness and diagonal compression field.
Driver	1997	University of Alberta, Canada	Connection	n/a	Single Connection	Cyclic loading created by moving beam and column segments, and applying a tensile force to the infill panel at a 45 to beam and column. This simulated the opening and closing that occurs at connections when shear forces are applied to a panel and the forces created by TFA. Total of 35 cycles were completed.	Fish plate weld connected infill plate to beam and column elements. Strap plate used for continuity between fish plates.	Tearing occurred at welds connecting fish plate to boundary elements and infill panel. Tears in welds occurred, but found not to be detrimental for strength of shear wall.

Table 2.1 continued: Summary of Physical Tests

Author	Year	Institute/ Country	Specimens	Stories	Parameters	Loading	Boundary Conditions	Failure Mode
Driver	1997	University of Alberta, Canada	1 4-story, single-bay, 1/2 scale	4	Built according to typical construction details, Panel thickness and grade of steel varied per story	Equal lateral loads applied at each floor. Slow cyclic loading according to ATC-24. Total of 30 cycles applied.	Beam-Column moment connections. No lateral supports. Welded connections for beam-column and plate. Deep, stiff, top beam. Plate weld connected to frame members using fish plates. Gravity loads applied to columns.	Column fractured at base. Fracture began at welded connection at column flange and continued through the web.
Elgaaly and Caccese	1998	University of Maine	7, 1/3 scale, single bay, 2-story	2	Column sections, application of axial load, welded vs. bolted, bolt spacing, stiffened openings placement	Reversed cyclic loading. Each level consisted of 3 complete cycles. Displacement controlled cyclic loading from 0 to maximum in 5 steps. 20 steps each cycle, 60 steps each displacement. If axial load applied: representative of 50% column capacity.	Plates bolted to fish plates welded to surrounding beams and columns. Columns welded to base plate. Stiff top beam used to anchor TFA. Beam webs welded to column flanges. Specimens braced at mid-floor level and top to prevent out of plane buckling.	Failures included local buckling of column, rupture of weld between column and base plate, and shearing of bolts connecting plates to midfloor beam. Due to high number of column failures, larger column sections were used and full post-buckling strength was reached in plates.
Rezai and Lubell	1998	University of British Columbia	1, 4-story, single bay, 1/3 scale, aspect ratio 1	4	Single specimen	Shake Table test. Different earthquake motions, recorded and generated, were applied. 3 records chosen to most likely damage structure. Stacks of steel plates attached at each level to model dead loads.	Full moment connections by continuous fillet welds of beam section to column flange, column base and bottom flange of lower beam welded to base plate, then bolted to shake table. 2 parallel frames for lateral support. Fish plates used to connect infill panel.	Failure was not reached. Infill plate remained basically elastic.

Table 2.1 continued: Summary of Physical Tests

Author	Year	Institute/ Country	Specimens	Stories	Parameters	Loading	Boundary Conditions	Failure Mode
Schumacher, Grondin and Kulak	1999	University of Alberta, Canada	4 Connections , full scale	n/a	1: corner where infill plate is welded directly to beam and column flanges, 2: corner where fish plates are welded to beam and column flanges then infill plate welded to fish plates, 3: fish plate welded to one boundary member and then infill welded to fish plate and also directly to adjacent boundary member. 4: Modified 2 where fish plates meet at 45 and corner is cut out to reduce area of high stress	Cyclic loading created by moving beam segment up and down, moving column segment from side to side, and applying a tensile force to the infill panel at a 45 to beam and column. This simulated opening and closing that occurs at connections when shear forces are applied to a panel and the forces created by TFA. ATC-24 was used to determine cyclic levels. Increasing levels of 3 cycles up to approximately 42 cycles per specimen.	Infill plate connected using only two fish plates. Panel welded directly to beam and column flanges in areas without fish plates. No strap plates used at fish plate connections. Beam and column segments fitted with a portion of panel	1: Joint between beam and column failed. Yielding along welds and traveling at 45. 2: Tear in welds at fish plate to infill connection and fish plate to boundary connection. All tears occurred at gap between fish plates. 3: Tear in welds along fish plate connections. Tears located at end of fish plate. 4: Tears in weld along fish plate connections. Tears located where gap in fish plates.
Lubell and Rezai	1999	University of British Columbia	2, 1/4 scale, single bay, single-story, aspect ration 1:1	1	Depth of top beam, Method of cyclic loading, Fabrication method. Deep top beam added to 2nd specimen. Extreme precautions made to 2nd specimen for weld distortions and excessive out-of-plane displacements.	Fully reversed, cyclic quasi-static loading. Applied with hydraulic actuator aligned at column web. First specimen loaded with 1 or 2 cycles at each load level. Second specimen tested following ATC-24.	Full moment connections at all beam-column joints with continuous fillet welds of entire beam section to column flanges. Infill plate connected using fish plates with 45 degree cuts at corners. Triangular stiffeners welded to column flanges at base. Lateral bracing supplied.	Specimen 1 had severe plate tearing and weld cracking. Testing was terminated due to distress in lateral bracing member. Specimen 2 failed due to an extensive column fracture just above the stiffener gusset plate at the base of the left column.

Table 2.1 continued: Summary of Physical Tests

Author	Year	Institute/ Country	Specimens	Stories	Parameters	Loading	Boundary Conditions	Failure Mode
Lubell and Rezai	1999	University of British Columbia	1, 1/4 scale, single bay, 4-story, panel aspect ratio = 1:1	4	None, single specimen, designed to model steel framed office building	Fully reversed, cyclic quasi-static loading. Applied with hydraulic actuator aligned at column web for each floor. Steel masses were attached at each level to simulate gravity load. ATC-24 was used.	Continuous columns through height of frame. Deep, stiff top beam. Full moment connections at all beam-column joints with continuous fillet welds of entire beam section to column flanges. Fish plates weld connected infill plate to beams and columns.	Global, out-of-plane buckling of the first story column.
Driver, Grondin, and Behbahanifard	2001	University of Alberta, Canada	1 1/2 scale, single-bay, 3-story	3	Single specimen. Top 3 panels used from previous experiment since there was little damage done.	Fully reversed cyclic loading based on ATC-24. Where yield displacement was estimated with finite element analysis. Equal loads applied at each level. Gravity loads applied for reasonable unfactored value in typical building by distributing beam placed at top of wall.	Beam-to-column moment connections with complete penetration groove welds on flanges and fillet welds on web. Columns welded to base plate. Infill connected using fish plates with strap plates at corners all fillet welded.	Rupture in beam flange to column flange connection in cycle 21 triggered large crack in middle panel. Repaired and test continued. Severe local buckling in column flange at base and level 1. Tears in bottom panel at bottom corner.

Table 2.1 continued: Summary of Physical Tests

Author	Year	Institute/ Country	Specimens	Stories	Parameters	Loading	Boundary Conditions	Failure Mode
Astaneh-Asl	2001	University of California, Berkley	2 1/2 scale, single-bay	varies	Story height. One specimen 2; one 3. Plate thickness.	Reversed cyclic loading with gradually increasing overall drift; Reference SAC protocol. Actuator applied load at deep top beam	Deep top beam. Boundary CFT column, WF beams, interior WF column. Roller at coupling beam due to symmetry. Boundary elements A572 Grade steel. Flux cored arc welds used to connect boundary elements to each other and steel infill plate. Bolted splice at mid-story height. Moment connects from CFT to WF beams.	Failure initiated in both specimens by a fracture in the top coupling beam along the column face. Resulted in total separation of coupling beam from specimen.
Berman and Bruneau	2003	University of Buffalo	3 large scale, single-story, single bay. Aspect ratio of 2:1 (L:h)	1	Three SPSW, 2 flat infill plates with different boundary conditions and 1 corrugated specimen.	Quasi-Static cyclic in accordance with ATC-24. Loading in increments of yield displacement estimated from numerical simulation using pushover analysis. Load applied with actuator at top of the specimen. Cycles completed varied fro 7 - 31.	Boundary frame designed to remain elastic with a safety factor of 2.5. Specimen 1 with flat infill, epoxy was used. Specimen 2 with flat infill was welded. Both were connected to intermediate WT then bolted to frame. Corrugated specimen was connected using epoxy to intermediate L. Sections connected with pop rivets.	Specimen 1 failed prematurely due to poor epoxy coverage. Specimen 2 failed due to fractures in the welds connecting infill to intermediate WT's at corners. Corrugated specimen failed due to infill plate fractures at areas of repeated local buckling.
Park and Kwack	2007	South Korea	5 1/3 Scale, 3-story, single bay	3	Plate thickness, Column strength	Reversed cyclic loading in increments of yield displacement calculated with finite element program	Built up members used for columns and beams. Lateral support preventing out of plane deformations. Stiff top beam at location of loading. Fish plates used to weld connect steel plates to frame members.	WC - Local buckling of columns. SC - Fracture of welded connections at column base, fracture at beam-column connection.

PART 3: ANALYSIS OF STEEL PLATE SHEAR WALL SPECIMENS

3.1 Abstract

Steel plate shear walls were the subject of two large scale tests conducted at the University of California at Berkley by Zhao and Astaneh-Asl in 2002. The following is an analysis of the data collected from two, ½ scale specimens subjected to quasi-static loading. Data was gathered from transducers, strain gages, and load cells. Analysis includes behavior of the overall system, components, and connections. Characteristics discussed include energy dissipation, axial forces and bending moments of WF columns, moment curvature of moment connections, and shear distribution inside the system. A comparison of test results with the AISC seismic provisions for special steel plate walls is also discussed.

3.2 Background

Specimens were designed to represent an innovative steel plate shear wall system developed by Magnusson Klemencic Associates. The design implements a “dual” system with both a steel shear wall and moment frame acting as lateral load resisting systems (Zhao and Astaneh-Ask, 2004). The system consists of steel infills spanning two bays, framed with concrete filled tubes (CFT), Wide Flange(WF) columns and WF beams as detailed in Figure 3.1 (All figures are included in the Appendix A). The high stiffness in the CFT columns allows them to carry the majority of the gravity load. The remaining members are responsible for resisting the internal forces created when lateral loads are applied.

Due to the symmetry of this design, test specimens were representative of half of the steel plate shear wall system. Rollers were placed at the centerline to simulate appropriate boundary conditions. A two-story and a three-story specimen were designed using different aspect ratios. All beams and columns were W 18 x 86 sections using A572 Grade 50 steel. Infill panels used A36 steel with thicknesses shown in Table 3.1 (All Tables found in Appendix). CFT columns were constructed using a 24-inch A572 Grade 50 steel tube 5/16 inch thick. Concrete with a minimum specified f'_c of 3 ksi filled the tube along with 1 ½ inch DYWIDAG W/FPU prestressed bars to simulate the gravity loads that would be applied by a structure. Shear studs were also welded into the steel tube prior to the concrete placement to ensure composite behavior (Zhao and Astaneh-Asl, 2004). Dimensions for specimens are detailed in Figure 3.2 and Figure 3.3.

Columns were connected to continuous beams using full penetration welds for WF sections. Infill panels were also welded to WF beam and column sections. Bolted splices were used to connect infill panels and column sections at mid-height of each story. Full moment resisting connections were used between the WF beams and CFT columns. Eight ¾ inch re-bars were embedded into the concrete and then fillet welded to the beam flanges. A reaction beam at the base and a loading beam at the top of the specimen ensured that the forces applied transferred directly to the steel plate shear wall system. Lateral bracing was applied to coupling beams and loading beam to prohibit out of plane deformations as shown in Figure 3.4 (Zhao and Astaneh-Asl, 2004).

Loading history for the test specimens was determined by the SAC Joint Venture developed after the 1994 Northridge earthquake. Displacement controlled, quasi-static, fully-reversed cyclic loading was applied to both test specimens with displacements described in Figure 3.5. The overall drift of the specimens is defined as the actuator displacement divided by the total specimen height. These loads were applied using a 1500 kip actuator placed at the center line of the loading beam. Load cells were also placed at the ends of coupling beams for reaction readings. Instrumentation for these specimens includes linear strain gages, strain gage rosettes, and transducers capable of reading a range of local and global displacements. Figure 3.6 through Figure 3.8 show the locations for instrumentation on specimen one and Figure 3.9 through Figure 3.11 show locations for specimen two (Zhao, 2004).

3.3 ENERGY DISSIPATION

Energy dissipation is a major concern with seismic design and defined as the area under the hysteresis loop. The total energy dissipation was calculated by integrating the area under the hysteresis curve as follows. After finding the energy dissipated by the entire structure, energy dissipated by the stories was also calculated as shown in Figure 3.12 and Figure 3.13.

$$EnergyDissipated = \sum \Delta_{energy} = \sum_{i=1}^{Enddata} \tfrac{1}{2}\left[P(i+1) + P(i)\right] * \left[\Delta(i+1) - \Delta(i)\right]$$

Δ_{energy} = Energy dissipated during single time step

P = Force applied at time step

Δ = Displacement at time step

The percentage of energy dissipated by the system and in each story is tabulated in Table 3.2 and Table 3.3 for specimens one and two respectively. In specimen one the majority of the energy dissipated is concentrated in the single story. In specimen two the two stories dissipated a comparable amount of the total energy, indicating that the energy dissipation is evenly distributed throughout the specimen. From the table, it is observed that the percent of energy dissipated by the infills increase as the lateral displacements increase.

3.4 Axial Loads and Bending Moments

A common material model used for steel structures is the elastic, perfectly-plastic model as shown in Figure 3.14. It is noted that this model is not accurate for cyclic loading due to plastic deformations after yielding; therefore, an elastic, perfectly plastic cyclic model was developed and is shown in Figure 3.15. The CFT and WF columns are A572 Gr. 50 with F_y = 50 ksi, and the infill plates are A36 with an assumed F_y = 45 ksi. Axial forces and bending moments were calculated from strain gage readings. An example of cases studied are shown in Figure 3.16. Strain gage locations for each specimen in which the axial force and bending moment was computed are shown in Figure 3.17 and Figure 3.18.

Axial forces in beams and columns on different sections under different overall drift values are plotted versus time in Figure 3.19 through Figure 3.26 for specimen one and Figure 3.27 through Figure 3.33 for specimen two. Bending moments are plotted versus time for coupling beams and columns in Figure 3.34 through Figure 3.41 for specimen one, and in Figure 3.42 through Figure 3.48 for specimen two. Distribution of the axial forces and moments were also investigated as shown in Figure 3.24 through Figure 3.26 for axial distribution for the WF column in specimen one and Figure 3.31 through Figure 3.33 for specimen two. Moment distribution along WF column is shown in Figure 3.39 through Figure 3.41 for specimen one and in Figure 3.46 through Figure 3.48 for specimen two.

As would be expected, axial forces and bending moments in WF column gradually increase as the loading progresses in both specimens. The coupling beams have shown low axial forces in the elastic region, with a more sudden increase after reaching the inelastic region. Bending moments in the coupling beams increase at a lower loading cycle than the column sections. During the elastic range of both test specimens, analysis shows that the columns are subjected to combined axial and low bending. The coupling beams are subjected to low axial forces and high bending moments during the early stages of loading. After yield occurs, first story columns in both specimens show an increased bending moment. First story column of specimen one yielded due to bending at the conclusion of testing. Second story coupling beam in specimen one yields due to bending, while the first story coupling beam shows decreased moment and increased axial force in the inelastic range. The column in specimen two yields due to both bending and axial forces at the second story cross-section. Specimen two coupling beam reaches high bending moments in the early loading levels, but then reaches axial capacity and has little bending moment by the conclusion of testing.

Profiles plotted for each specimen along the height of the WF column were analyzed at a low loading with an overall drift of 0.004, yield loading with an verall drift of 0.006, and high loading with an overall drift of 0.02. Column profiles show an axial force increase as the distance to the column base decreases for both specimens. The distribution of axial forces also remains constant as the lateral load increases. Moment distribution of the WF column for specimen one behaves as expected for a frame with a moderately uniform distribution throughout loading. Specimen two moments were calculated at the base of each story. For the low and yield cycles plotted, high moments are present at the base compared along the height of the column. The low bending moment at the high loading level is due to the formation of a plastic hinge at the column base.

3.5 ANGLE OF INCLINATION IN INFILL PANELS

Strain gage rosette readings were collected throughout each test for the infill panels. From these readings principal strains, principal stresses, and the angles of principal stresses can be found with the following equations.

$$\varepsilon_1 = \frac{\varepsilon_T + \varepsilon_L}{2} + \frac{1}{\sqrt{2}}\sqrt{(\varepsilon_T - \varepsilon_D)^2 + (\varepsilon_D - \varepsilon_L)^2}$$

$$\varepsilon_2 = \frac{\varepsilon_T + \varepsilon_L}{2} - \frac{1}{\sqrt{2}}\sqrt{(\varepsilon_T - \varepsilon_D)^2 + (\varepsilon_D - \varepsilon_L)^2}$$

$$\sigma_1 = \frac{E}{(1-\nu^2)}(\varepsilon_1 + \nu\varepsilon_2)$$

$$\sigma_2 = \frac{E}{(1-\nu^2)}(\varepsilon_2 + \nu\varepsilon_1)$$

$$\theta = \tfrac{1}{2}\tan^{-1}\left(\frac{\varepsilon_T - 2\varepsilon_D + \varepsilon_L}{\varepsilon_T - \varepsilon_L}\right)$$

ε_1 = Major principal strain

ε_2 = Minor principal strain

ε_T = Strain reading in transverse direction

ε_L = Strain reading in lateral direction

ε_D = Strain reading in diagonal direction

σ_1 = Major principal stress

σ_2 = Minor principal stress

E = Young's Modulus

v = Poisson's ratio

θ = Angle at which major principal stress acts

Locations for strain gage readings are shown in Figure 3.49 and Figure 3.53. Analysis for these values was conducted for a peak load value in the elastic range, yield range, formation of tension field range and inelastic range of testing. Values for major and minor principal stresses along with the angle of inclination are tabulated in Table 3.4 and Table 3.5 for specimens one and two respectively. These stresses are then represented by arrows with a magnitude representing the stress value and positioned at the appropriate angle of inclination in their corresponding locations on the steel plate shear wall specimens as shown in Figure 3.50 through Figure 3.52 for specimen one and Figure 3.54 through Figure 3.56 for specimen two.

The angle of principal stresses is representative of the formation of tension field action. By analyzing these angles, it is determined how buckling in the panels occur. Angles in the panels average between 33° and 38° with a maximum of 45°. Lower angles are present along the base of the first story infill panels and high compressive stresses are found at the corners of the panels. High compressive forces at corners would be expected due to the opening and closing of boundary elements present when a shear force is applied to a frame. Once the specimens reach the inelastic range of loading, there is not a predictable pattern for the angle of principal stresses.

Angle of inclination can be compared between specimens, since the infills vary in size. Specimen one infill has an aspect ratio (W:H) of 1.3 and specimen two infills have an aspect ratio of 0.85. The average angle of principal stresses for specimen one is 35.2° at the significant yield point. If the interior readings are only considered the average angle is then 40.0°. The infills for specimen two have an average angle of inclination of 33.7° at the significant yield point. Interior readings have an average angle of 37.3° for specimen two.

3.6 Moment versus Curvature

Moment versus curvature has been studied at the moment connections for WF sections. Strain gage data and transducer readings along with information from the load cells are used to determine the moment and curvature at location near the moment connections. Moment versus curvature plots from strain gage data are included in Figure 3.58 to Figure 3.60 for specimen one and Figure 3.63 for specimen two. Strain gage locations are shown in Figure 3.17 and Figure

3.18. The first story coupling beam in specimen one remained elastic according to testing notes as shown in Figure 3.57. Analysis of this connection shows a higher stiffness is present during the pushing of the actuator, while a lower stiffness is shown for pulling. This behavior is also shown in the elastic region of the second story coupling beams in both specimens. This difference could be caused by the fact that the specimens do not truly act as a symmetrical system. The roller supports designed to simulate the symmetry are causing an increase in stiffness when the actuator applies a pushing force. Coupling beam for specimen one at the second story shows robust hysteresis loops after sudden yielding. Specimen two coupling beam at the second story shows elastic behavior until web and flange buckling occur, which causes permanent deformations and a shift in the moment versus curvature plot.

Moment versus curvature was also plotted for transducer readings as shown in Figure 3.61 and Figure 3.62 for specimen one and Figure 3.64 through Figure 3.66 for specimen two. First story plots for both specimens show the effects of local buckling in the flange of the column. Transducers were connected to the outside flange of the WF column. After local buckling of the column, permanent deformations are present. This accounts for the drift in the moment versus curvature plots. Both first story readings are only plotted for data collected on day one and day three due to an instrumentation malfunction in day two. Transducer readings for middle and top levels of specimen two show a large amount of energy dissipation with robust hysteresis loops after yielding for both specimens.

3.7 COMPARISON OF TEST RESULTS AND CODE CALCULATIONS

3.7.1 TEST RESULTS

Shear forces have been determined at a cross-section for each specimen through strain gage readings. Each cross section studied is identified in Figure 3.67 and Figure 3.68 for specimen one and two respectively. Using Mohr's circle, the shear strains at each location were determined in order to calculate shear force in columns as shown below.

$$\gamma_{xy} = \frac{1}{2}\sqrt{(\varepsilon_1 - \varepsilon_2)^2 - (\varepsilon_x - \varepsilon_y)^2}$$

$$\tau_{xy} = \gamma_{xy} G = \gamma_{xy} \frac{E}{2(1+\nu)}$$

γ_{xy} = Shear strain

ε_x = Strain in x direction

ε_y = Strain in y direction

τ_{xy} = Shear stress

G = Shear Modulus

Assuming composite behavior in the CFT, the shear strain reading recorded on the outside of the steel tube was also taken as the shear strain in the concrete. Calculations for shear forces in the CFT are shown in Appendix B. Distribution of shear across both the circular CFT section and the WF was assumed to be uniform. Shear strain values in the CFT and WF were also assumed to be uniform across the height of the columns. For each panel, shear forces were calculated as the integration of shear stresses across the panel width. Shear distributions for specimen two cross-sections are shown in **Error! Reference source not found.** and **Error! Reference source not found.**. Shear forces taken by the CFT, infill, and WF column are tabulated in Table 3.3 and Table 3.4 for specimens one and two respectively.

The distribution of shear forces was analyzed to determine the contribution of each element throughout loading. Distributions of shear forces for each cross-section are shown in Figure 3.81 through Figure 3.84 for specimen one and Figure 3.87 through Figure 3.90 for specimen two. A comparison of the infill panels is shown in Figure 3.85 and Figure 3.86 for specimen one and Figure 3.91 and Figure 3.92 for specimen two. CFT behavior is compared in Figure 3.93 and Figure 3.94 for specimens one and two respectively. All shear distributions were determined for actuator movement to the right and to the left in order to examine if the specimens behaved symmetrically. These figures show that the infill panels in both specimens have a major contribution to the specimen shear strength while the specimen remains elastic. As loading progresses into the inelastic loading region, shear forces in the panels decrease. The CFT column remains elastic throughout testing, so the shear forces are redistributed to the CFT column after infill panel yields. When the actuator moves to the left the CFT carries less shear load in both specimens. Shear contribution of the WF column is small in comparison to other components and levels out early in the loading cycles.

From the table, it’s shown that summation of the shear forces from the CFT, infill, and WF column vary within 20% of the total base shear readings from the actuator. Errors in calculations could be due to the determination of shear forces in CFT or infill. True behavior of the CFT is not fully understood, so several assumptions stated earlier were used for calculations. If the shear distribution is not truly uniform or the shear strains in the concrete are not truly equal to the steel, errors would occur in the calculations. Also, in determining the shear forces of the infill, a linear distribution between readings was assumed, which is not the true behavior of the plate and will cause inaccuracy in the infill shear forces calculated.

Shear forces in the infill panels show several trends through loading. During the elastic stage of loading, the shear forces of the infill range from 50% to 70% of the total base shear. As tension field action forms and the plates begin to buckle, strain gage readings are not as reliable due to additional localized deformation, but it is clear that the plates continue to resist shear forces. The effect of buckling on the strain gages explains the peaks and irregular behavior of the infills after yielding. Aside from the unpredictable pattern of the infills in the inelastic region, it is also clear that the panels are exceptionally ductile. After yielding the shear capacity of the infills maintain a reasonable level of resistance until the shear strength gradually diminishes.

3.7.2 AISC Code

The American Institute of Steel Construction has recently included provisions for Special Steel Plate Walls (AISC, 2007). Calculations for plate girder analogy and special steel plate wall were completed according to the following equations and sample calculations are included in Appendix B.

<u>Plate Girder:</u>

$$V_n = 0.6F_yA_w\left(C_v + \frac{1-C_v}{1.15\sqrt{1+\left(a/h\right)^2}}\right)$$

$$C_v = \frac{1.51Ek_v}{\left(h/t_w\right)^2 F_y}$$

$$k_v = 5 + \frac{5}{\left(a/h\right)^2}$$

V_n = Nominal shear strength for plate girder

F_y = Yield stress

A_w = Area of web

a = Clear distance between transverse stiffners

h = Clear distance between flanges

t_w = Thickness of web

<u>Special Steel Plate Wall:</u>

$$V_n = 0.42F_yt_wL_{cf}\sin 2\alpha$$

$$\tan^4\alpha = \frac{1+\dfrac{t_wL}{2A_c}}{1+t_wh\left(\dfrac{1}{A_b}+\dfrac{h^3}{360I_cL}\right)}$$

V_n = Nominal shear strength for strip model

F_y = Yield stress of infill

t_w = Thickness of web plate

L_{cf} = Clear distance between HBE flanges

α = Angle of inclination for tension field

L = Distance between VBE centerlines

A_c = Cross-sectional area of VBE

h = Distance between HBE centerlines

A_b = Cross-sectional area of HBE

I_c = Moment of inertia of VBE taken perpendicular to the direction of the web-plate line

Analyzed as a plate girder, specimen one nominal shear capacity is 282.3 kips and specimen two capacity is 589.9 kips. These values are extremely conservative when compared to the experimental shear capacities of 917 kips and 1225 kips for specimens one and two respectively. This comparison verifies that steel plate shear walls cannot be designed as plate girders since the additional strength and stiffness of the boundary elements are not accounted for.

Shear capacity for the infill panels were calculated with reasonable accuracy using the special steel plate wall equations when compared to the experimental values determined for the panels. AISC code is designed for symmetrical systems, so two calculations were completed for each specimen. One shear value was calculated as if the specimen consisted of two CFT columns and another as if the specimen consisted of two WF columns. AISC code results in a shear value of 425.4 kip or 426.8 kip for specimen one and 639.3 kip or 648.4 kip for specimen two. Specimen one resulted in a maximum shear force in the infill at yield of 447.6 kip and a value of 630.0 kip for specimen two. Both shear forces are close to the calculated values; however the value at yield would not be the highest value for shear. Additional values for the maximum shear forces in the infill panels were computed by subtracting the shear values of the CFT column and WF column from the base shear. This approach resulted in a shear value of 356 kip and 540 kip for specimens one and two respectively. Both values are considerably lower than the calculated value possibly due to a higher calculated shear value in the CFT than the true shear force. Values calculated for the infills are compared to the AISC predictions in Table 3.10.

3.8 CONCLUSION

Data collected from two 1/2 scale test specimens was analyzed. Factors considered are energy dissipation of the system, axial forces and bending moments in frame elements, angle of inclination for the infill panels, moment versus curvature behavior for moment connections, and shear distribution across system components. Results are as follows:

- Steel panels contributed a large percentage to the total energy dissipated in both specimens. Specimen two infill panels dissipate comparable amounts of energy indicating that energy dissipation is evenly distributed between the two stories.
- First story columns are subjected to high axial forces and low bending moments in the elastic region, but after yielding bending moment will significantly increase at the column base. Coupling beams are subjected to high bending moment, but once reaching the inelastic region axial forces suddenly increase.

- Principal stresses act at the angle of inclination which was determined to range from 33º to 40º. As the infill plate's ratio of height to width decreases the angle of inclination of tension field action will also decrease.
- Principal stresses are fairly uniform throughout the interior of the panels, but high compression stresses are present at the corners due to opening and closing of the connections during loading.
- Moment connections used in the specimen had stable hysteretic behavior showing that there was no sudden loss of moment carrying capacity.
- Shear distribution of both specimens proves that the infill panels are responsible for resisting the majority of the shear forces in the elastic region and maintain strength into inelastic loading by allowing tension field action to form and the plate to buckle. After reaching the ultimate capacity of the infill, the secondary system consisting of the frame and CFT successfully maintains the systems shear capacity.
- Equations supplied under the AISC provisions for special steel plate walls can conservatively and with reasonable accuracy predict the shear capacity of a steel plate shear wall system.

APPENDICES

APPENDIX A: FIGURES AND TABLES

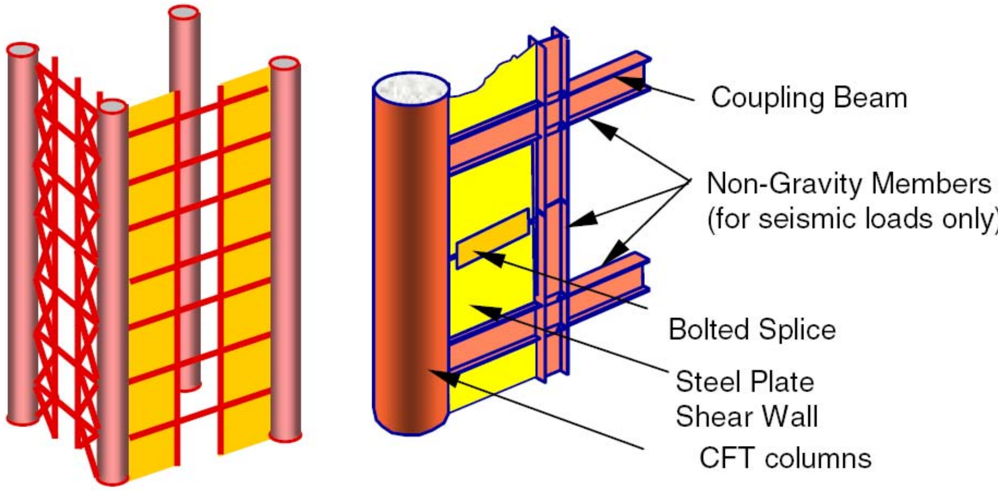

Figure 3.1: Components of Lateral Load Resisting System Studied (Zhao and Astaneh-Asl, 2004)

Table 3.1: Section Properties for Test Specimens (Zhao and Astaneh-Asl, 2004)

Specimen No. and Designation	Steel Wall Plate Thickness	CFT Column		Beam Section*	Column Section*
		Thickness	Diameter		
1 Two-Story	6mm(1/4 inch)	8mm (5/16 inch)	610 mm (24 inch)	W 18x86	W 18x86
2 Three-Story	10 mm (3/8 inch)	8mm (5/16 inch)	610 mm (24 inch)	W 18x86	W 18x86

* Properties of Cross Sections refer to the AISC Manual.

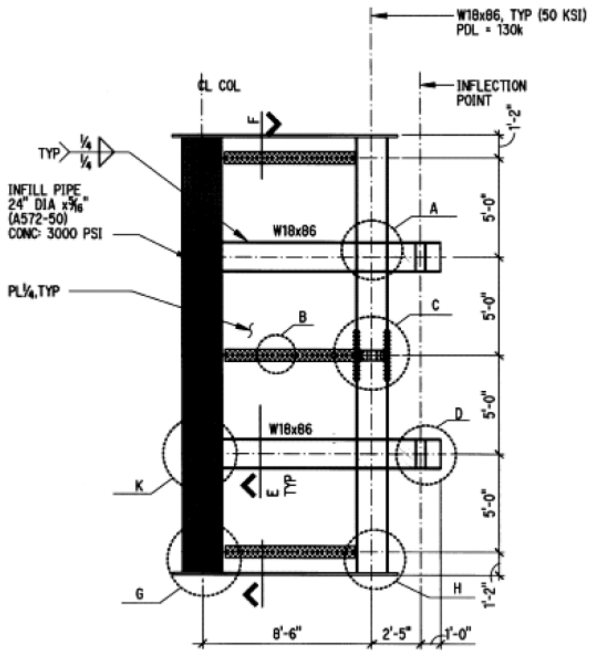

Figure 3.2: Structural Details for Specimen One (Zhao, 2004)

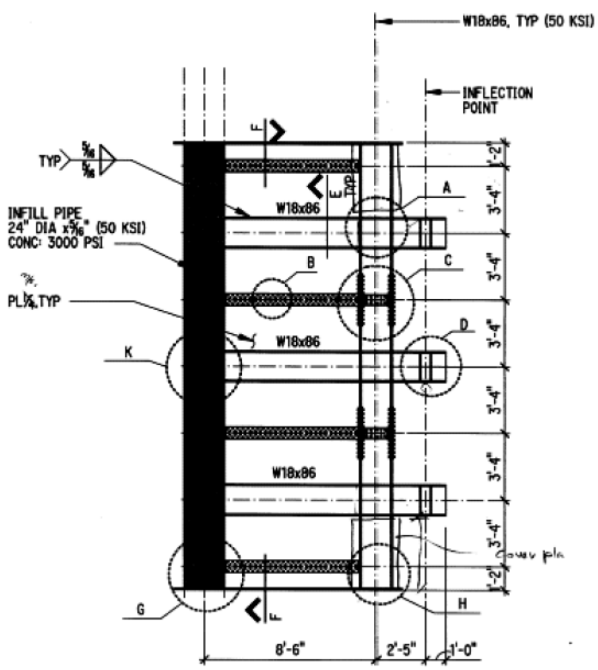

Figure 3.3: Structural Details for Specimen Two (Zhao, 2004)

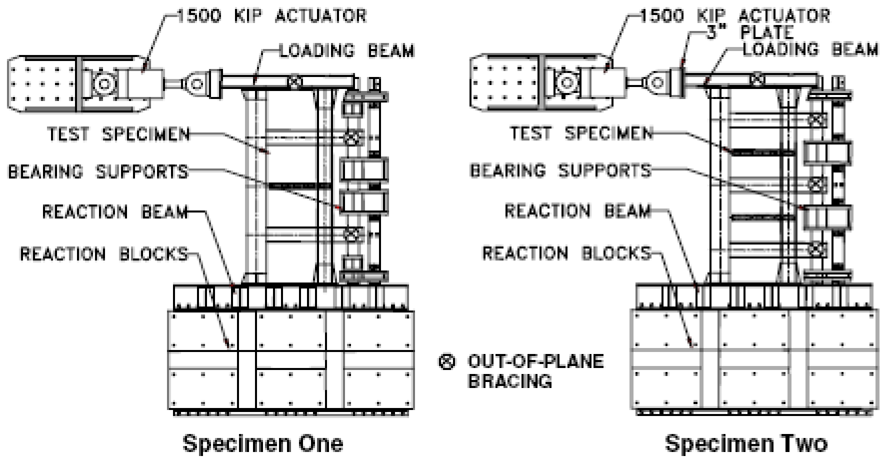

Figure 3.4: Testing Set-Up (Zhao and Astaneh-Asl, 2004)

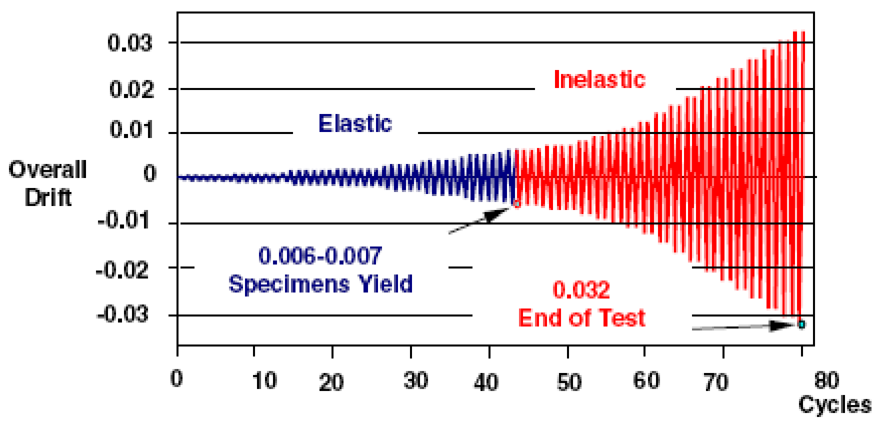

Figure 3.5: Loading History Applied to Both Specimens (Zhao and Astaneh-Asl, 2004)

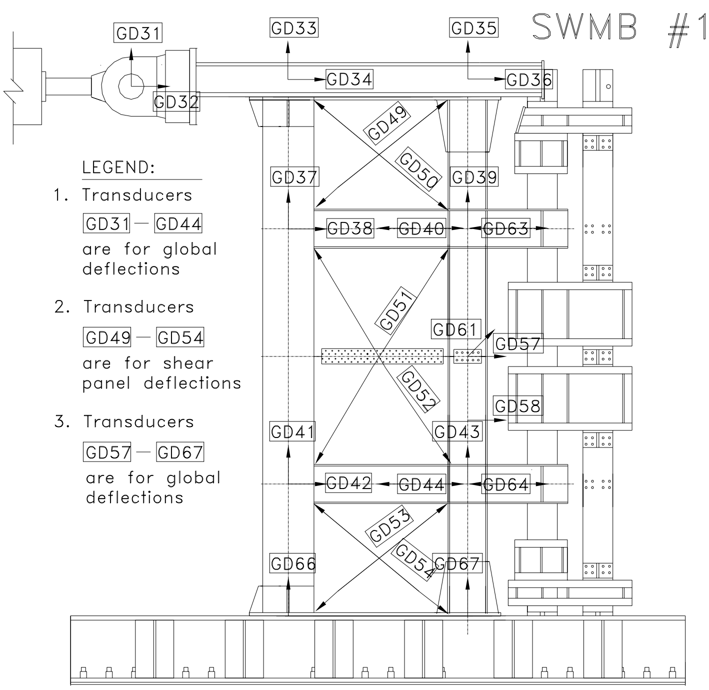

Figure 3.6: Global Displacement Transducers on Specimen One (Zhao, 2004)

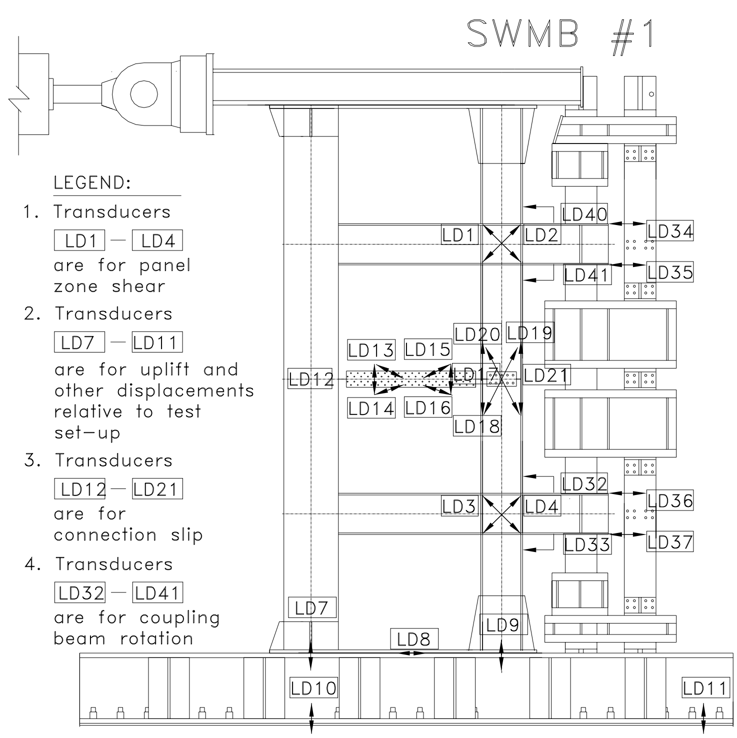

Figure 3.7: Local Displacement Transducers on Specimen One (Zhao, 2004)

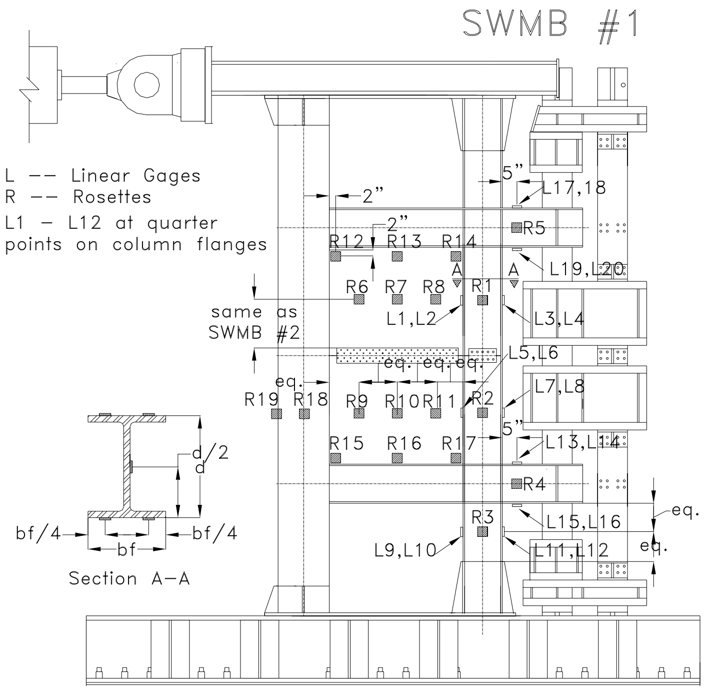

Figure 3.8: Strain Gage Locations on Specimen One (Zhao, 2004)

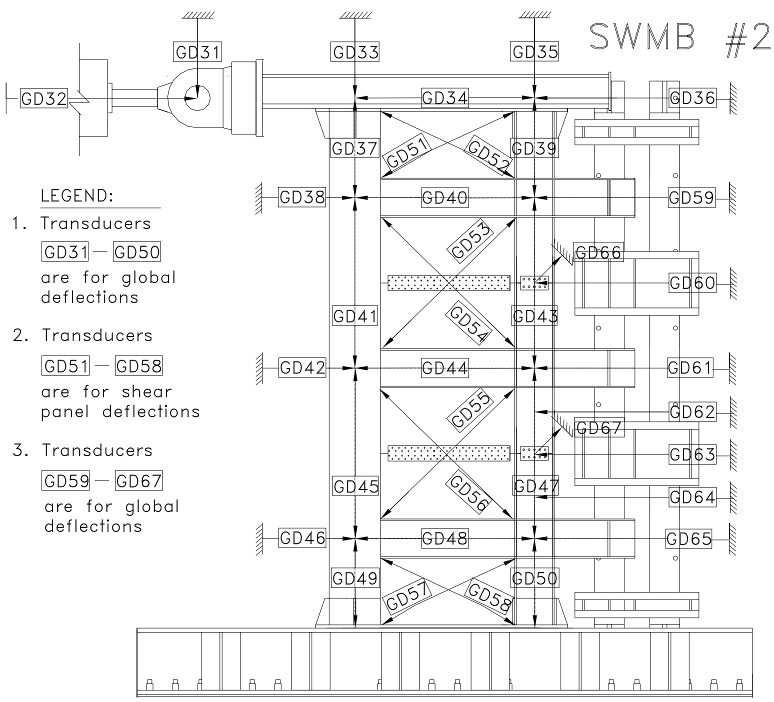

Figure 3.9: Global Displacement Transducers on Specimen Two (Zhao, 2004)

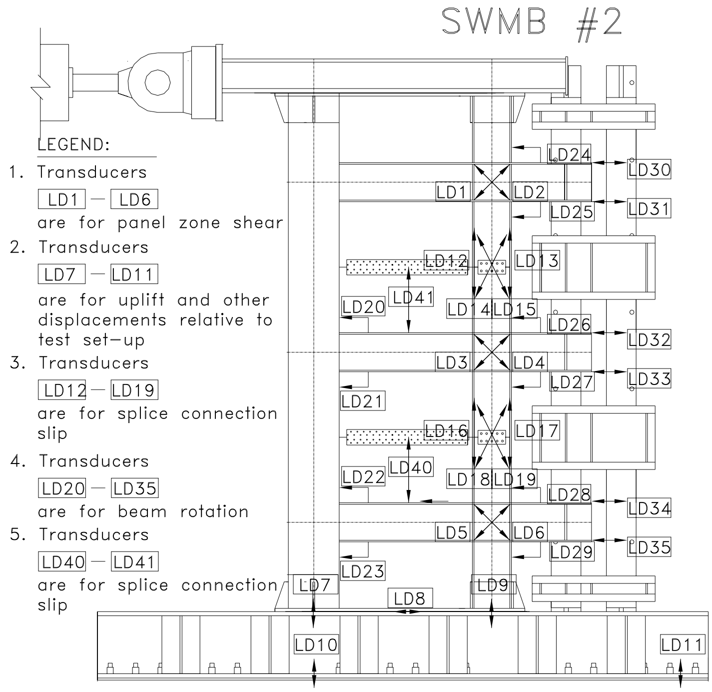

Figure 3.10: Local Displacement Transducers on Specimen Two (Zhao, 2004)

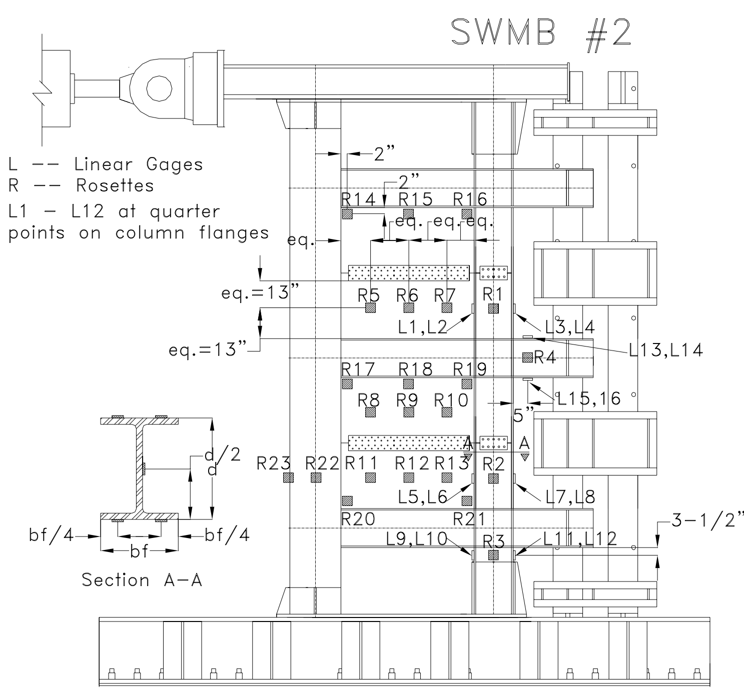

Figure 3.11: Strain Gage Locations on Specimen Two (Zhao, 2004)

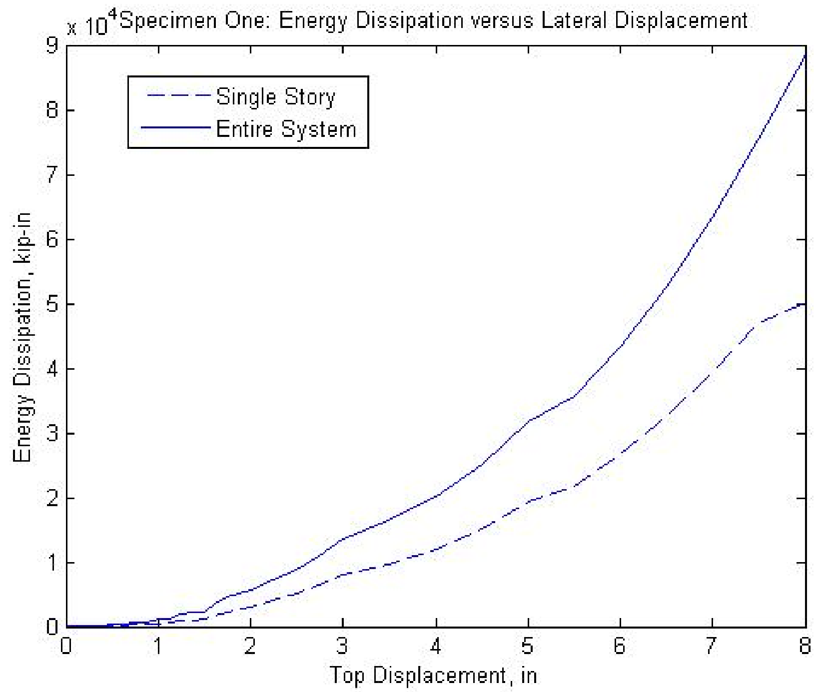

Figure 3.12: Energy Dissipation for Specimen One

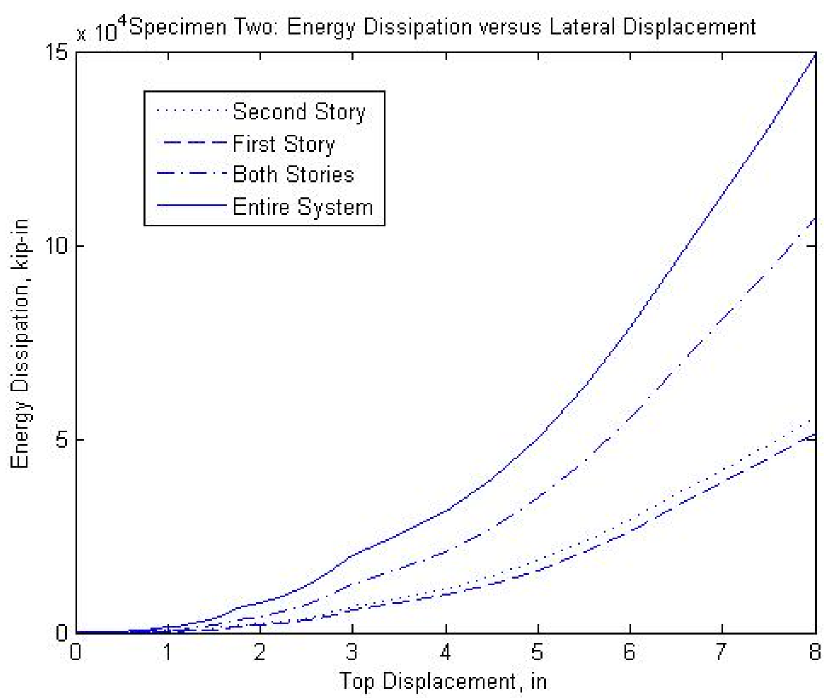

Figure 3.13: Energy Dissipation for Specimen Two

Table 3.2: Specimen One Energy Dissipation

Top Displacement, in	Energy Dissipated by Entire System	Energy Dissipated by Single Story	
		kip - in	Percent of Total
1	1080.42	489.24	45.28
2	5676.63	3037.53	53.51
3	13454.39	7901.10	58.73
4	20123.12	12018.98	59.73
5	31747.54	19311.53	60.83
6	43187.23	26611.34	61.62
7	63330.60	39311.59	62.07
8	88455.17	50024.40	56.55

Table 3.3: Specimen Two Energy Dissipation

Top Displacement, in	Energy Dissipated by Entire System	Energy Dissipated by First Story		Energy Dissipated by Second Story		Energy Dissipated by Both Stories	
		kip - in	Percent of Total	kip - in	Percent of Total	kip - in	Percent of Total
1	1501.22	283.47	18.88	462.04	30.78	745.51	49.66
2	7858.32	1858.77	23.65	2436.23	31.00	4295.00	54.66
3	19801.08	5823.83	29.41	6863.63	34.66	12687.45	64.07
4	31287.81	9674.08	30.92	11337.87	36.24	21011.95	67.16
5	50291.98	16210.27	32.23	18632.04	37.05	34842.31	69.28
6	78670.24	26294.88	33.42	29233.72	37.16	55528.60	70.58
7	113064.87	38652.96	34.19	42048.84	37.19	80701.80	71.38
8	149483.87	51639.04	34.54	55624.74	37.21	107263.78	71.76

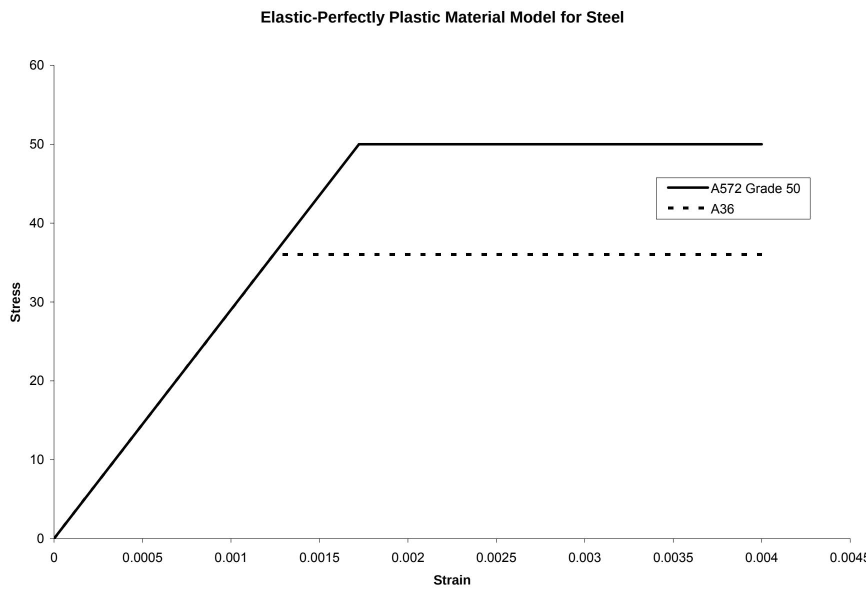

Figure 3.14: Elastic-Perfectly Plastic Material Model

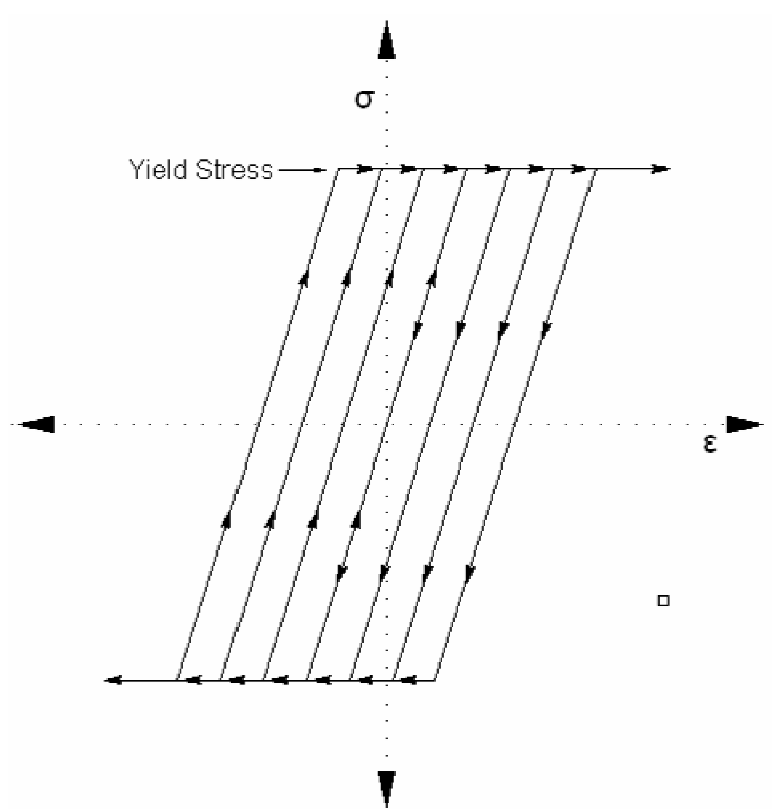

Figure 3.15: Cyclic Material Model Accounting for Permanent Deformations

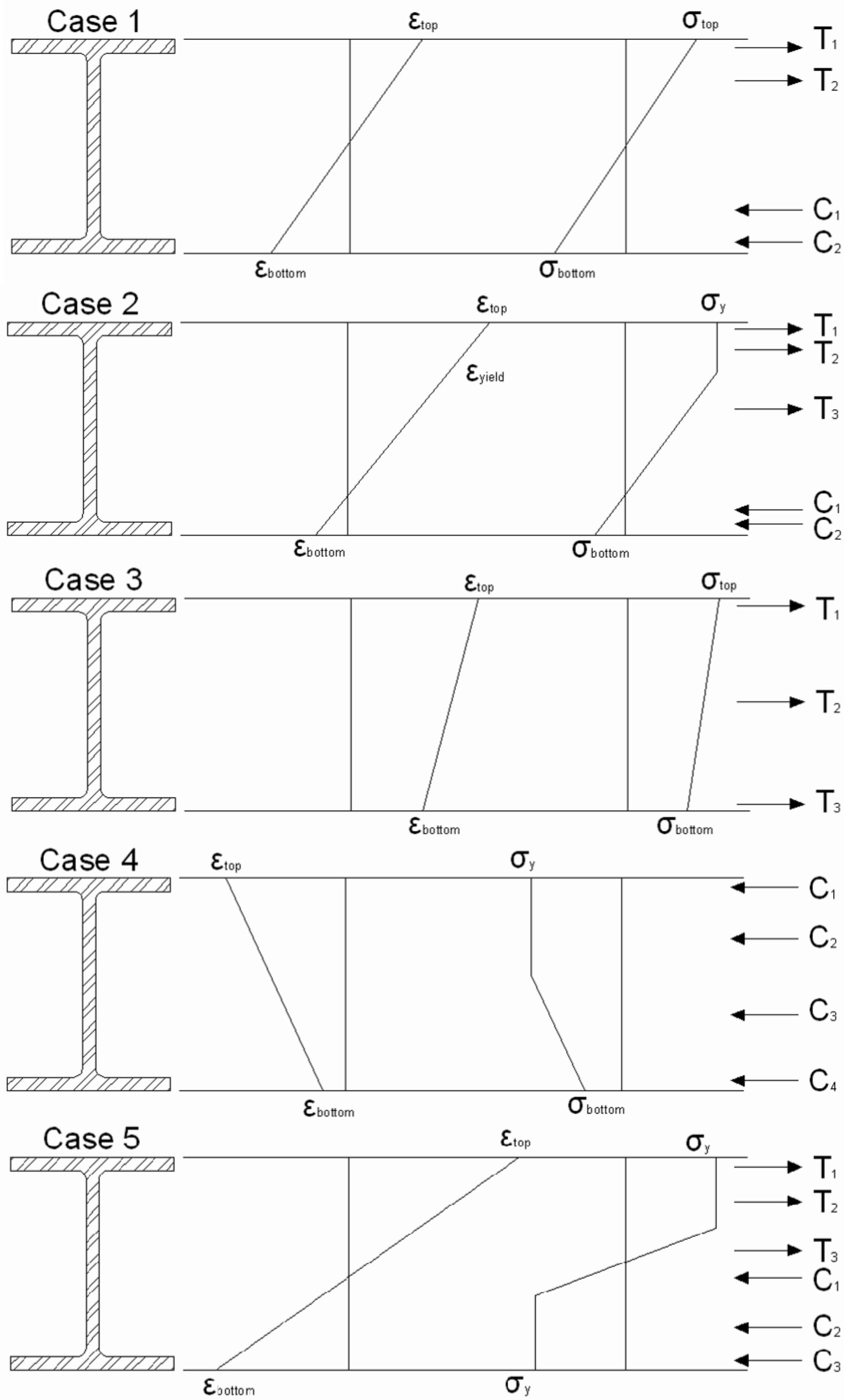

Figure 3.16: Sample Cases for Bending Moment and Axial Force Calculations

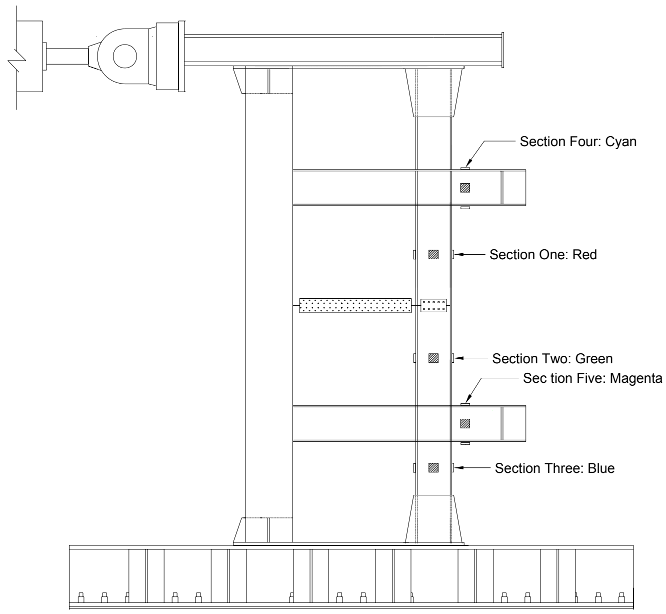

Figure 3.17: Specimen One Cross Sections Analyzed using Strain Gages

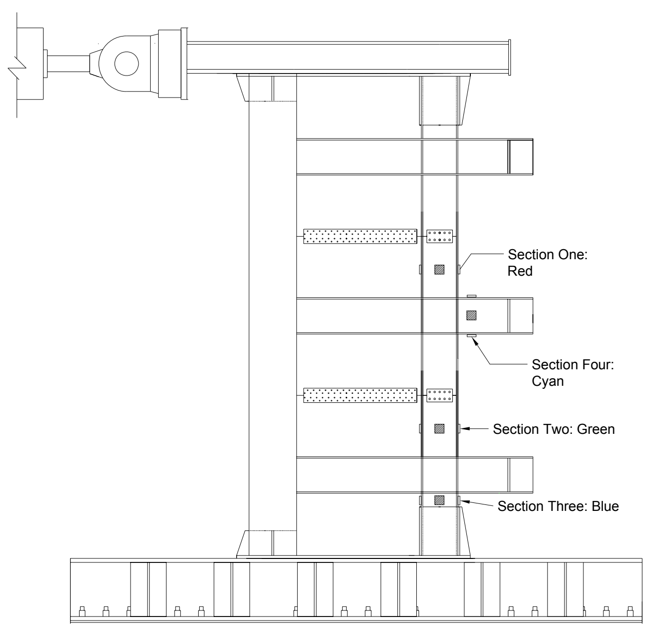

Figure 3.18: Specimen Two Cross Sections Analyzed using Strain Gages

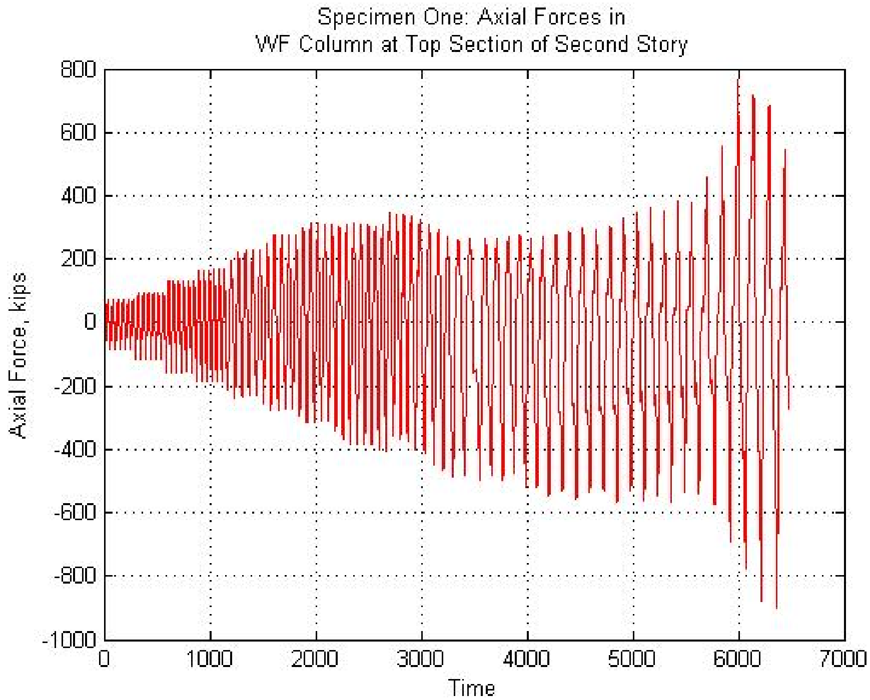

Figure 3.19: Specimen One Axial Forces in WF Column at Section One

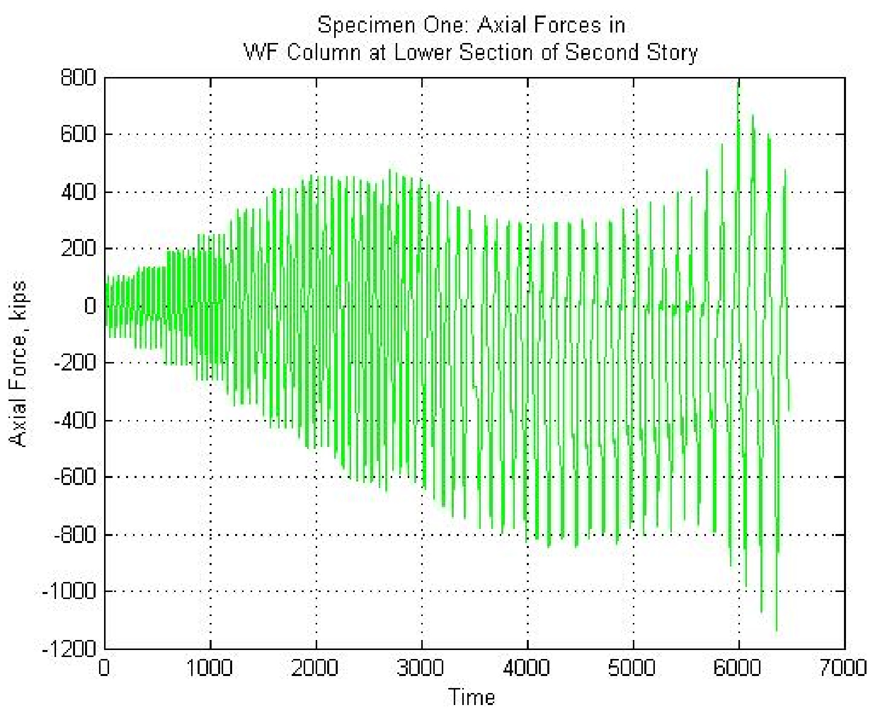

Figure 3.20: Specimen One Axial Forces in WF Column at Section Two

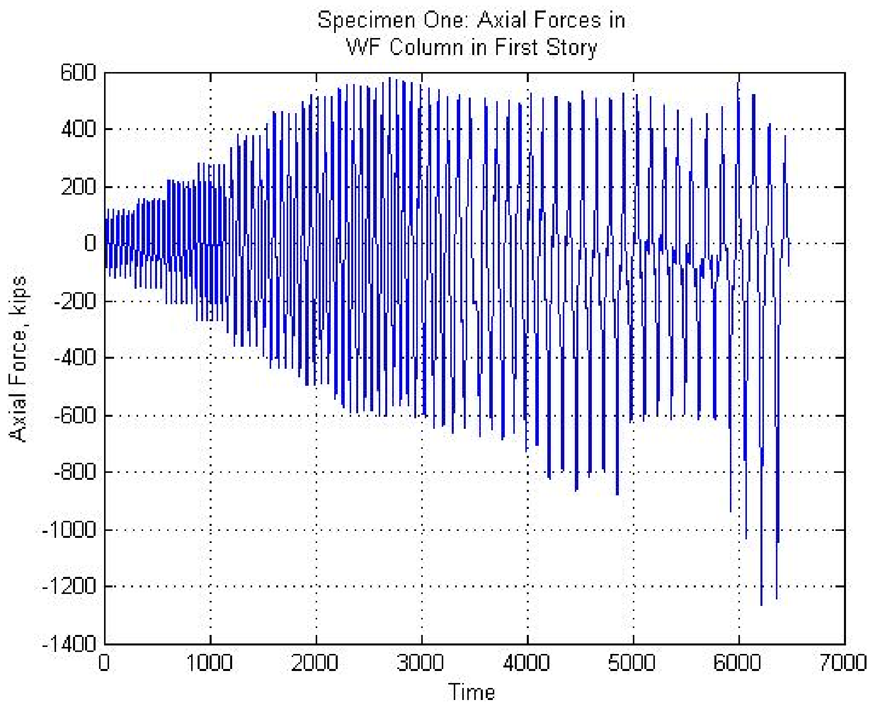

Figure 3.21: Specimen One Axial Forces in WF Column at Section Three

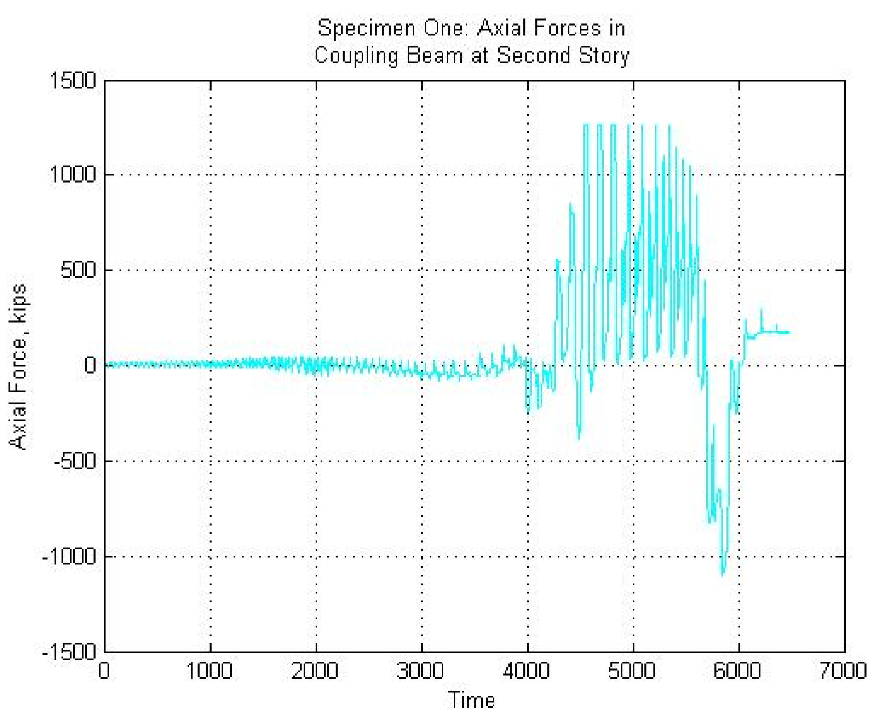

Figure 3.22: Specimen One Axial Forces in Coupling Beam at Section Four

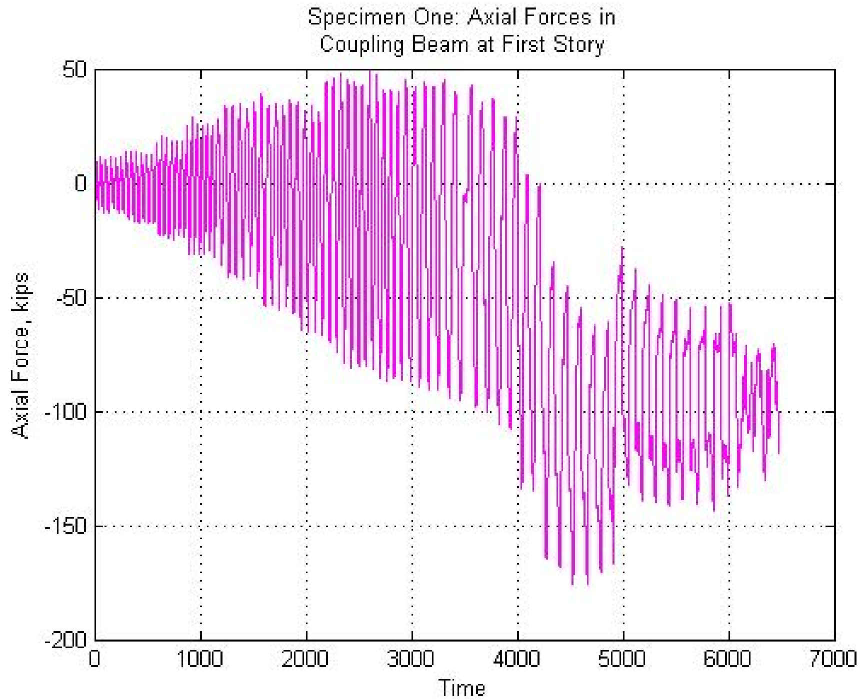

Figure 3.23: Specimen One Axial Forces in Coupling Beam at Section Five

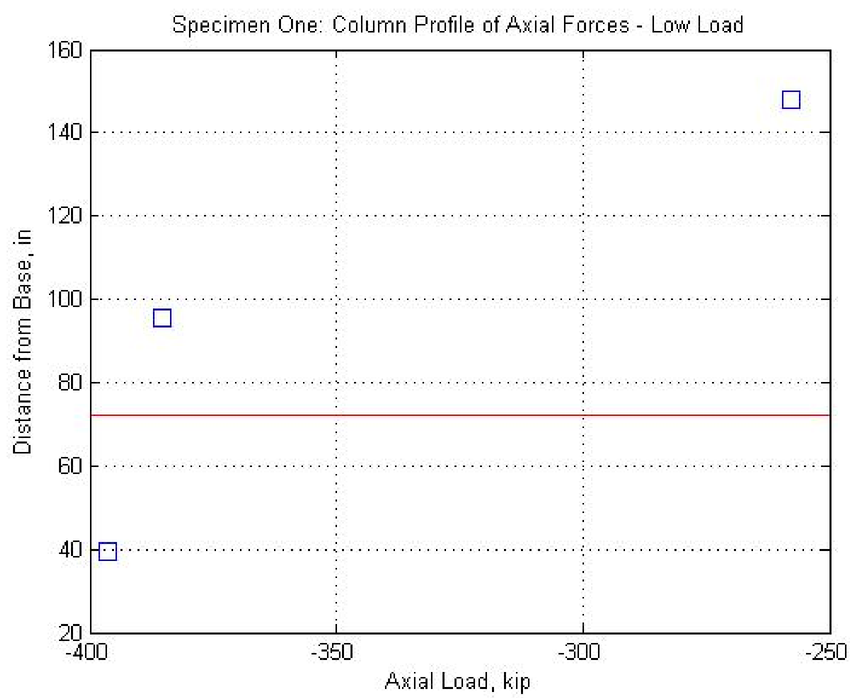

Figure 3.24: Specimen One Axial Distribution along WF Column (Drift = 0.004)

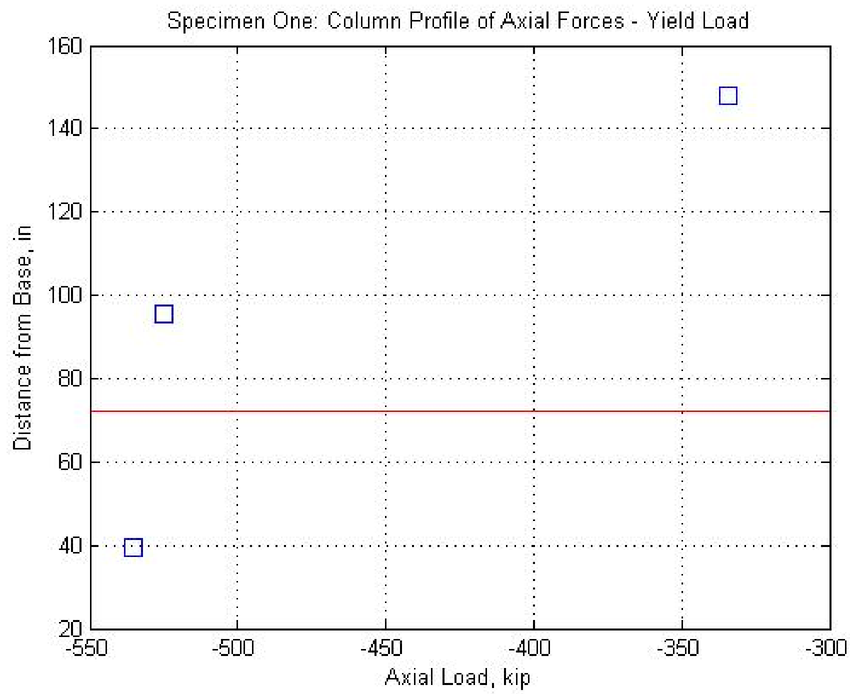

Figure 3.25: Specimen One Axial Distribution along WF Column (Drift = 0.006)

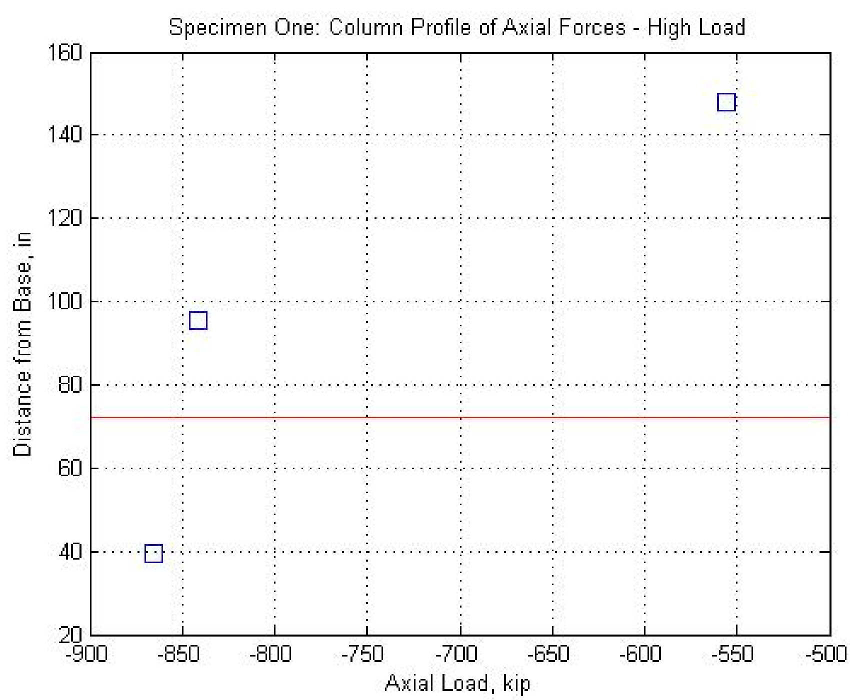

Figure 3.26: Specimen One Axial Distribution along WF Column (Drift = 0.02)

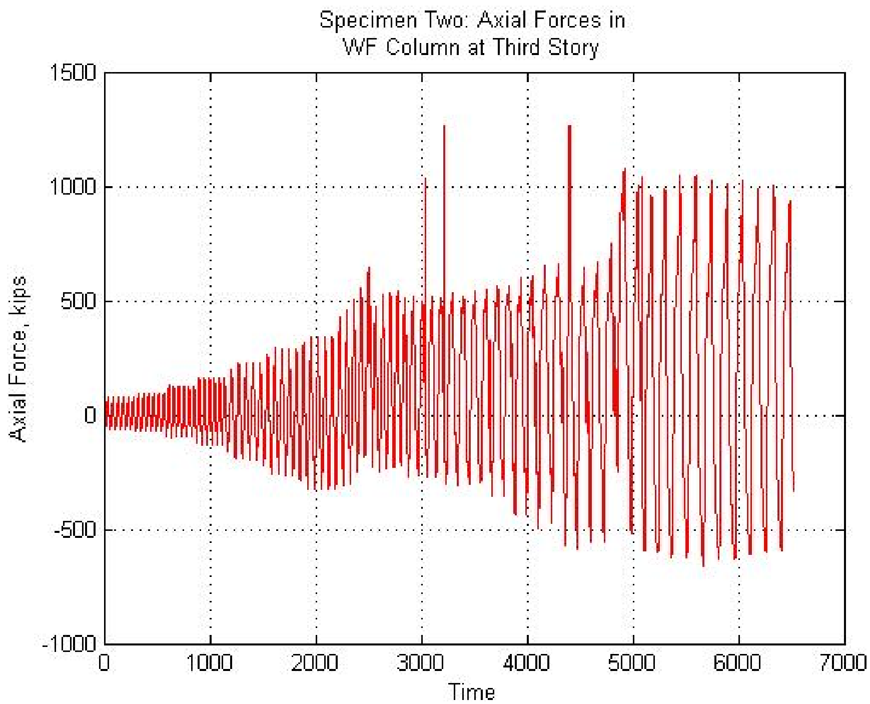

Figure 3.27: Specimen Two Axial Forces in WF Column at Section One

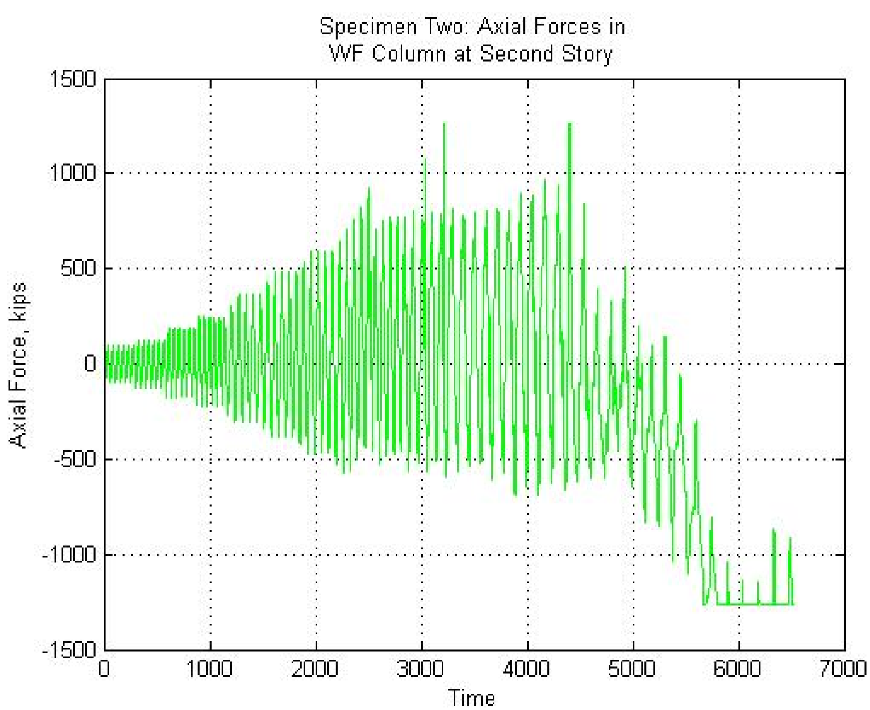

Figure 3.28: Specimen Two Axial Forces in WF Column at Section Two

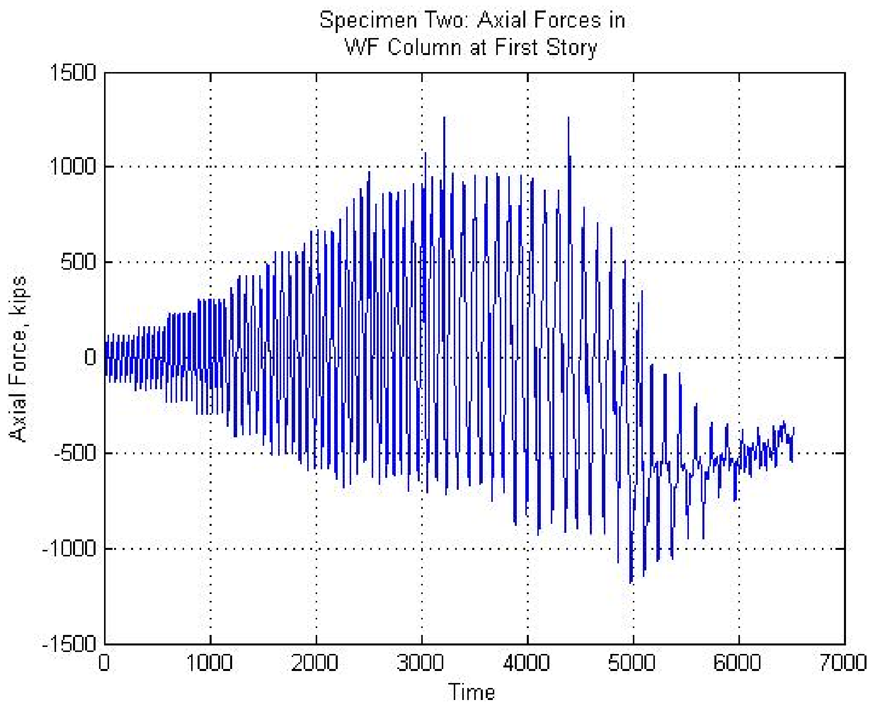

Figure 3.29: Specimen Two Axial Forces in WF Column at Section Three

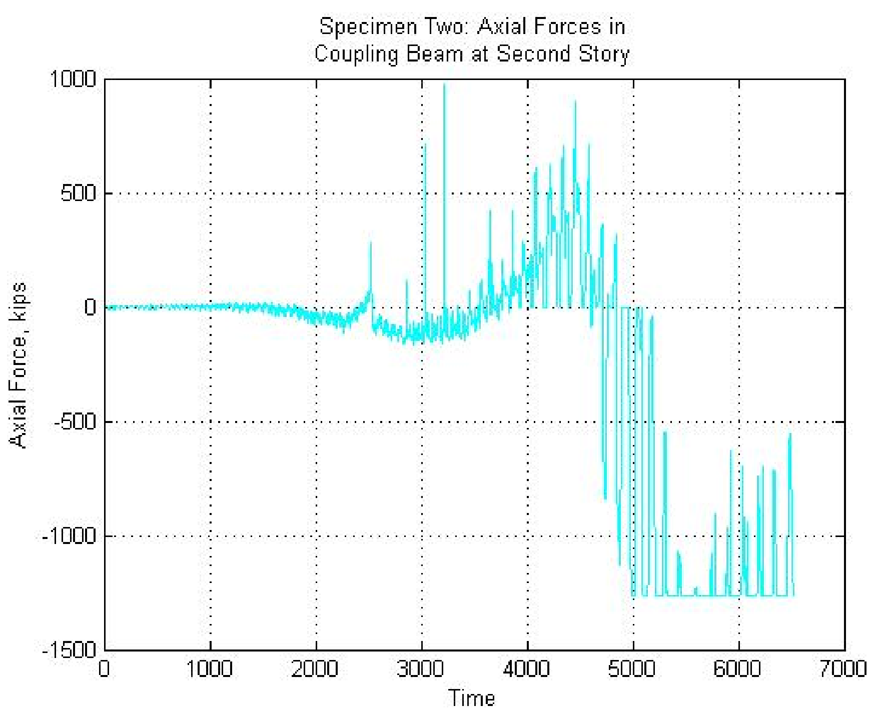

Figure 3.30: Specimen Two Axial Forces in Coupling Beam at Section Four

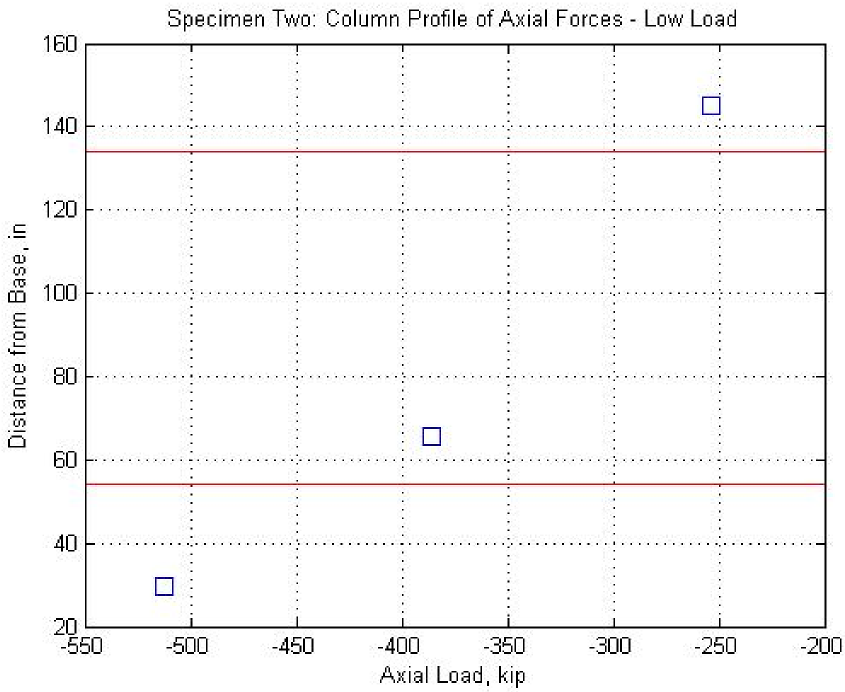

Figure 3.31: Specimen Two Axial Distribution along WF Column (Drift = 0.004)

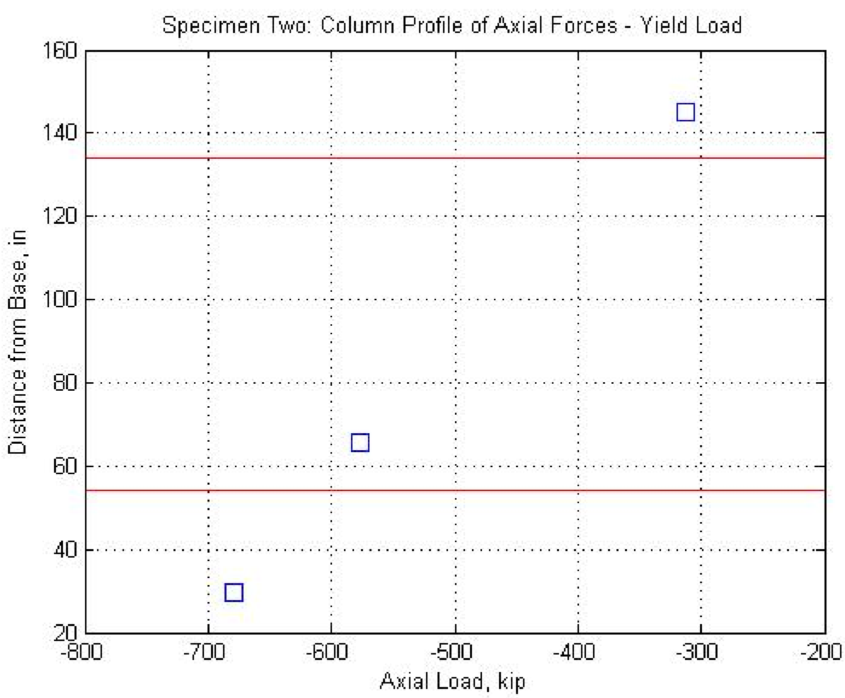

Figure 3.32: Specimen Two Axial Distribution along WF Column (Drift = 0.006)

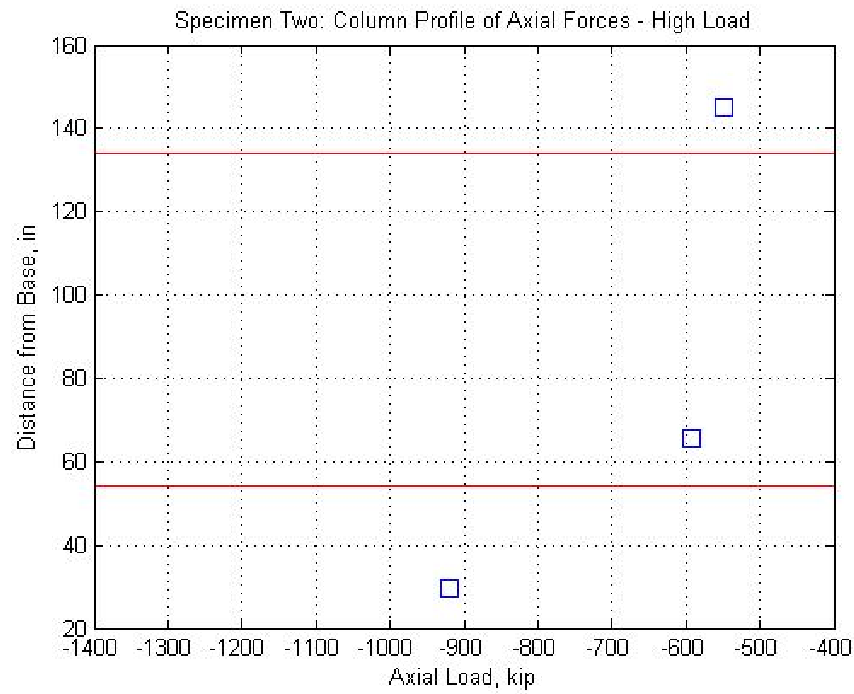

Figure 3.33: Specimen Two Axial Distribution along WF Column (Drift = 0.02)

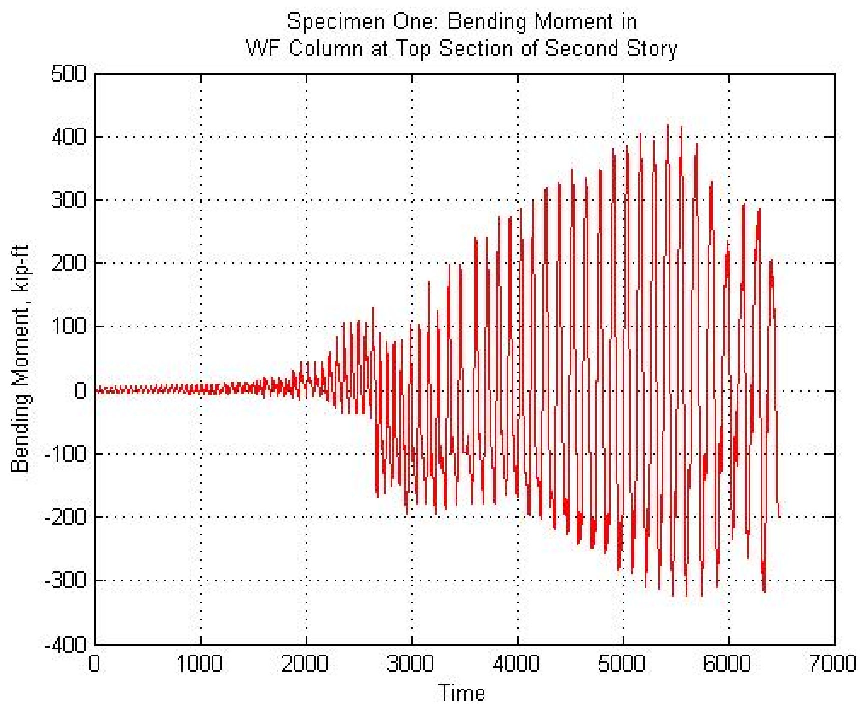

Figure 3.34: Specimen One Moment in WF Column at Section One

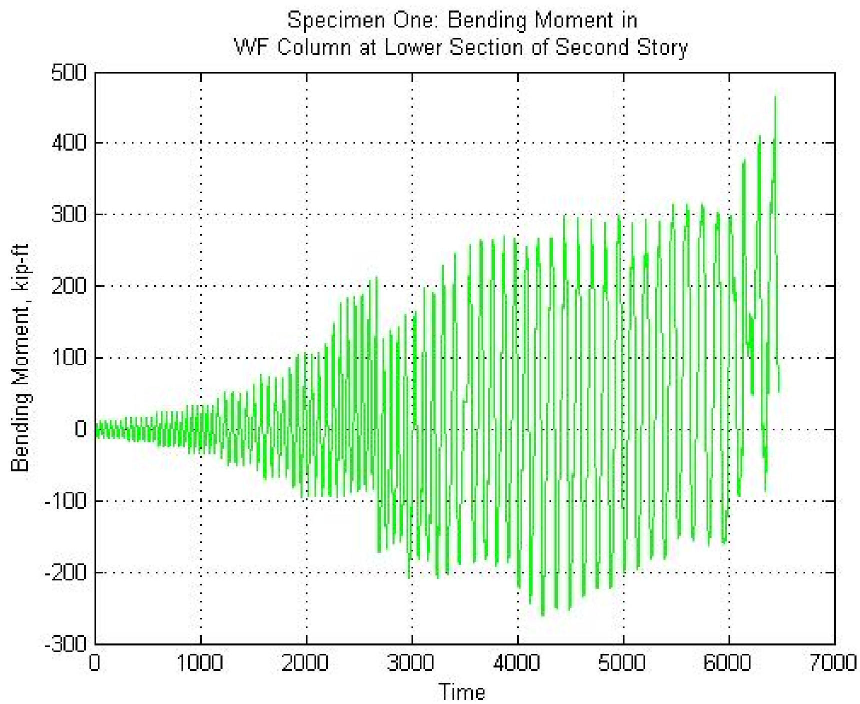

Figure 3.35: Specimen One Moment in WF Column at Section Two

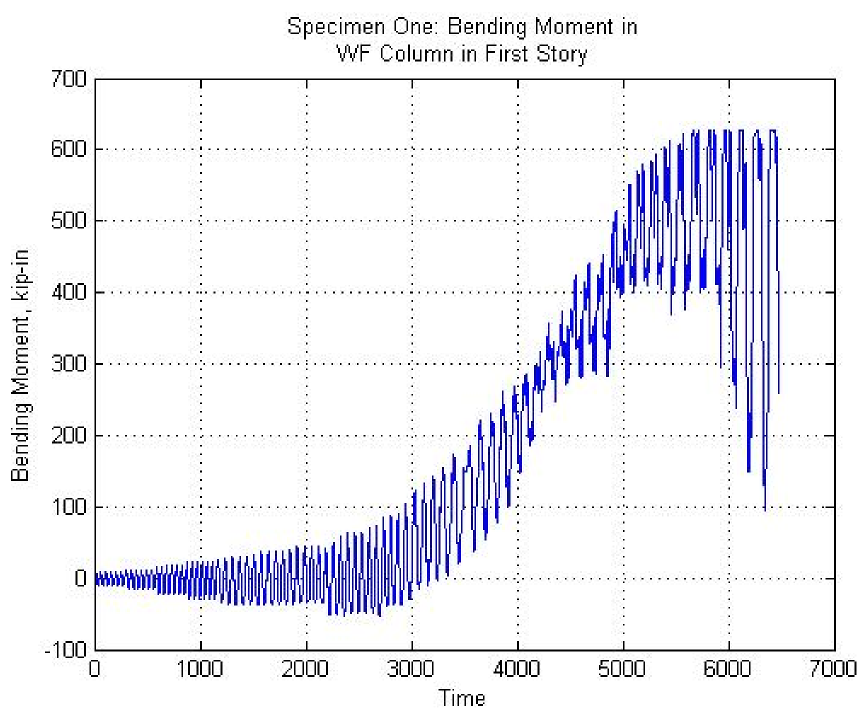

Figure 3.36: Specimen One Moment in WF Column at Section Three

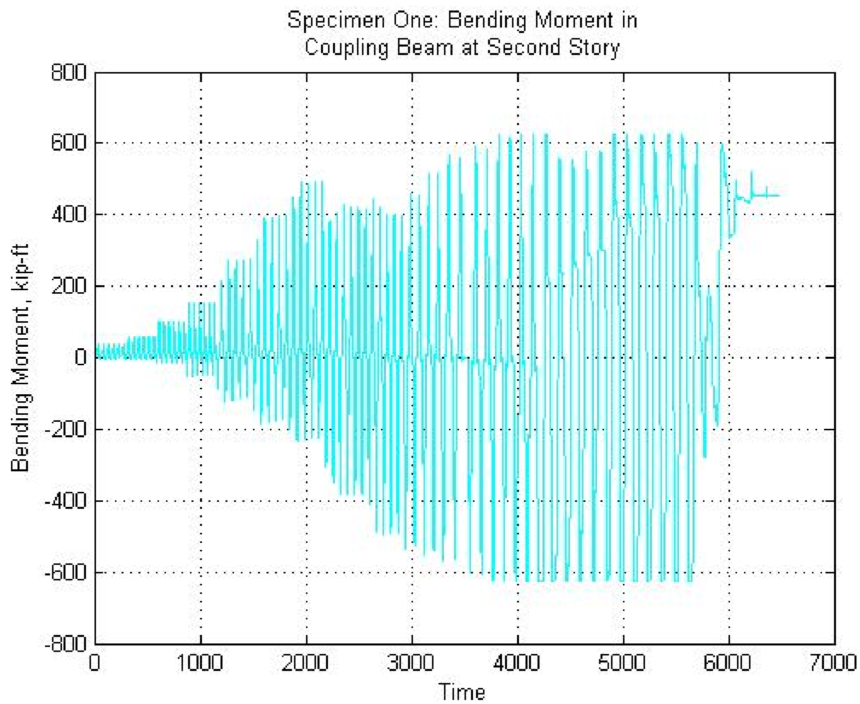

Figure 3.37: Specimen One Moment in Coupling Beam at Section Four

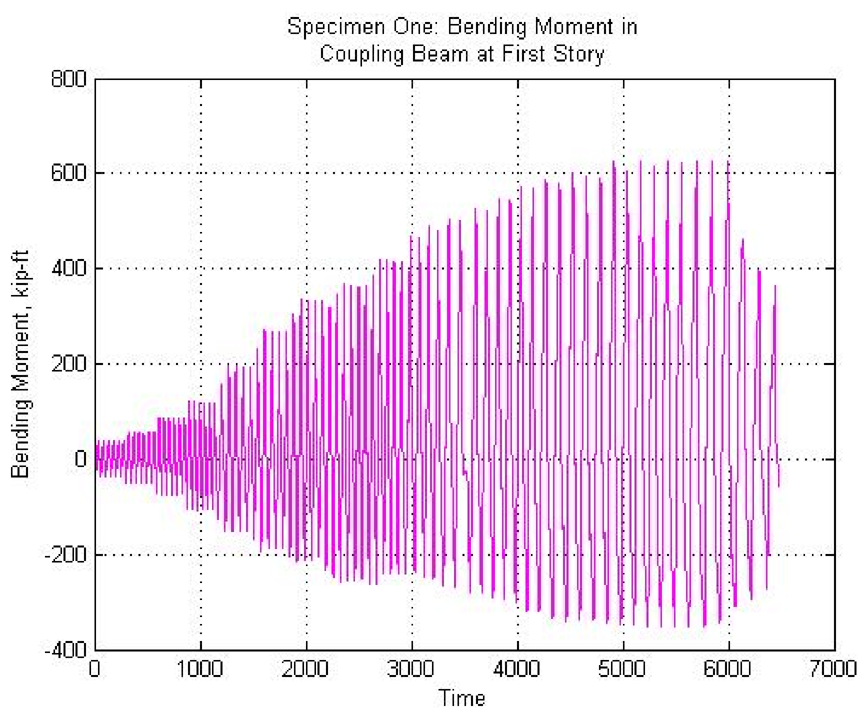

Figure 3.38: Specimen One Moment in Coupling Beam at Section Five

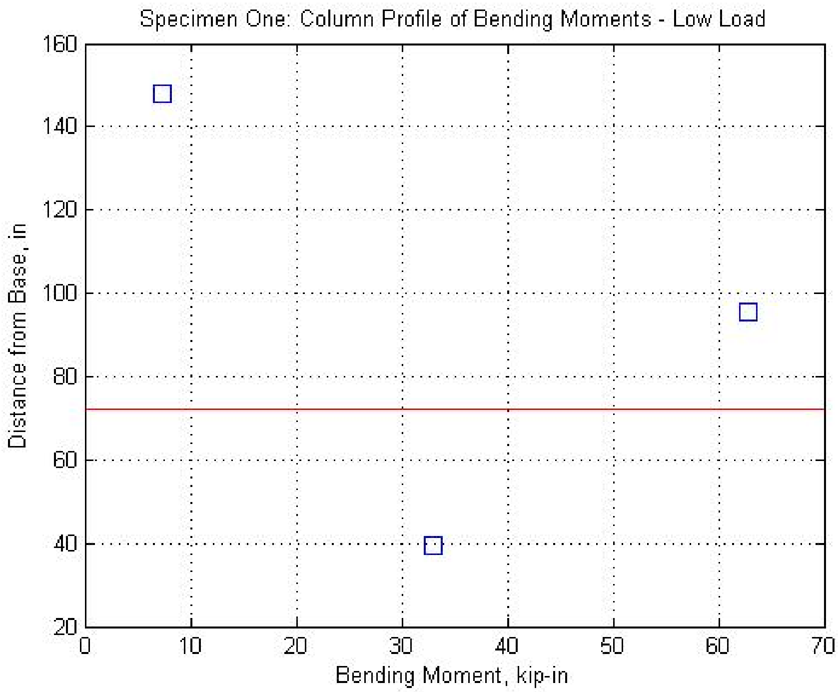

Figure 3.39: Specimen One Moment Distribution along WF Column (Drift = 0.004)

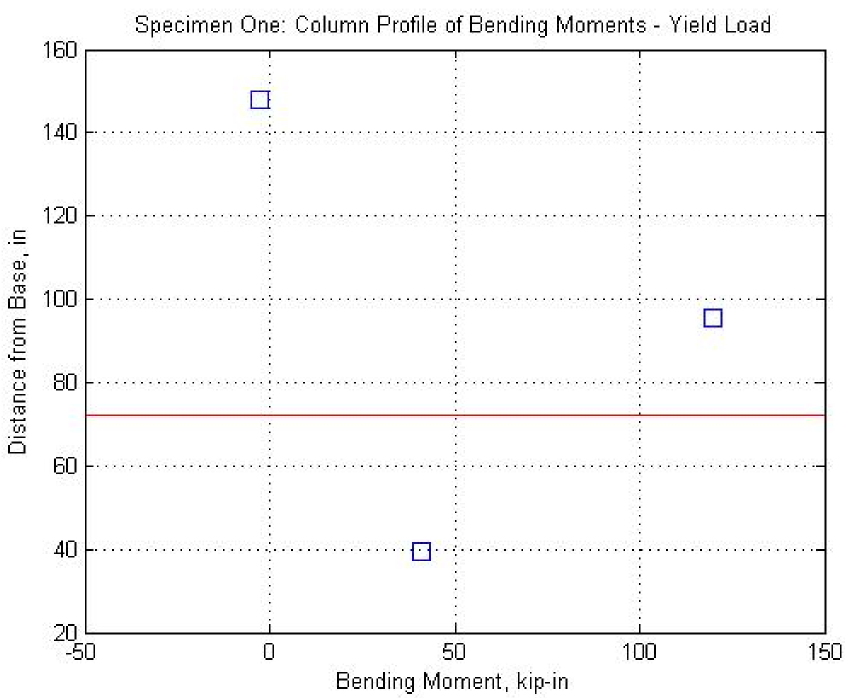

Figure 3.40: Specimen One Moment Distribution along WF Column (Drift = 0.006)

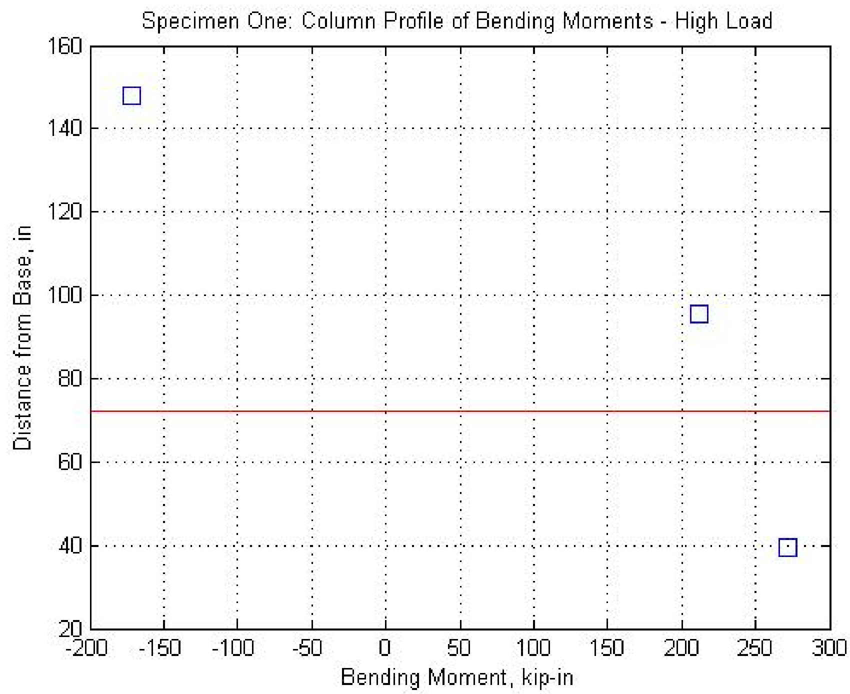

Figure 3.41: Specimen One Moment Distribution along WF Column (Drift = 0.02)

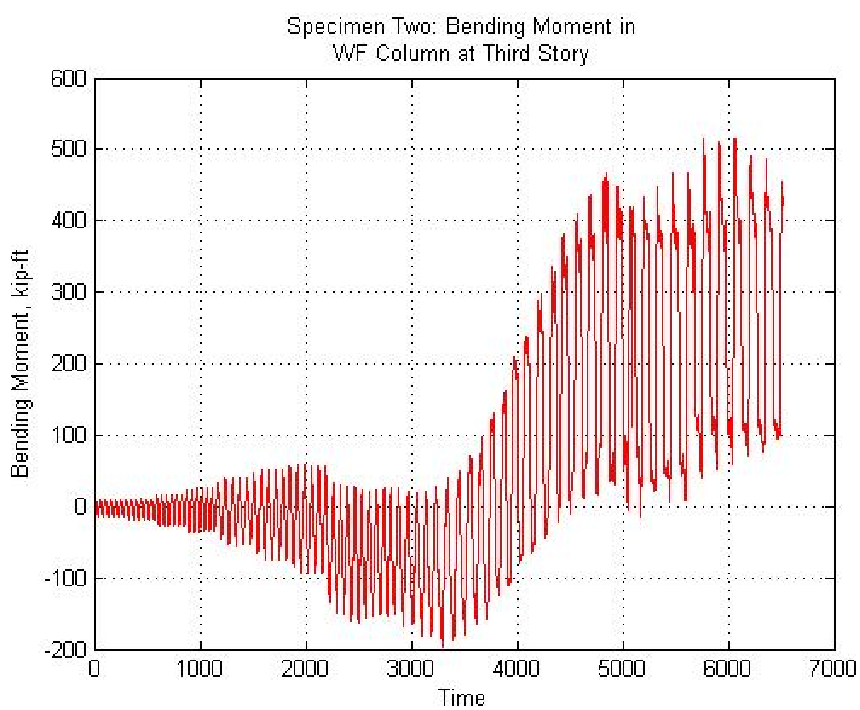

Figure 3.42: Specimen Two Moment in WF Column at Section One

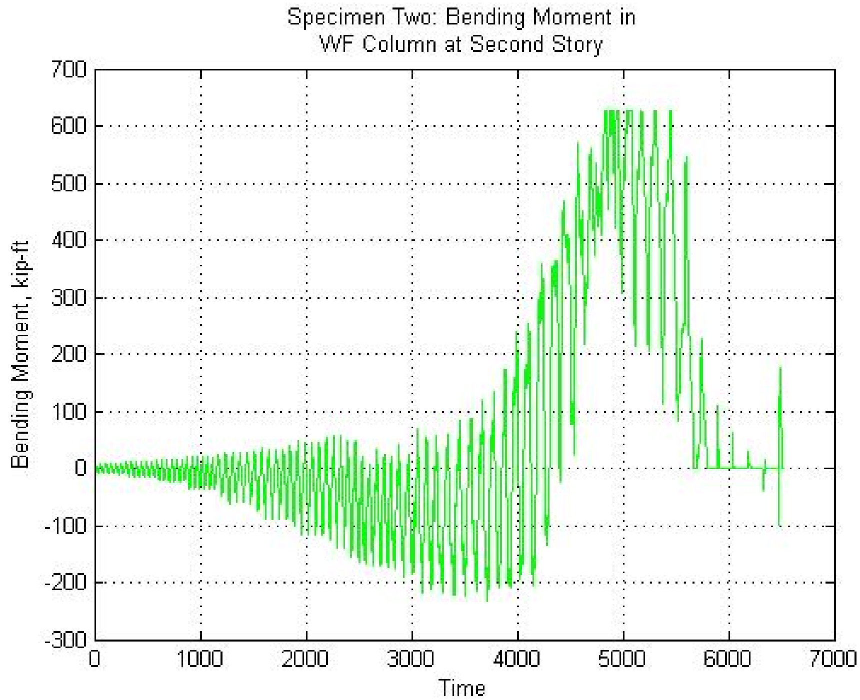

Figure 3.43: Specimen Two Moment in WF Column at Section Two

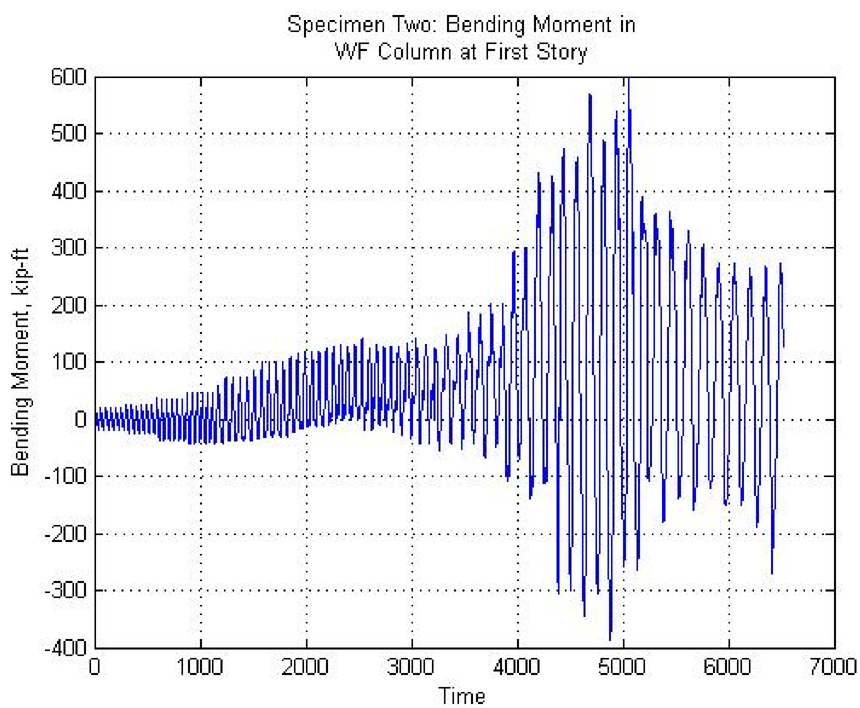

Figure 3.44: Specimen Two Moment in WF Column at Section Three

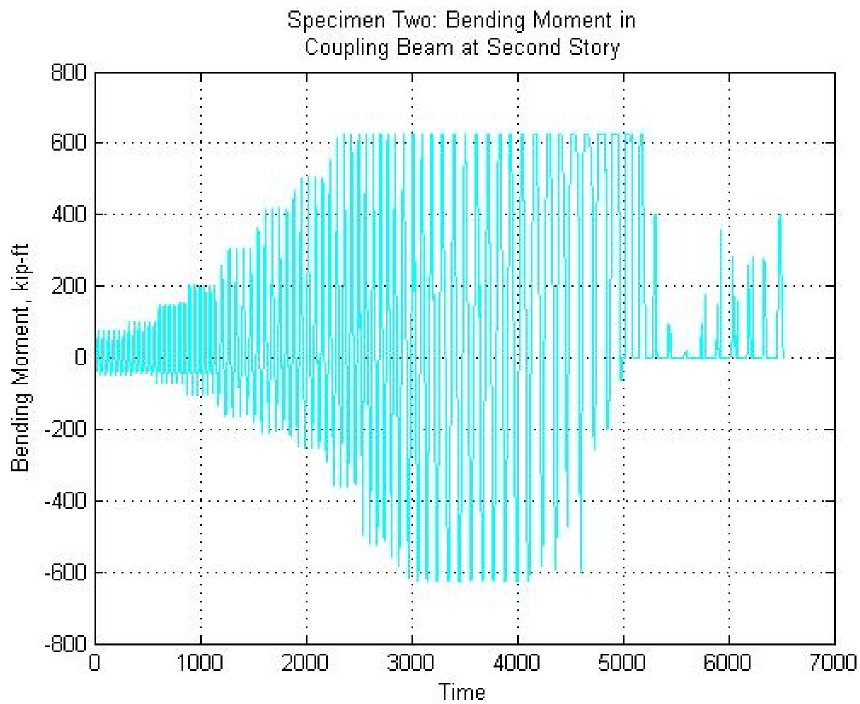

Figure 3.45: Specimen Two Moment in Coupling Beam at Section Four

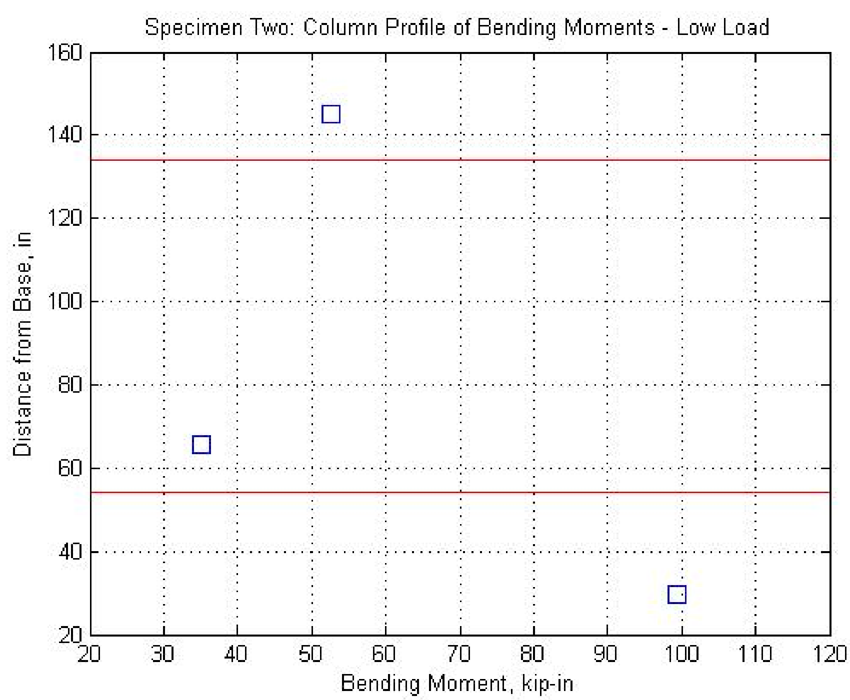

Figure 3.46: Specimen Two Moment Distribution along WF Column (Drift = 0.004)

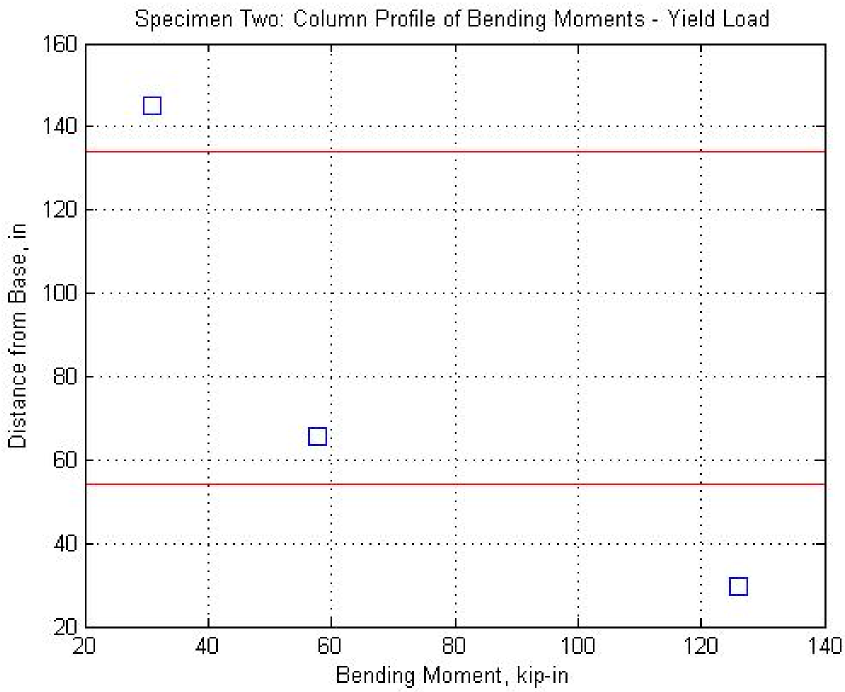

Figure 3.47: Specimen Two Moment Distribution along WF Column (Drift = 0.006)

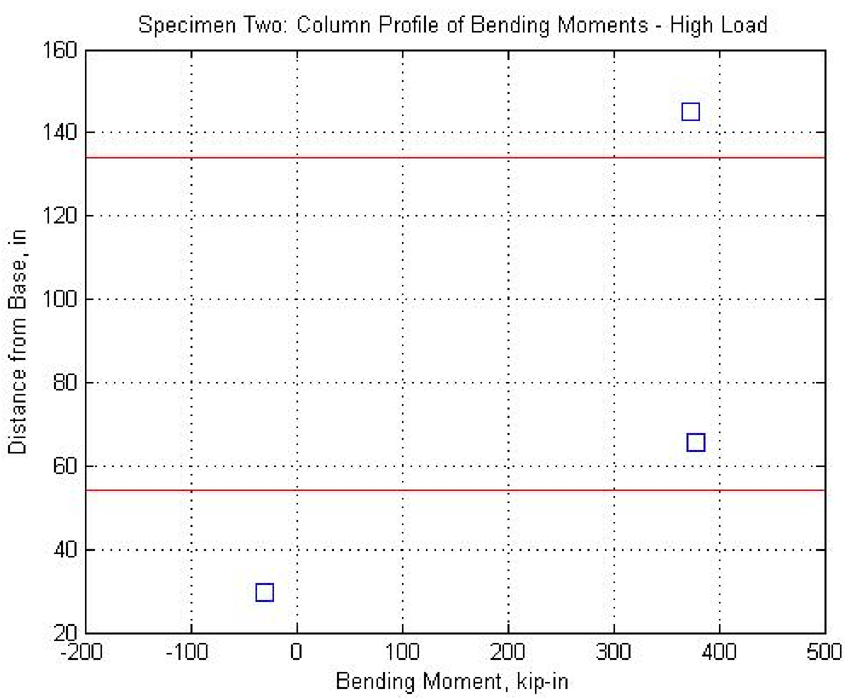

Figure 3.48: Specimen Two Moment Distribution along WF Column (Drift = 0.02)

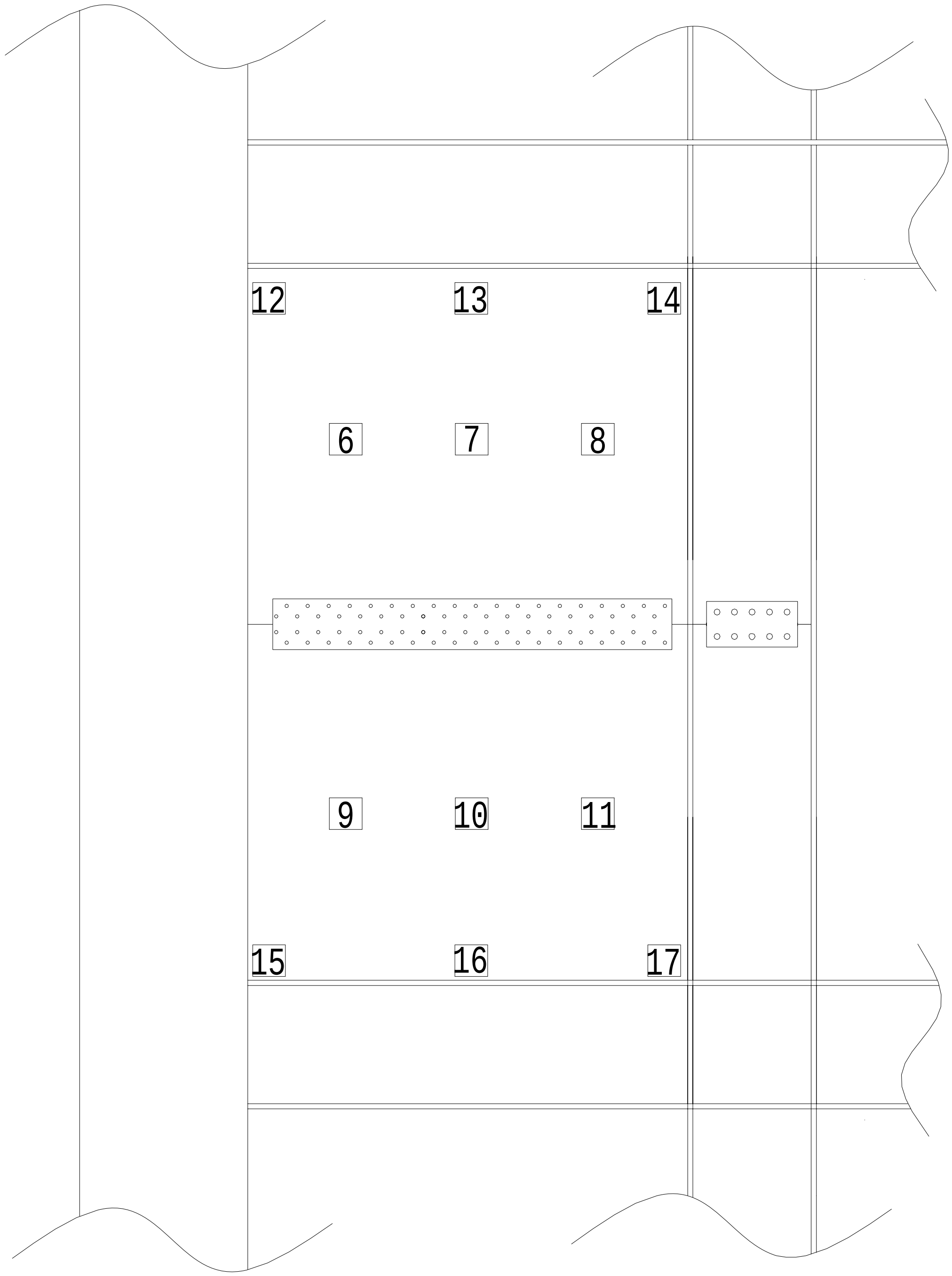

Figure 3.49: Specimen One Strain Gage Placement for Infill Panel

Table 3.4: Tabulated Principal Stresses and Angles for Specimen One Infills

		Elastic Range		Yield Range		Inelastic Range	
		Pt. 1510, 1st peak, cycle 30, 0.004 Drift, F = 408 k		Pt. 2192, 1st peak, cycle 40, 0.006 Drift; F = 519 k		Pt. 4466, 1st peak, cycle 65, 0.02 Drift, F = 797 k	
Specimen 1		**Phi**	**Stress**	**Phi**	**Stress**	**Phi**	**Stress**
6	major	41.8305	10.2245	41.9479	17.0448	31.2958	45
	minor		-29.7635		-38.7313		45
7	major	41.376	30.3113	44.9598	43.9597	28.6881	45
	minor		9.9121		5.3821		-18.9039
8	major	36.8985	32.7303	39.5954	45	44.0129	45
	minor		9.426		40.9082		45
9	major	41.7842	29.4271	41.2993	45	-12.4836	45
	minor		6.6339		18.3088		33.7455
10	major	42.6426	25.3542	42.6778	44.1413	27.1787	42.1925
	minor		9.3216		21.4156		17.1166
11	major	41.0832	0.2987	39.5397	-37.9531	41.2448	29.1973
	minor		-45		-45		-4.2809
12	major	32.8321	45	28.1906	45	5.082	34.8726
	minor		-31.1296		-41.1807		-34.3792
13	major	41.7745	23.0186	43.5694	35.4103	27.9009	16.395
	minor		-14.6123		-23.4433		-41.684
14	major	35.8969	-5.2769	33.2766	11.8599	41.8091	39.3943
	minor		-22.584		-24.7004		-45
15	major	-0.9917	10.3248	4.4635	19.6105	22.4766	45
	minor		-21.4234		-41.2347		16.2949
16	major	23.3299	26.6406	10.0668	31.7847	-26.068	45
	minor		-2.834		-3.9404		18.343
17	major	40.2327	5.2895	42.03	7.0019	-31.9718	45
	minor		-20.066		-19.7943		-1.436

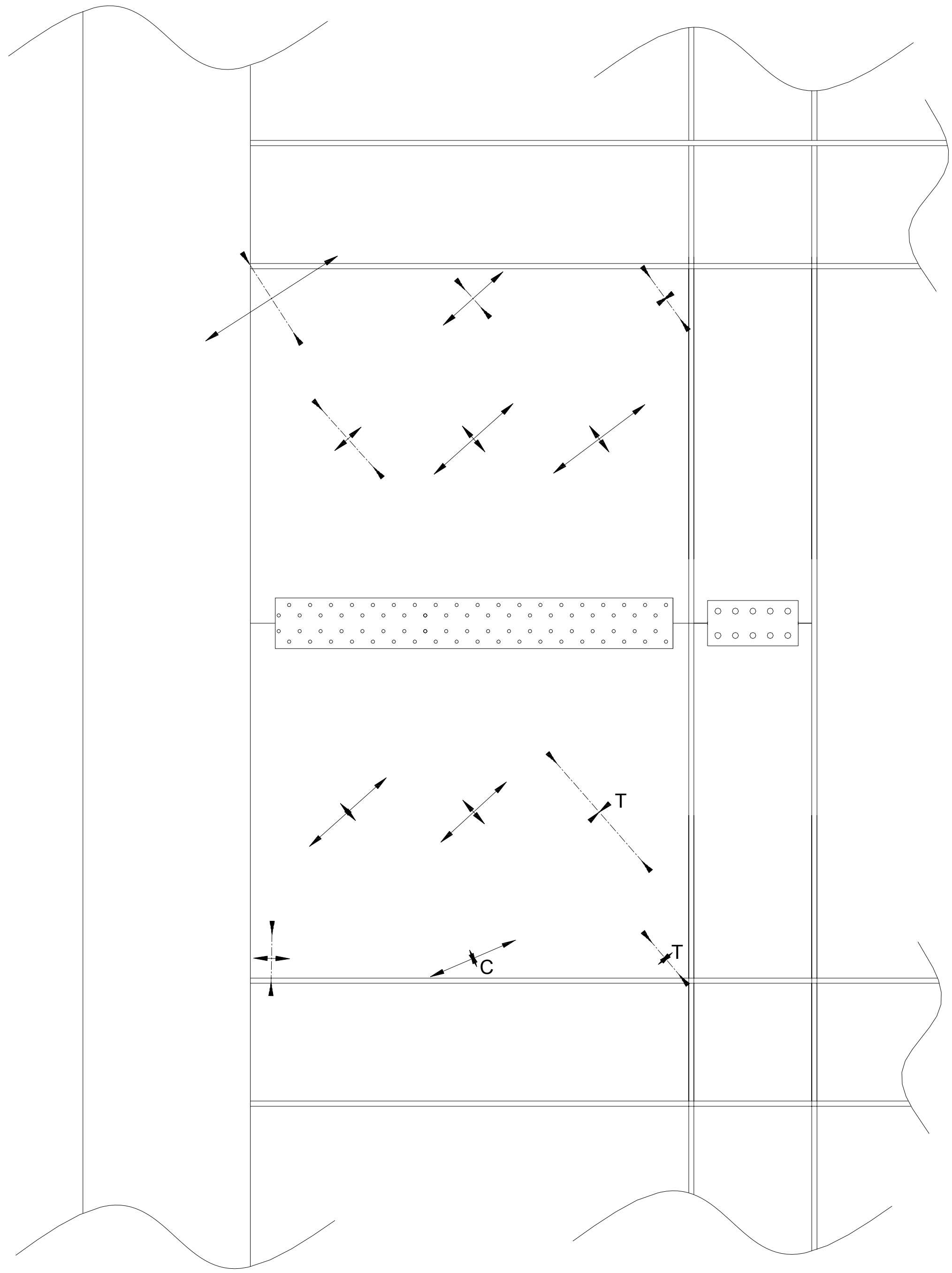

Figure 3.50: Specimen One Angles of Major and Minor Principal Stresses of Infill Panels during Elastic Range of Loading
(Length signifies magnitude of tensile or compressive stress)

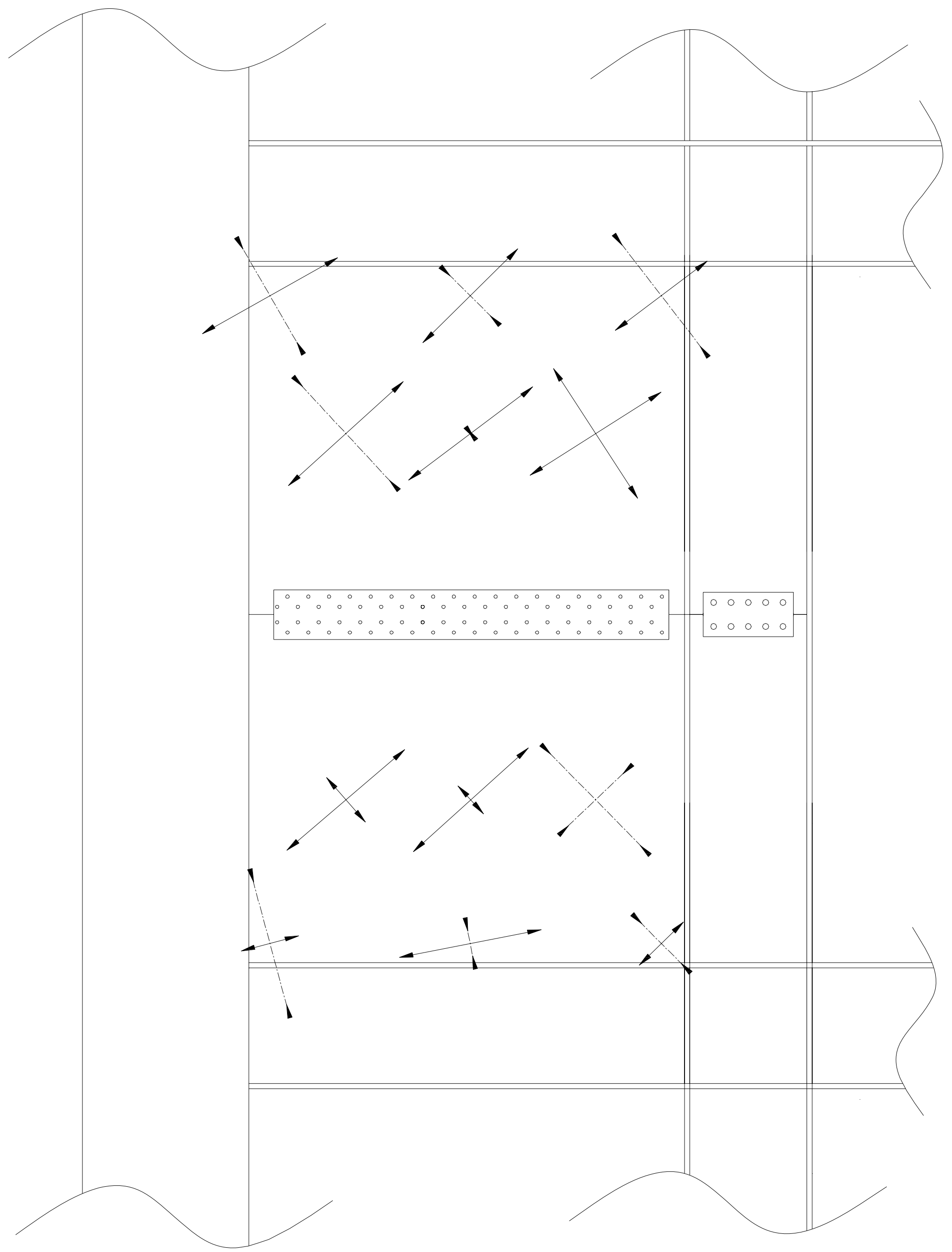

Figure 3.51: Specimen One Angles of Major and Minor Principal Stresses of Infill Panels during Yield Range of Loading (Length signifies magnitude of tensile or compressive stress)

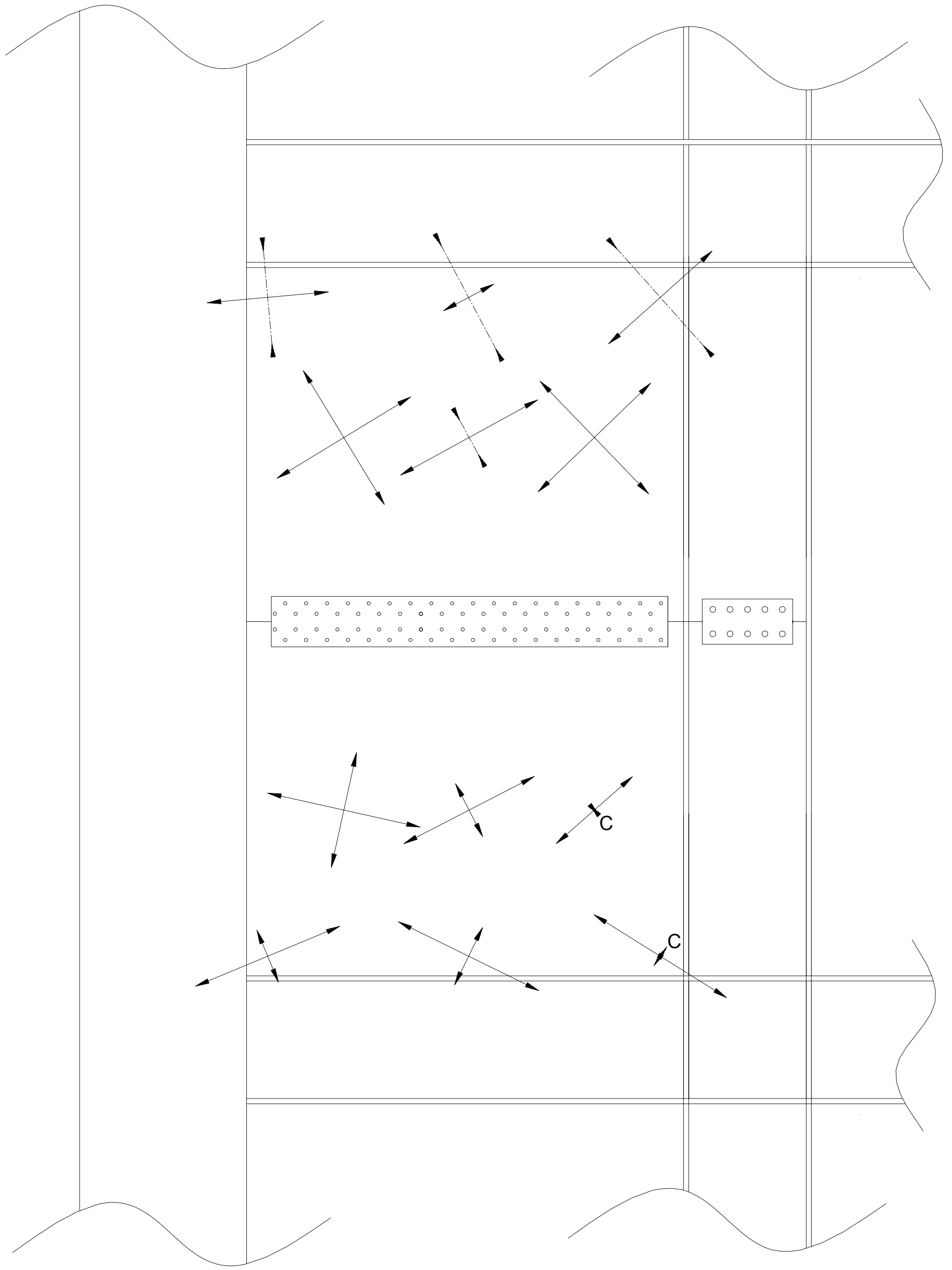

**Figure 3.52: Specimen One Angles of Major and Minor Principal Stresses of Infill Panels during Inelastic Range of Loading
(Length signifies magnitude of tensile or compressive stress)**

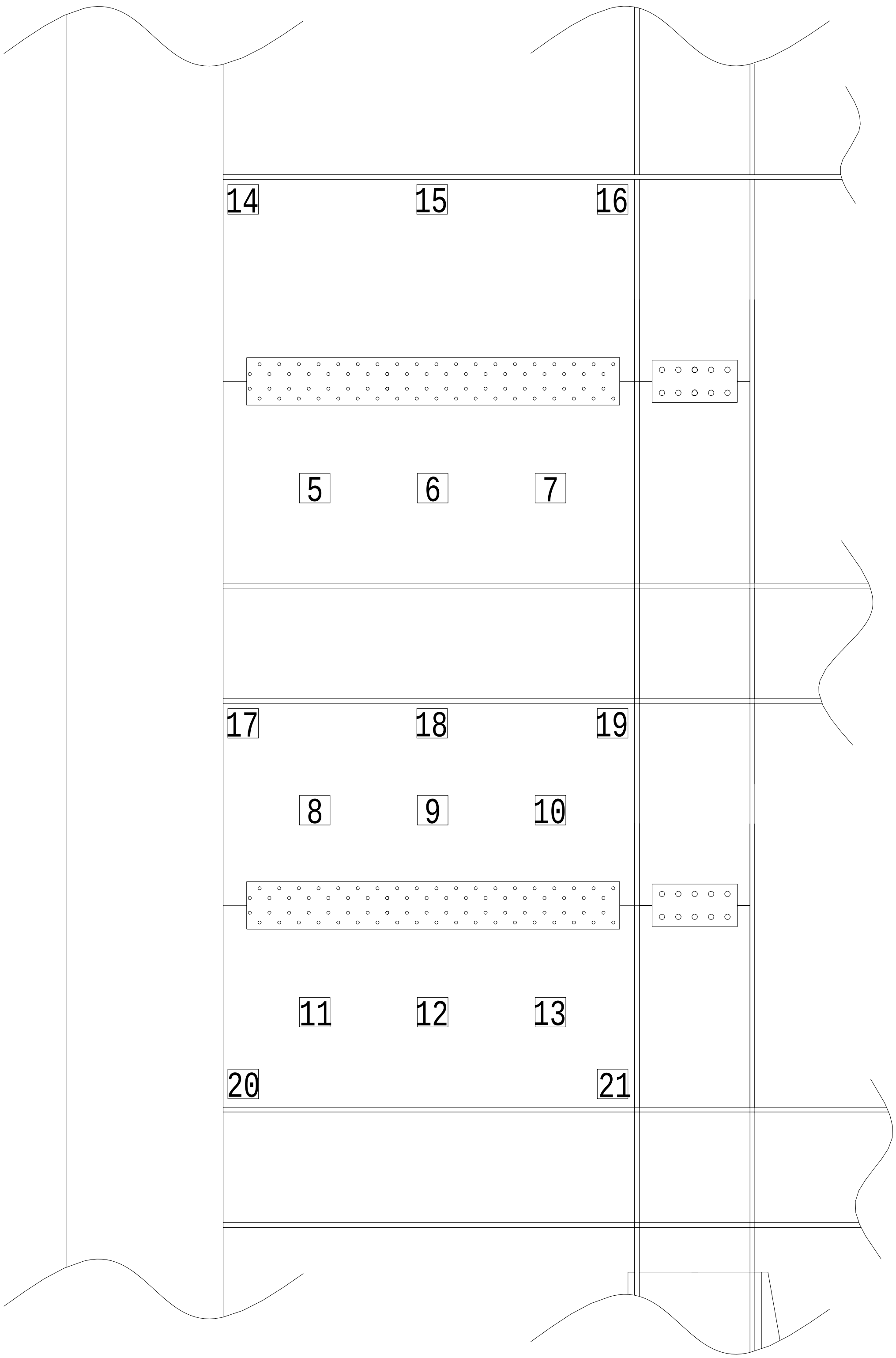

Figure 3.53: Specimen Two Strain Gage Placement of Infill Panel

Table 3.5: Tabulated Principal Stresses and Angles for Specimen Two Infills

Specimen 2		Elastic Range: Pt. 1513, 1st peak, cycle 30, 0.004 Drift, F= 491 k		Yield Range: Pt. 2195, 1st peak, cycle 40, 0.006 Drift, F = 753 k		Inelastic Range: Pt. 4472, 1st peak, cycle 65, 0.02 Drift, F = 1071 k	
		Phi	Stress	Phi	Stress	Phi	Stress
5	major	38.6213	11.8567	38.2904	18.7744	41.1562	45
	minor		-11.6897		-19.0356		-31.4337
6	major	38.6184	13.3373	37.5814	21.568	-22.2301	45
	minor		-10.4371		-13.8673		25.8607
7	major	43.0402	12.7669	43.8336	20.3713	-14.0618	19.7135
	minor		-12.1774		-16.2491		-40.4421
8	major	36.9618	15.3112	35.6213	23.0788	24.7068	-5.7689
	minor		-3.4597		-4.6352		-9.3022
9	major	43.9144	11.6391	44.9715	18.653	14.5682	45
	minor		-6.9496		-8.7839		27.4537
10	major	39.3453	8.084	39.6519	13.6964	42.1413	33.0477
	minor		-14.9667		-22.6934		-45
11	major	35.1103	13.9515	33.1915	23.1222	42.5186	45
	minor		-8.3677		-11.8361		-45
12	major	39.826	13.2038	37.2163	21.642	-18.1438	45
	minor		-9.9677		-13.8991		25.3662
13	major	44.545	12.5211	42.581	19.2411	-23.8989	17.9069
	minor		-10.0546		-13.7593		-45
14	major	42.9764	12.0048	41.4702	15.0657	-17.8602	45
	minor		-9.1054		-16.8204		-45
15	major	44.0728	13.1278	42.7556	20.4342	33.6482	43.0417
	minor		-9.0367		-12.6779		-45
16	major	24.8682	6.9318	9.6592	18.5854	44.3965	45
	minor		-12.4269		-14.3265		-45
17	major	36.087	45	35.1668	45	-30.2646	10.0924
	minor		-10.422		-17.1551		-27.9339
18	major	43.7182	9.559	43.9101	14.4681	33.3008	19.9719
	minor		-8.2955		-12.3198		-45
19	major	33.9955	11.7644	30.2819	21.2182	44.3201	45
	minor		-21.7678		-42.7069		-45
20	major	11.7746	17.1695	-2.4756	42.3226	23.006	7.875
	minor		-7.9981		-26.3902		-45
21	major	41.7753	-2.1527	42.1247	-1.768	-42.0462	45
	minor		-14.6293		-21.4985		-45

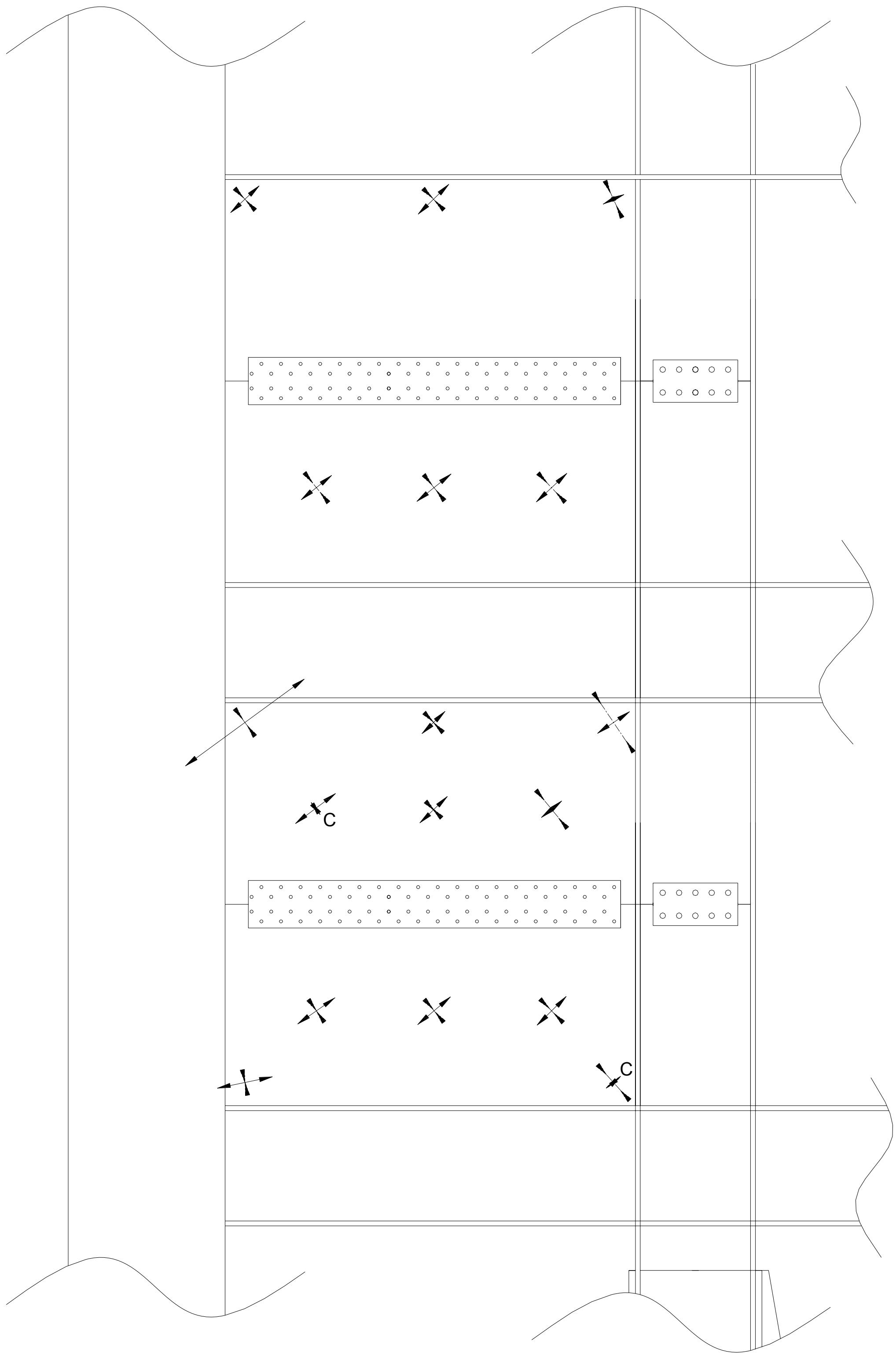

Figure 3.54: Specimen Two Angles of Major and Minor Principal Stresses of Infill Panels during Elastic Range of Loading
(Length signifies magnitude of tensile or compressive stress)

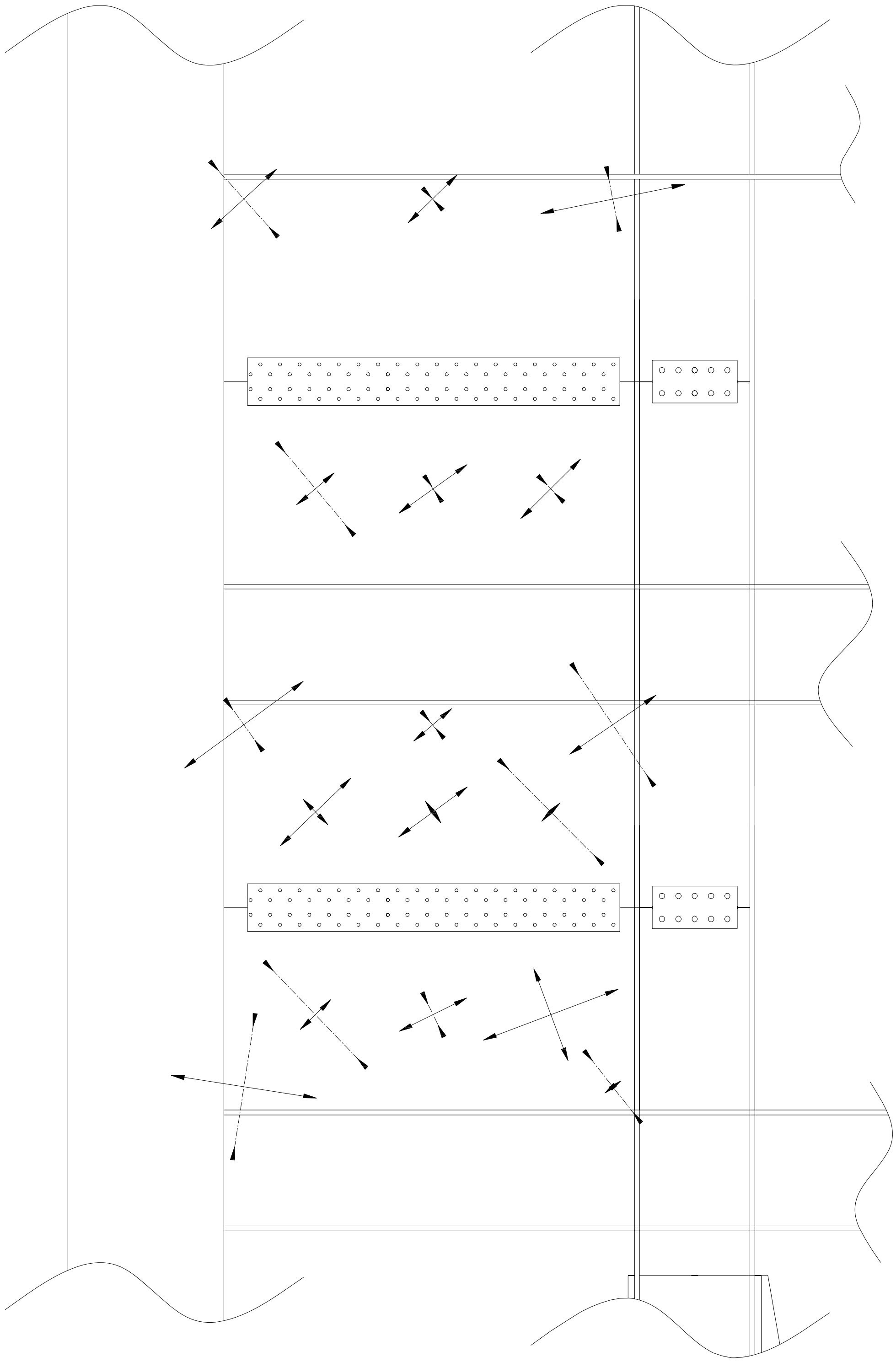

**Figure 3.55: Specimen Two Angles of Major and Minor Principal Stresses of Infill Panels during Yield Range of Loading
(Length signifies magnitude of tensile or compressive stress)**

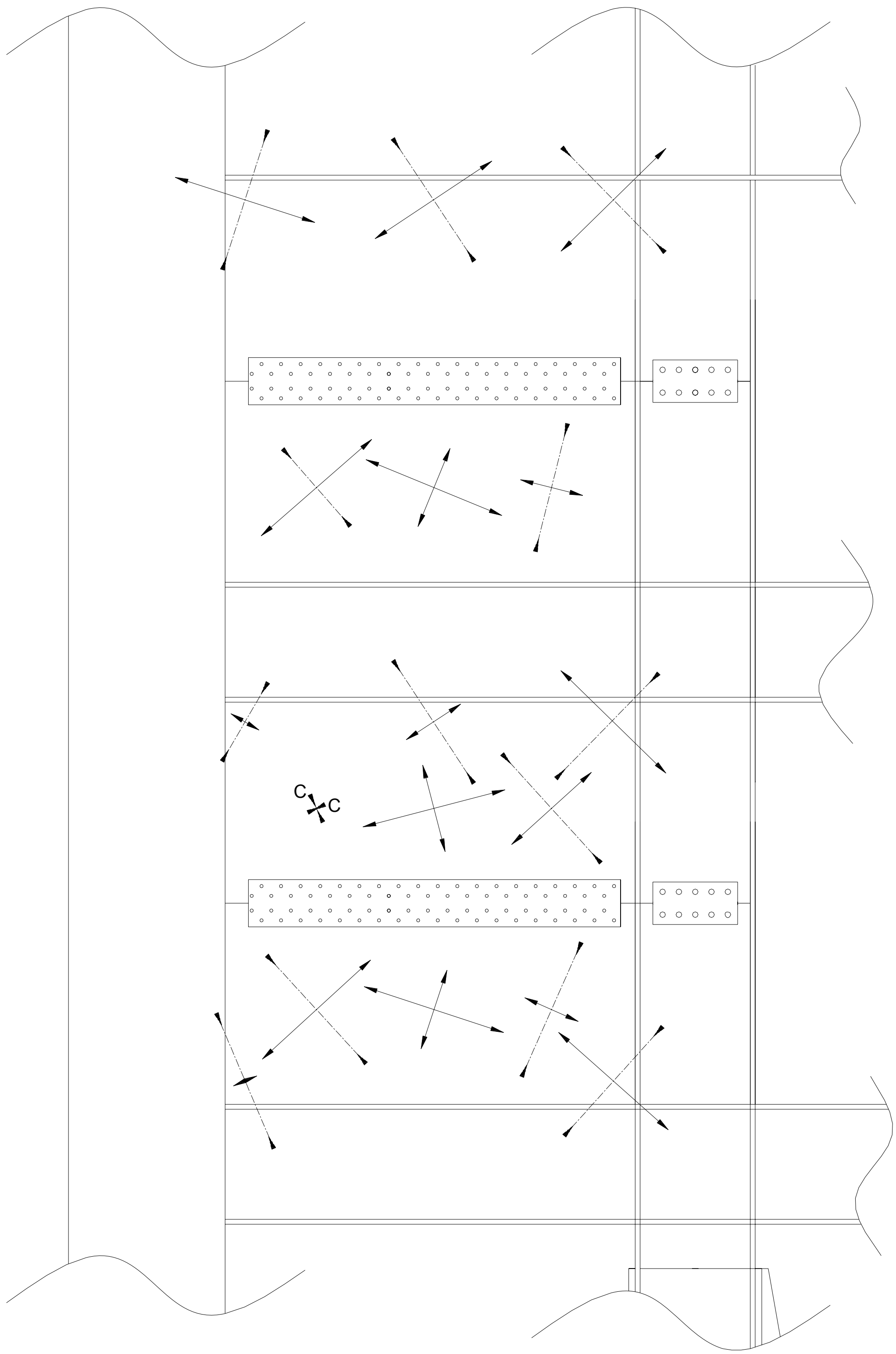

Figure 3.56: Specimen Two Angles of Major and Minor Principal Stresses of Infill Panels during Inelastic Range of Loading
(Length signifies magnitude of tensile or compressive stress)

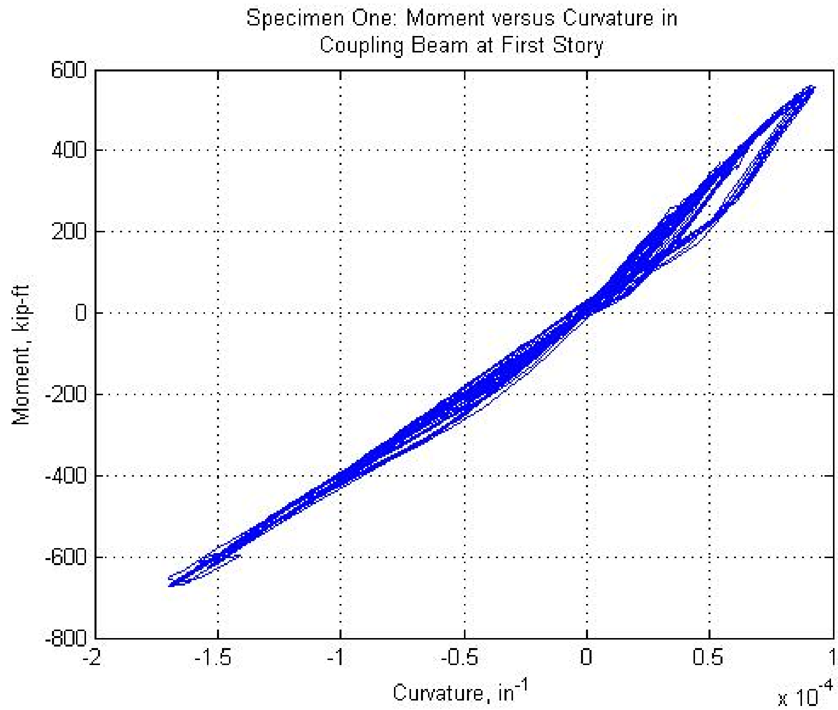

Figure 3.57: Elastic Behavior from Strain Gages showing Different Stiffness for Pushing and Pulling

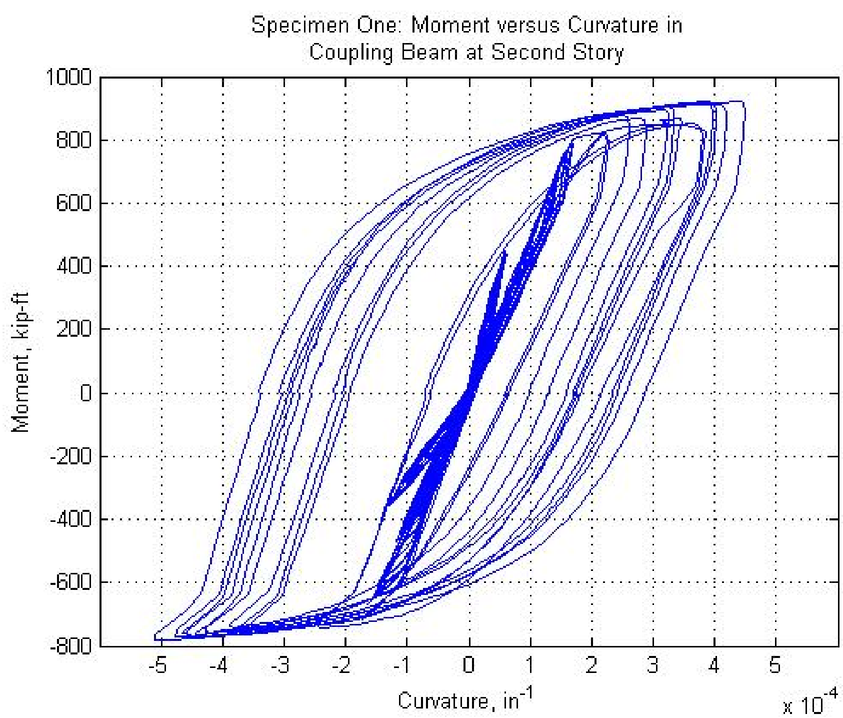

Figure 3.58: Moment versus Curvature using Strain Gage Data

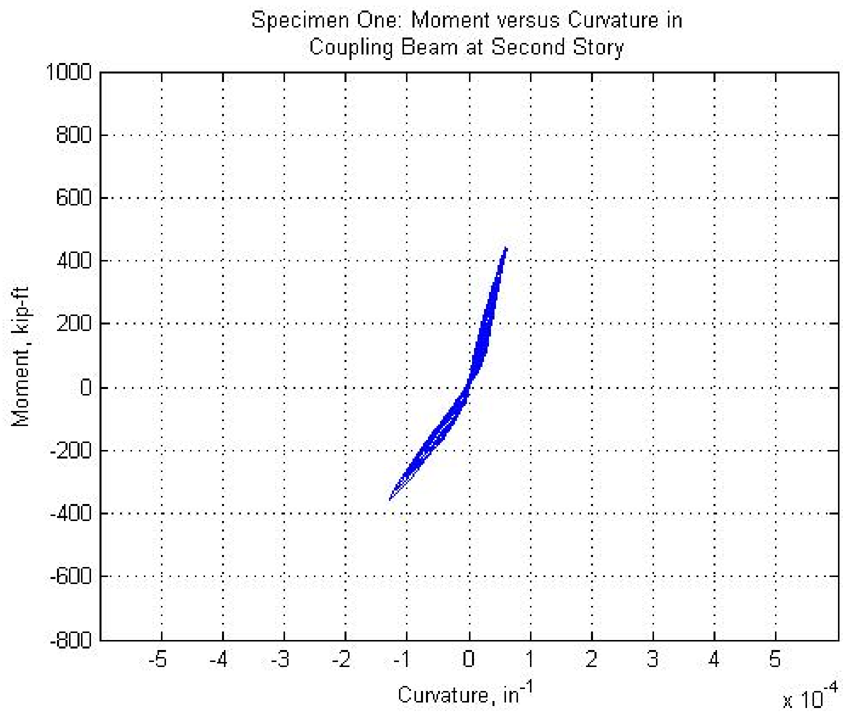

Figure 3.59: Strain Gage Data showing Different Stiffness at Low Loading

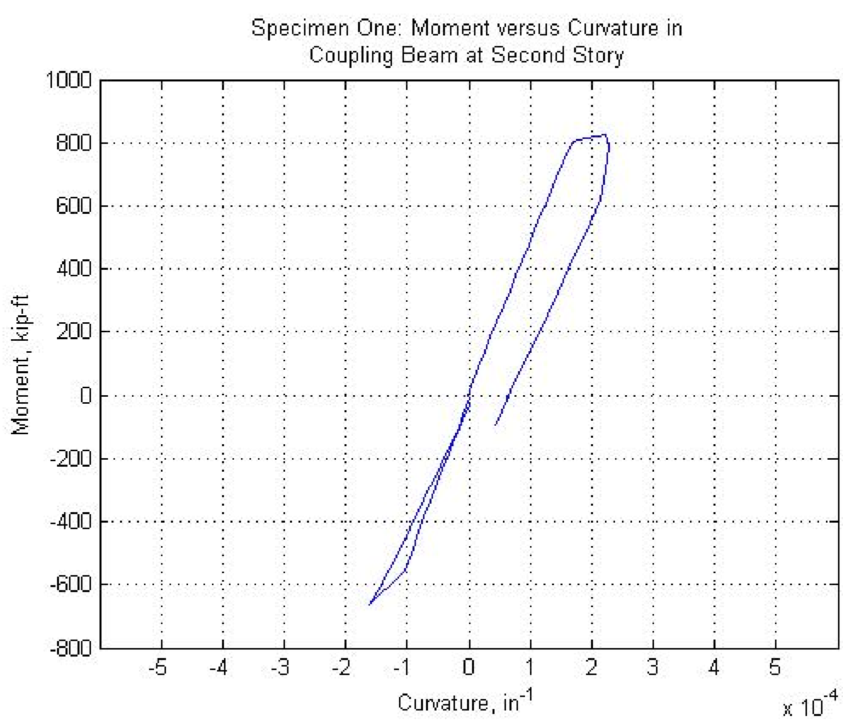

Figure 3.60: Evidence of Yielding

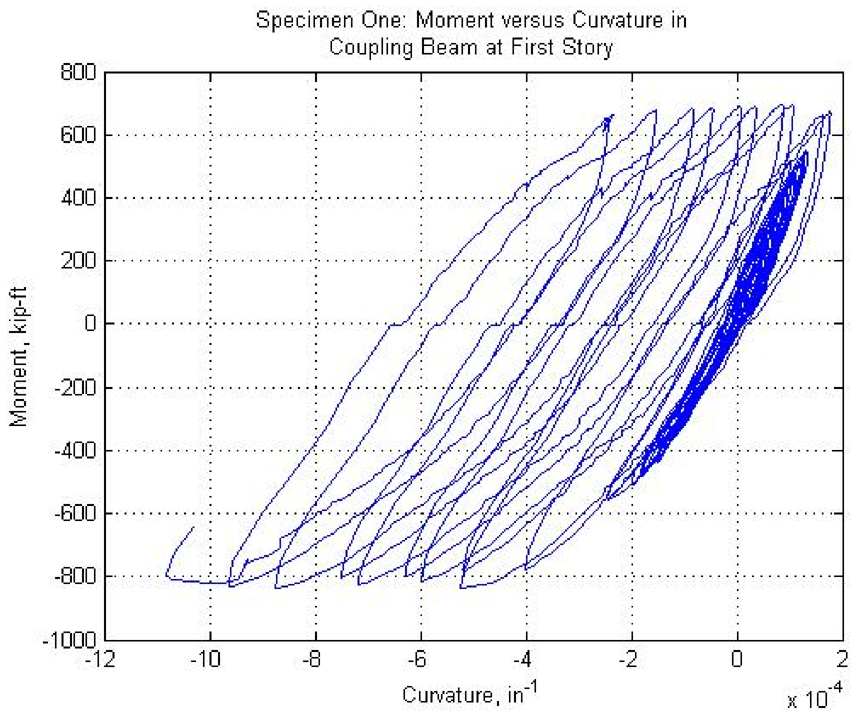

Figure 3.61: Moment Curvature using Transducer Readings

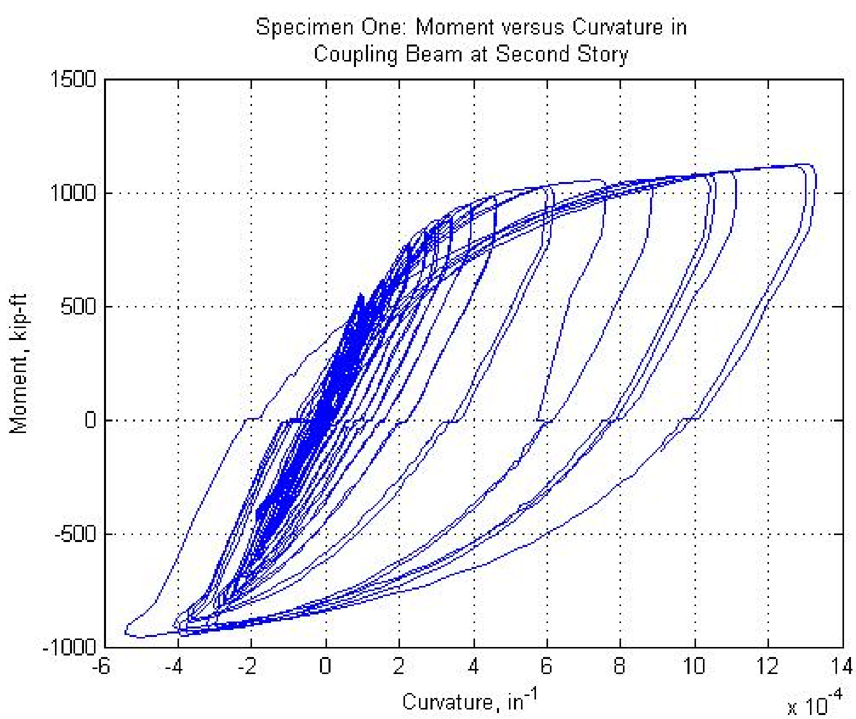

Figure 3.62: Moment Curvature using Transducer Readings

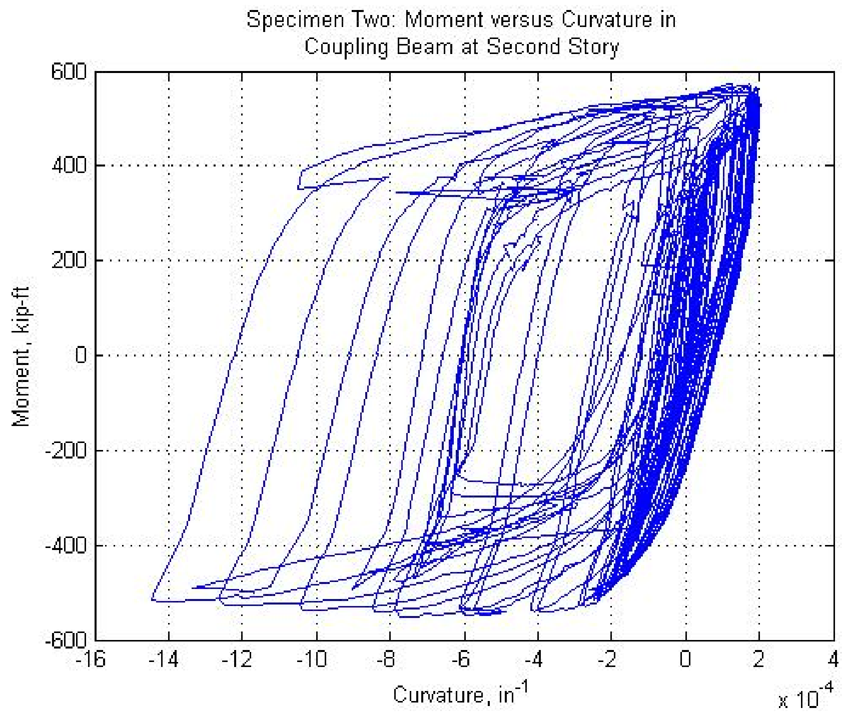

Figure 3.63: Moment Curvature using Strain Gage Data

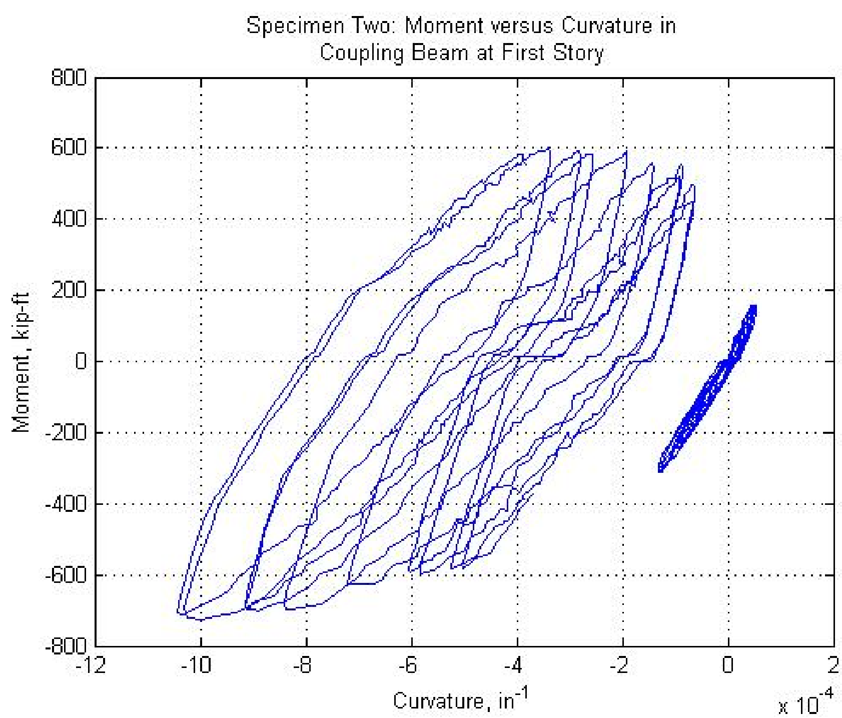

Figure 3.64: Moment versus Curvature using Transducer Readings

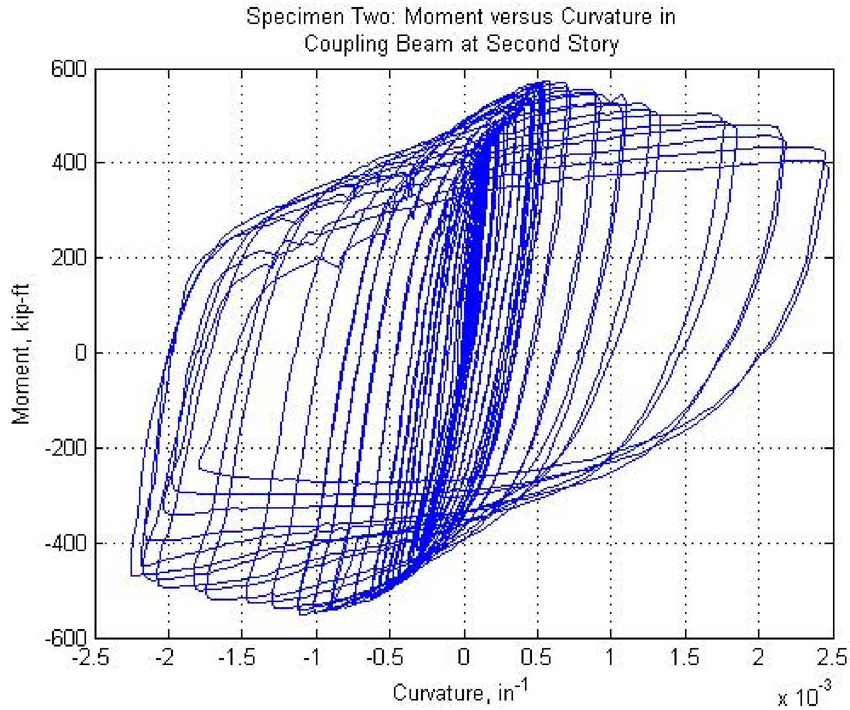

Figure 3.65: Moment versus Curvature using Transducer Readings

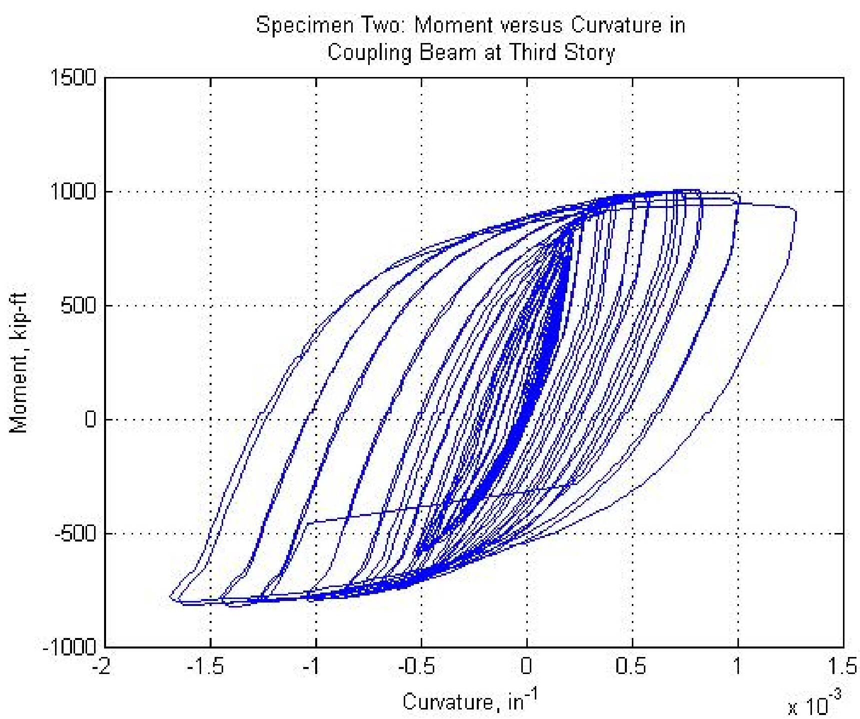

Figure 3.66: Moment versus Curvature for Transducer Readings

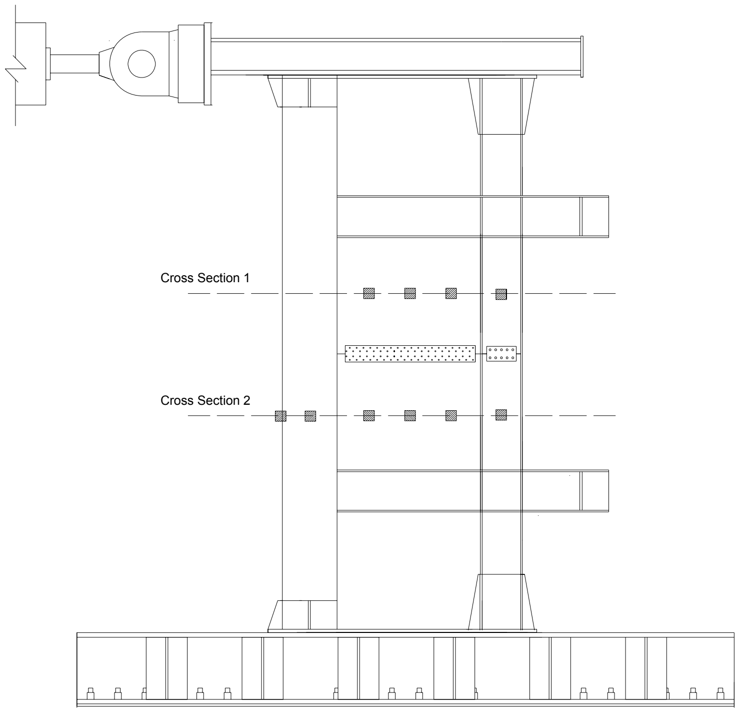

Figure 3.67: Specimen One Cross Sections where Shear Distribution is Analyzed

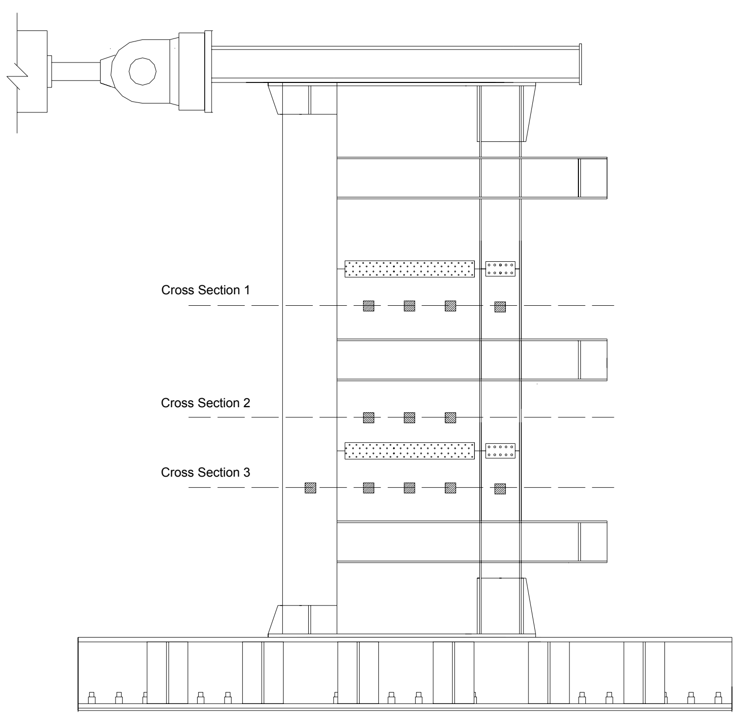

Figure 3.68: Specimen Two Cross Sections where Shear Distribution is Analyzed

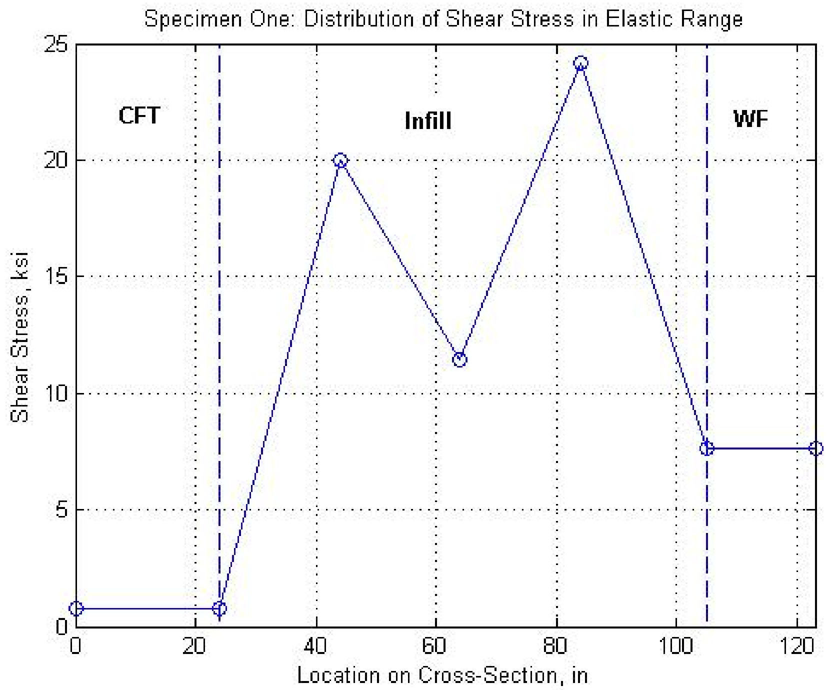

Figure 3.69: Specimen One Shear Stress Distribution in Elastic Range at Upper Section of Panel (Drift = 0.004)

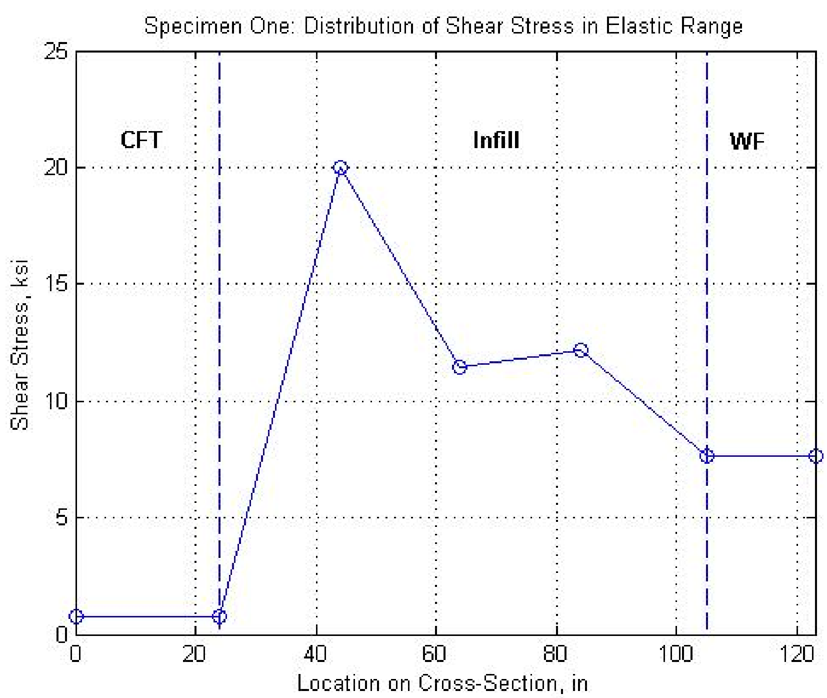

Figure 3.70: Specimen One Shear Stress Distribution in Elastic Range at Lower Section of Panel (Drift = 0.004)

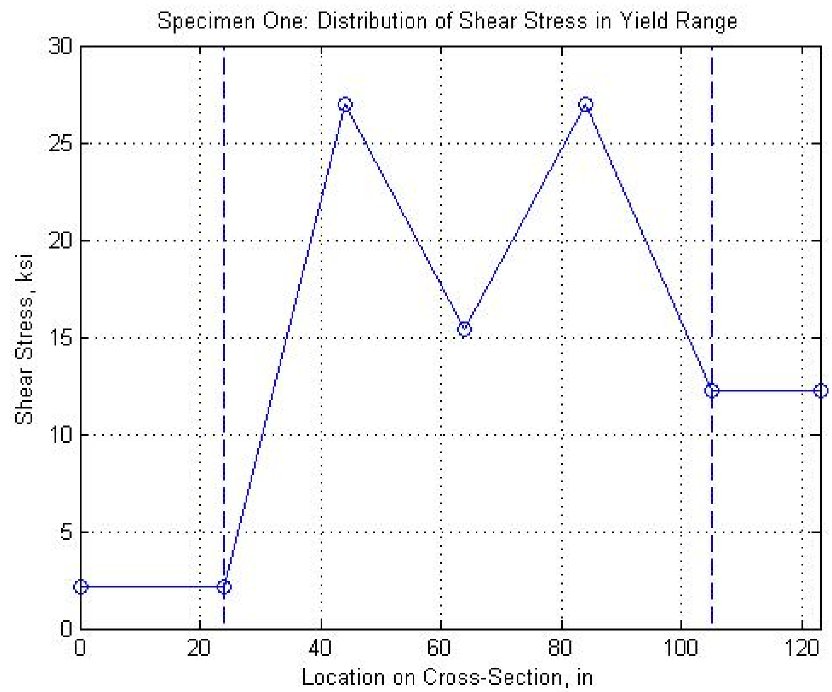

Figure 3.71: Specimen One Shear Stress Distribution in Yield Range at Upper Section of Panel (Drift = 0.006)

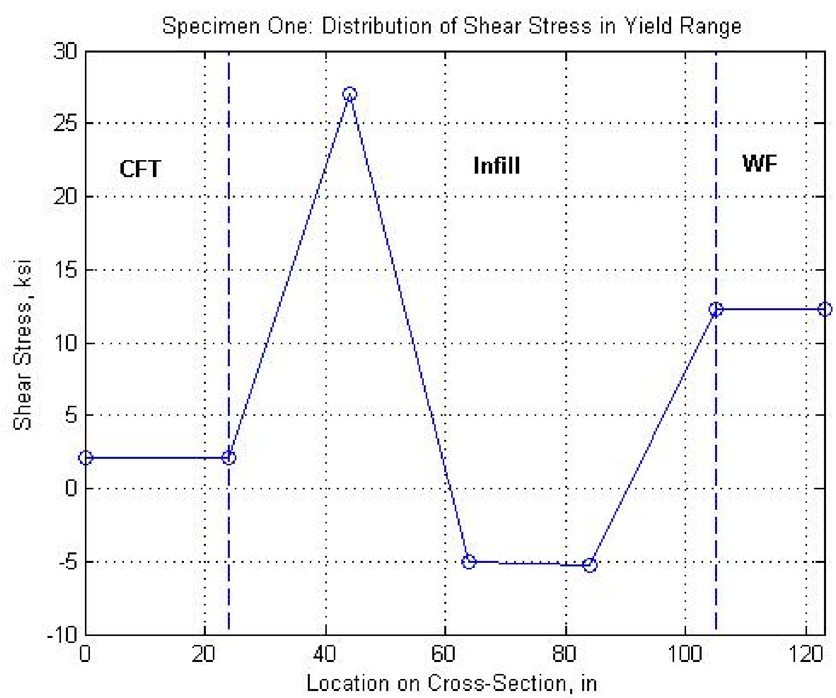

Figure 3.72: Specimen One Shear Stress Distribution in Yield Range at Lower Section of Panel (Drift = 0.006)

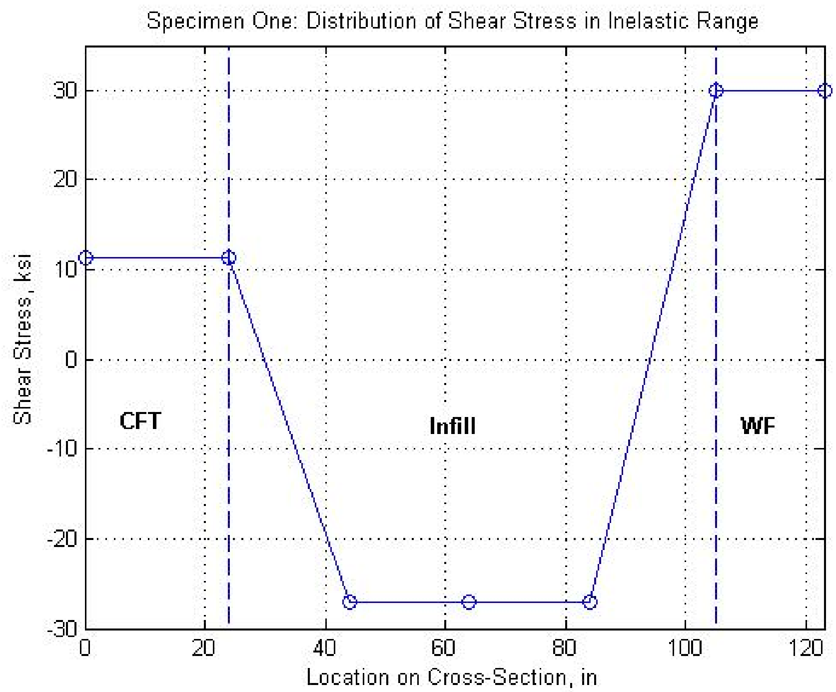

Figure 3.73: Specimen One Shear Stress Distribution in Inelastic Range at Upper Section of Panel (Drift = 0.02)

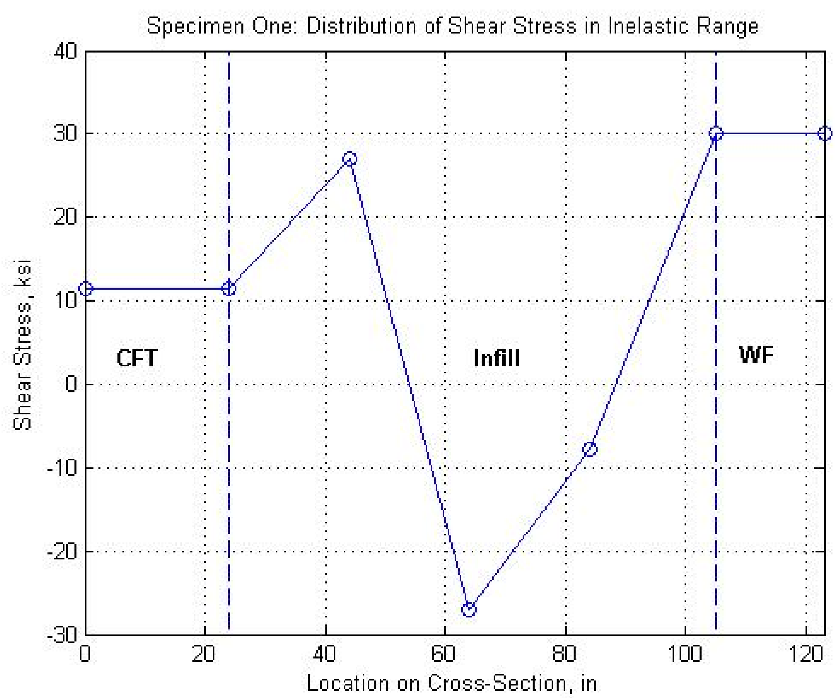

Figure 3.74: Specimen One Shear Stress Distribution in Inelastic Range at Lower Section of Panel (Drift = 0.02)

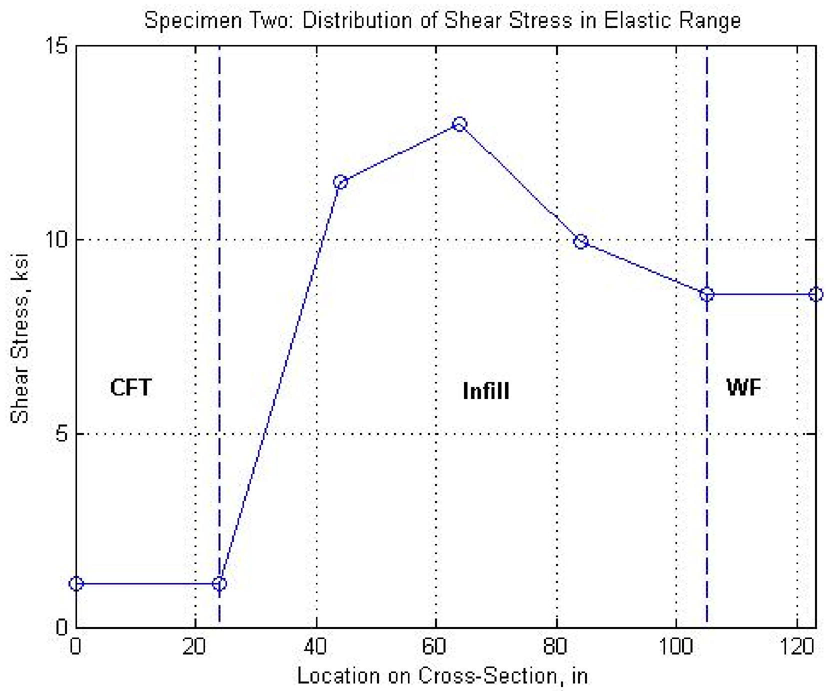

Figure 3.75: Specimen Two Shear Stress Distribution in Elastic Range at Top Section of Panel (Drift = 0.004)

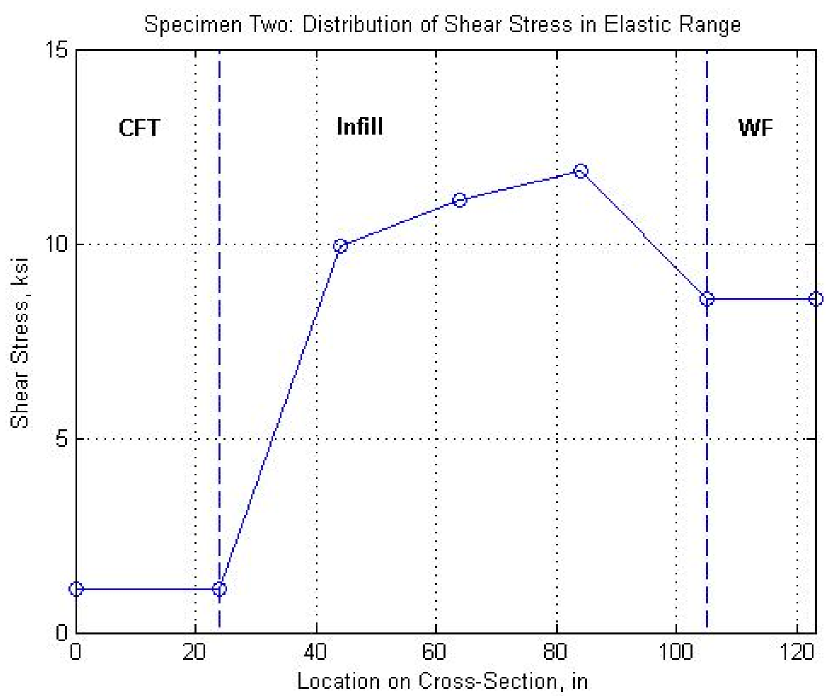

Figure 3.76: Specimen Two Shear Stress Distribution in Elastic Range at Bottom Section of Panel (Drift = 0.004)

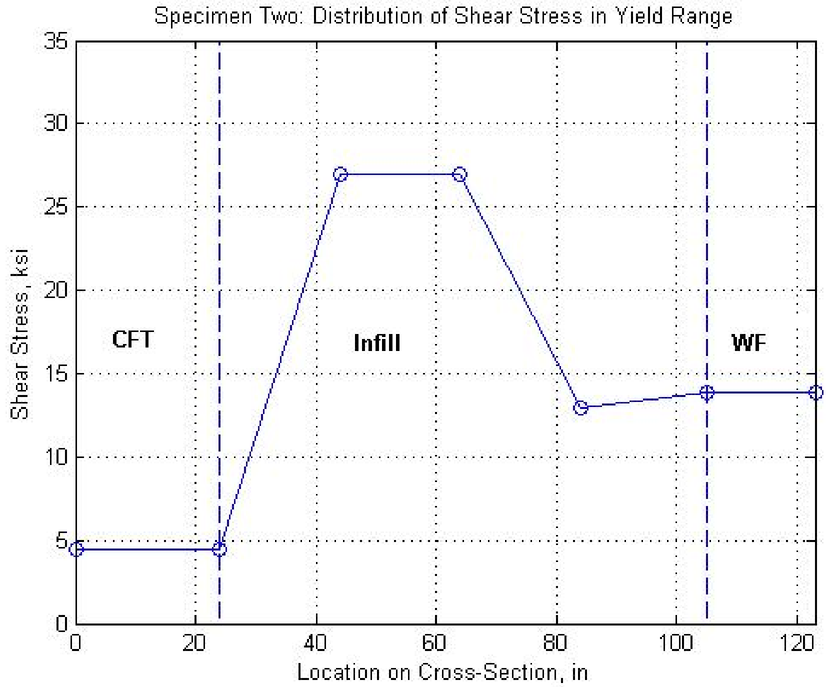

Figure 3.77: Specimen Two Shear Stress Distribution in Yield Range at Top Section of Panel (Drift = 0.006)

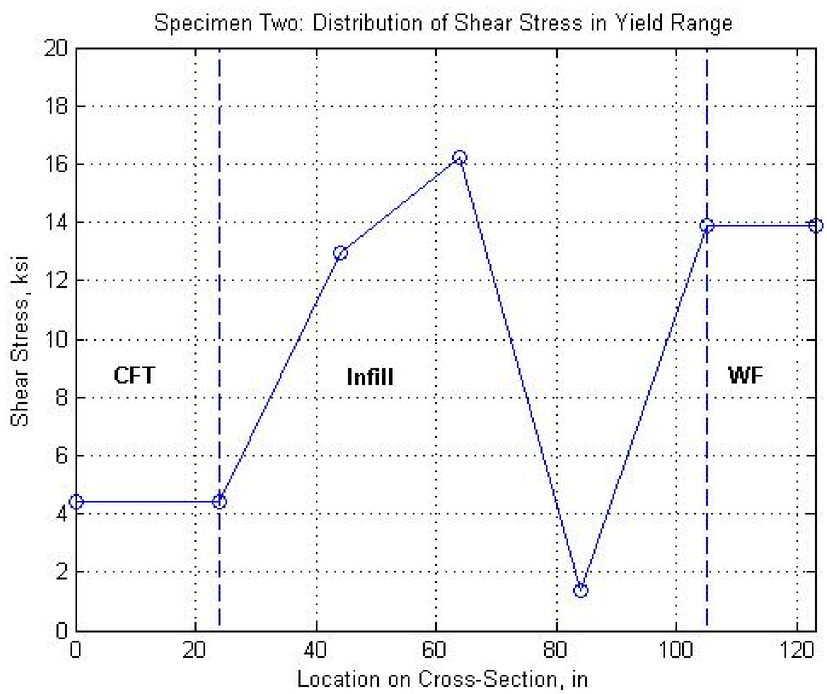

Figure 3.78: Specimen Two Shear Stress Distribution in Yield Range at Bottom Section of Panel (Drift = 0.006)

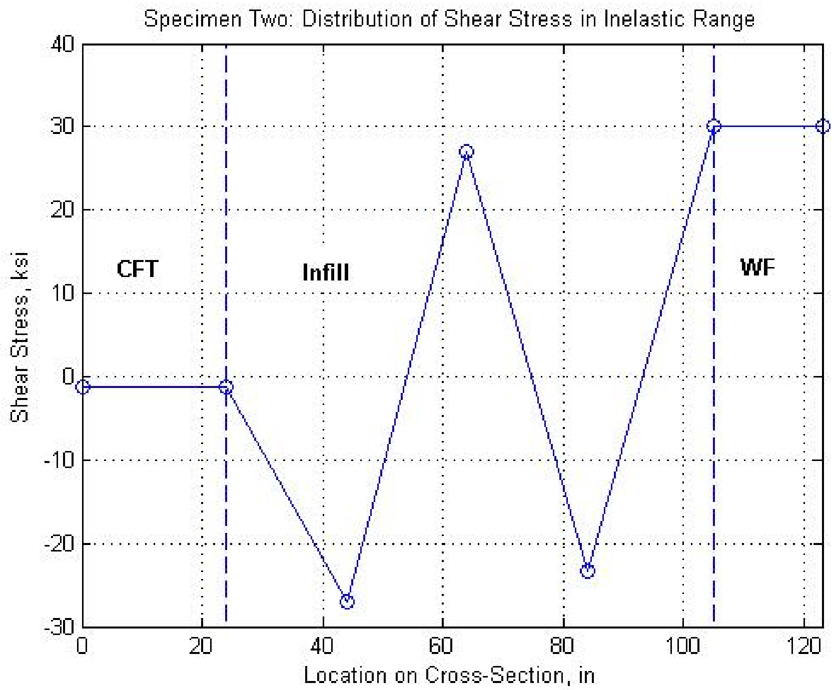

Figure 3.79: Specimen Two Shear Stress Distribution in Inelastic Range at Top of Plate (Drift = 0.02)

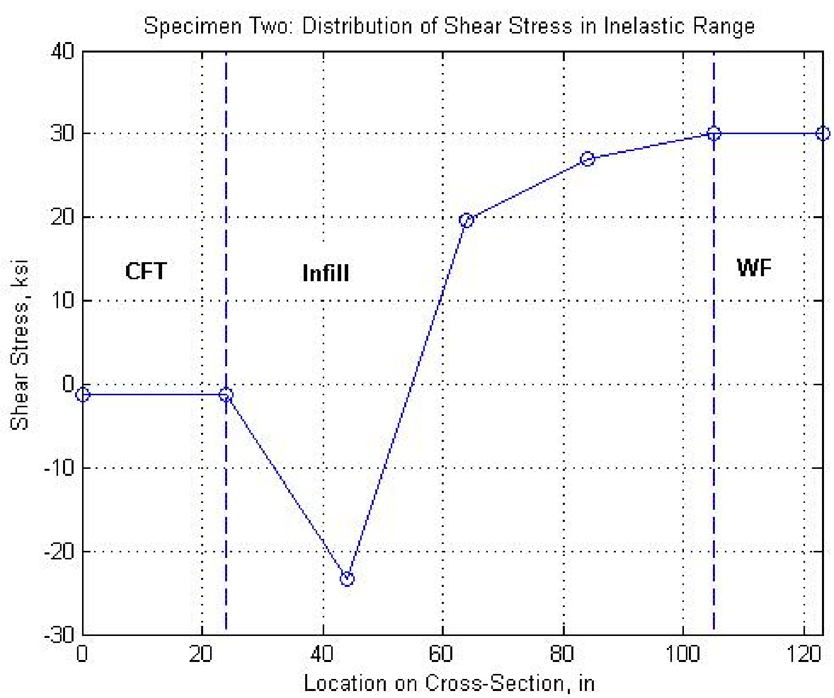

Figure 3.80: Specimen Two Shear Stress Distribution in Inelastic Range at Bottom of Plate (Drift = 0.02)

Table 3.6: Specimen One Shear Forces and Percentages taken by Components when Actuator moves to Right

Overall Drift	V_{BASE}, kip	V_{CFT}, kip	V_{CFT}/ V_{BASE}, %	Top Cross-Section					Bottom Cross-Section				
				V_{infill}, kip	%	V_{WF}, kip	%	% Total	V_{infill}, kip	%	V_{WF}, kip	%	% Total
0.00075	88	11.9	13.6	52.6	59.9	9.5	10.8	84.3	56.5	64.4	11.9	13.6	91.6
0.001	114	13.8	12.1	69.9	61.4	13.7	12.0	85.5	76.8	67.4	16.6	14.6	94.1
0.0015	166	19.1	11.5	101.1	60.8	22.3	13.4	85.7	111.2	66.9	24.6	14.8	93.2
0.002	227	24.4	10.8	133.8	59.1	36.8	16.2	86.1	147.2	65.0	34.1	15.1	90.8
0.0025	287	41.5	14.4	166.3	57.9	49.4	17.2	89.5	182.9	63.6	43.9	15.3	93.3
0.003	344	52.7	15.3	198.5	57.8	61.3	17.8	91.0	208.2	60.6	53.0	15.4	91.4
0.0035	408	81.8	20.0	228.5	56.0	72.1	17.7	93.7	243.9	59.8	62.6	15.3	95.2
0.004	468	106.8	22.8	263.2	56.2	85.0	18.2	97.2	263.9	56.4	73.7	15.7	94.9
0.0045	532	116.7	21.9	146.3	27.5	93.2	17.5	66.9	375.6	70.6	81.6	15.3	107.8
0.005	580	133.8	23.1	194.0	33.4	105.8	18.2	74.7	385.8	66.5	91.1	15.7	105.2
0.0055*	555	149.0	26.9	274.7	49.5	135.1	24.4	100.8	384.6	69.3	102.3	18.4	114.7
0.006	585	171.4	29.3	378.7	64.8	152.8	26.1	120.2	450.6	77.1	110.5	18.9	125.3
0.0065	607	199.1	32.8	364.8	60.1	168.0	27.7	120.5	453.4	74.7	115.4	19.0	126.4
0.007	599	242.0	40.4	227.3	38.0	156.5	26.1	104.5	458.6	76.6	125.8	21.0	138.0
0.008	654	290.1	44.4	479.3	73.3	189.3	28.9	146.6	464.6	71.0	138.2	21.1	136.5
0.009	695	324.4	46.7	488.3	70.3	214.9	30.9	147.9	329.2	47.4	148.6	21.4	115.5
0.010	717	365.3	51.0	492.5	68.7	221.9	31.0	150.7	365.3	51.0	152.3	21.3	123.2
0.011	737	399.6	54.3	496.2	67.4	228.9	31.1	152.7	351.3	47.7	162.9	22.1	124.1
0.012	751	427.6	57.0	499.1	66.5	233.7	31.1	154.6	131.8	17.6	59.2	7.9	82.4
0.014	774	466.9	60.3	503.8	65.1	243.9	31.5	156.8	121.1	15.6	64.2	8.3	84.2
0.016	790	507.0	64.2	507.4	64.3	248.6	31.5	160.0	82.1	10.4	74.1	9.4	84.0
0.018	796	466.9	58.7	505.1	63.5	247.6	31.1	153.2	70.3	8.8	84.8	10.7	78.1
0.020	801	498.0	62.2	503.1	62.8	235.3	29.4	154.4	119.6	14.9	109.6	13.7	90.8
0.022	809	513.1	63.5	235.3	29.1	252.0	31.2	123.7	114.2	14.1	118.8	14.7	92.3
0.024	814	524.3	64.4	236.6	29.1	254.6	31.3	124.8	114.6	14.1	129.5	15.9	94.4
0.026	803	540.4	67.3	236.0	29.4	249.5	31.1	127.7	103.2	12.8	126.9	15.8	95.9
0.028	693	554.2	80.0	222.8	32.2	201.0	29.0	141.2	93.4	13.5	178.7	25.8	119.3
0.030	540	511.5	94.7	199.1	36.9	125.7	23.3	154.9	55.5	10.3	265.0	49.1	154.1

***Significant Yield Point according to testing notes**

Table 3.7: Specimen One Shear Forces and Percentages taken by Components when Actuator moves to Left

Drift	V_{BASE}, kip	V_{CFT}, kip	V_{CFT}/ V_{BASE}, %	Top Cross-Section					Bottom Cross-Section				
				V_{infill}, kip	%	V_{WF}, kip	%	% Total	V_{infill}, kip	%	V_{WF}, kip	%	% Total
0.00075	81	7.2	8.9	53.7	66.0	12.3	15.1	89.9	53.5	65.7	11.8	14.5	89.1
0.001	112	2.0	1.8	72.0	64.5	16.2	14.5	80.7	73.0	65.3	15.9	14.2	81.3
0.0015	170	9.2	5.4	108.6	63.9	24.6	14.5	83.7	110.3	64.9	24.9	14.6	84.9
0.002	235	17.1	7.3	145.5	61.9	35.6	15.1	84.3	149.6	63.6	36.7	15.6	86.5
0.0025	301	28.3	9.4	177.0	58.8	46.4	15.4	83.6	194.9	64.8	47.9	15.9	90.1
0.003	363	36.3	10.0	208.7	57.5	56.4	15.5	83.1	244.3	67.3	59.1	16.3	93.6
0.0035	422	38.9	9.2	235.9	55.9	65.5	15.5	80.7	302.9	71.8	67.5	16.0	97.0
0.004	483	58.0	12.0	271.5	56.2	76.7	15.9	84.1	346.8	71.8	78.7	16.3	100.1
0.0045	535	65.3	12.2	345.4	64.6	83.6	15.6	92.4	248.5	46.4	88.1	16.5	75.1
0.005	581	80.4	13.8	372.2	64.1	94.6	16.3	94.2	274.4	47.2	97.2	16.7	77.8
0.0055*	572	122.6	21.4	447.6	78.3	109.0	19.0	118.7	109.0	19.0	127.1	22.2	62.7
0.006	596	141.8	23.8	451.5	75.8	119.1	20.0	119.5	152.6	25.6	143.7	24.1	73.5
0.0065	614	154.9	25.2	180.4	29.4	124.7	20.3	74.9	204.7	33.3	154.9	25.2	83.8
0.007	631	178.1	28.2	182.4	28.9	127.3	20.2	77.3	226.8	35.9	153.5	24.3	88.5
0.008	664	209.1	31.5	187.5	28.3	139.8	21.1	80.8	103.8	15.6	162.1	24.4	71.6
0.009	695	240.6	34.6	200.4	28.8	153.9	22.2	85.6	122.2	17.6	176.0	25.3	77.6
0.010	720	272.4	37.8	347.9	48.3	168.1	23.3	109.5	51.0	7.1	185.0	25.7	70.6
0.011	745	298.0	40.0	344.0	46.2	176.9	23.7	109.9	42.0	5.6	265.0	35.6	81.2
0.012	768	329.9	43.0	340.5	44.3	183.5	23.9	111.2	7.9	1.0	265.0	34.5	78.5
0.014	806	376.6	46.8	336.1	41.7	190.5	23.6	112.1	28.6	3.5	265.0	32.9	83.2
0.016	841	427.9	50.9	333.9	39.7	189.1	22.5	113.1	94.8	11.3	265.0	31.5	93.7
0.018	863	548.6	63.6	326.4	37.8	193.3	22.4	123.8	122.5	14.2	265.0	30.7	108.5
0.020	889	579.5	65.2	323.5	36.4	197.9	22.3	123.9	75.8	8.5	265.0	29.8	103.5
0.022	902	614.5	68.1	51.5	5.7	186.7	20.7	94.5	19.3	2.1	265.0	29.4	99.6
0.024	917	638.8	69.6	55.7	6.1	167.9	18.3	94.0	171.5	18.7	265.0	28.9	117.2
0.026	902	678.9	75.3	59.0	6.5	149.0	16.5	98.3	5.9	0.7	264.7	29.3	105.3
0.028	761	705.2	92.6	17.4	2.3	97.1	12.7	107.6	4.1	0.5	265.0	34.8	128.0
0.030	559	791.2	141.5	80.6	14.4	53.5	9.6	165.4	26.4	4.7	137.3	24.6	170.7

***Significant Yield Point according to testing notes**

Table 3.8: Specimen Two Shear Forces and Percentages taken by Components when Actuator Moves to Right

Drift	V_{BASE}, kip	V_{CFT}, kip	V_{CFT}/ V_{BASE}, %	First Story Cross-Section					Second Story Cross-Section				
				V_{infill}, kip	%	V_{WF}, kip	%	% Total	V_{infill}, kip	%	V_{WF}, kip	%	% Total
0.00075	103	17.2	16.7	60.4	58.6	12.0	11.7	92.0	60.1	58.3	17.5	17.0	86.9
0.001	135	29.1	21.5	82.2	60.7	17.3	12.7	97.3	81.3	60.1	21.3	15.8	94.9
0.0015	205	41.5	20.3	122.7	59.9	25.7	12.5	99.6	125.6	61.3	37.0	18.0	92.7
0.002	274	58.6	21.4	165.2	60.3	34.3	12.5	105.1	175.5	64.0	54.0	19.7	94.1
0.0025	355	58.0	16.3	204.1	57.6	42.8	12.1	100.2	225.5	63.6	71.8	20.3	86.0
0.003	419	81.7	19.5	243.3	58.0	52.6	12.5	104.4	269.6	64.3	86.4	20.6	90.0
0.0035	491	108.7	22.2	281.4	57.3	62.4	12.7	108.4	320.8	65.4	102.1	20.8	92.2
0.004	561	125.9	22.4	322.9	57.6	72.2	12.9	109.5	369.3	65.8	118.9	21.2	92.9
0.0045	630	143.1	22.7	354.4	56.2	84.4	13.4	110.0	415.7	66.0	134.6	21.4	92.3
0.005	698	165.5	23.7	395.6	56.7	97.8	14.0	111.8	465.1	66.6	149.5	21.4	94.4
0.0055	753	178.6	23.7	429.7	57.1	112.1	14.9	112.3	507.8	67.4	159.2	21.1	95.7
0.006	811	201.0	24.8	464.4	57.3	123.8	15.3	114.5	557.2	68.7	170.1	21.0	97.3
0.0065	782	207.8	26.6	480.7	61.5	156.3	20.0	115.3	536.3	68.6	157.1	20.1	108.1
0.007*	876	243.8	27.8	295.8	33.8	160.0	18.3	119.3	630.0	72.0	170.7	19.5	79.9
0.008	946	336.2	35.5	508.8	53.8	161.3	17.0	101.2	437.7	46.3	183.7	19.4	106.4
0.009	962	436.7	45.4	389.3	40.5	156.4	16.3	118.8	522.3	54.3	183.3	19.1	102.1
0.010	988	557.6	56.4	555.5	56.2	185.7	18.8	136.2	593.8	60.1	194.2	19.7	131.5
0.011	970	678.4	69.9	483.4	49.8	188.6	19.4	107.3	324.7	33.5	38.1	3.9	139.2
0.012	987	760.9	77.1	448.5	45.4	265.0	26.8	118.5	170.0	17.2	238.5	24.2	149.4
0.014	1018	587.2	57.7	282.4	27.8	265.0	26.0	100.6	198.1	19.5	238.5	23.4	111.5
0.016	1037	702.6	67.7	158.3	15.3	224.2	21.6	107.4	172.5	16.6	238.5	23.0	104.6
0.018	1073	598.3	55.8	78.3	7.3	254.4	23.7	94.2	173.7	16.2	238.5	22.2	86.8
0.020	1097	292.5	26.7	285.0	26.0	264.5	24.1	57.2	95.9	8.7	238.5	21.7	76.8
0.022	1085	316.1	29.1	49.9	4.6	265.0	24.4	57.8	72.6	6.7	238.5	22.0	58.2
0.024	1056	337.0	31.9	62.7	5.9	265.0	25.1	62.2	81.2	7.7	238.5	22.6	62.9
0.026	1029	310.5	30.2	143.0	13.9	253.0	24.6	59.2	60.1	5.8	238.5	23.2	68.7
0.028	763	325.1	42.6	235.0	30.8	265.0	34.7	79.9	46.2	6.1	238.5	31.3	108.2
0.030	769	324.2	42.2	232.0	30.2	255.7	33.3	79.2	46.1	6.0	238.5	31.0	105.6

*Significant Yield Point according to testing notes

Table 3.9: Specimen Two Shear Forces and Percentages taken by Components when Actuator Moves to Left

Drift	V_{BASE}, kip	V_{CFT}, kip	V_{CFT}/ V_{BASE}, %	First Story Cross-Section					Second Story Cross-Section				
				V_{infill}, kip	%	V_{WF}, kip	%	% Total	V_{infill}, kip	%	V_{WF}, kip	%	% Total
0.00075	96	3.3	3.4	51.5	53.5	11.0	11.4	87.6	59.8	62.2	21.2	22.1	68.3
0.001	136	0.6	0.4	71.0	52.3	16.1	11.9	82.4	81.9	60.3	29.4	21.7	64.6
0.0015	209	0.8	0.4	111.7	53.4	24.6	11.7	80.5	123.5	59.0	44.2	21.1	65.5
0.002	300	10.6	3.5	158.6	52.9	39.2	13.1	81.6	173.1	57.7	61.1	20.4	69.5
0.0025	387	28.5	7.4	203.5	52.6	51.0	13.2	83.9	219.1	56.6	77.1	19.9	73.1
0.003	466	35.1	7.5	244.2	52.5	63.0	13.5	84.0	264.4	56.8	91.8	19.7	73.5
0.0035	551	54.2	9.8	286.6	52.0	75.8	13.7	86.0	311.9	56.6	108.2	19.6	75.5
0.004	632	70.0	11.1	329.9	52.2	86.9	13.8	87.0	357.8	56.6	121.7	19.3	77.1
0.0045	705	89.1	12.6	368.6	52.3	96.4	13.7	87.5	395.3	56.1	132.9	18.8	78.6
0.005	775	108.9	14.1	412.7	53.3	106.0	13.7	88.6	434.4	56.1	143.4	18.5	81.0
0.0055	836	119.3	14.3	449.9	53.8	108.6	13.0	88.6	468.3	56.0	152.7	18.3	81.1
0.006	900	139.2	15.5	482.0	53.6	112.9	12.5	89.4	505.1	56.1	160.0	17.8	81.6
0.0065	914	171.2	18.7	511.7	56.0	112.4	12.3	91.9	515.3	56.4	153.3	16.8	87.0
0.007*	943	191.9	20.4	327.1	34.7	119.5	12.7	49.7	126.7	13.4	150.1	15.9	67.7
0.008	936	262.2	28.0	411.6	44.0	118.0	12.6	123.1	711.7	76.1	177.6	19.0	84.6
0.009	981	289.7	29.5	428.9	43.7	146.5	14.9	83.0	331.0	33.7	193.7	19.7	88.2
0.010	1019	264.6	26.0	382.2	37.5	165.7	16.3	112.7	695.7	68.3	188.0	18.4	79.7
0.011	1039	239.6	23.1	44.6	4.3	166.1	16.0	47.5	15.5	1.5	238.5	23.0	43.3
0.012	1069	256.6	24.0	67.7	6.3	103.8	9.7	63.2	180.7	16.9	238.5	22.3	40.1
0.014	1119	535.4	47.8	336.9	30.1	104.2	9.3	85.1	178.9	16.0	238.5	21.3	87.2
0.016	1162	301.2	25.9	79.3	6.8	265.0	22.8	66.5	232.9	20.0	238.5	20.5	55.5
0.018	1209	147.3	12.2	153.9	12.7	265.0	21.9	39.5	91.1	7.5	238.6	19.7	46.8
0.020	1241	365.1	29.4	301.6	24.3	265.0	21.4	59.0	128.8	10.4	238.5	19.2	75.1
0.022	1226	449.6	36.7	169.4	13.8	265.0	21.6	66.1	122.4	10.0	238.5	19.5	72.1
0.024	1091	521.0	47.8	222.6	20.4	265.0	24.3	80.2	115.7	10.6	238.5	21.9	92.5
0.026	1069	522.4	48.9	274.1	25.6	265.0	24.8	82.6	121.9	11.4	238.5	22.3	99.3
0.028	1063	383.0	36.0	278.0	26.2	265.0	24.9	72.2	145.6	13.7	238.5	22.4	87.1
0.030	1052	267.1	25.4	130.4	12.4	264.9	25.2	64.2	169.9	16.2	238.5	22.7	63.0

*Significant Yield Point according to testing notes

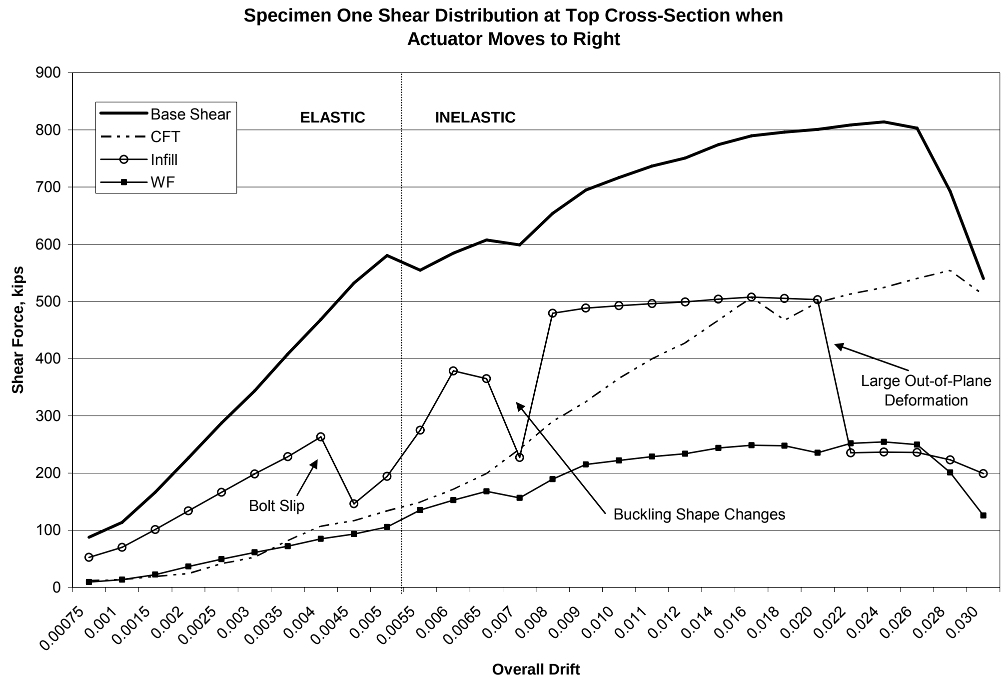

Figure 3.81: Specimen One Shear Distribution for Top Cross-Section when Actuator Moves to Right

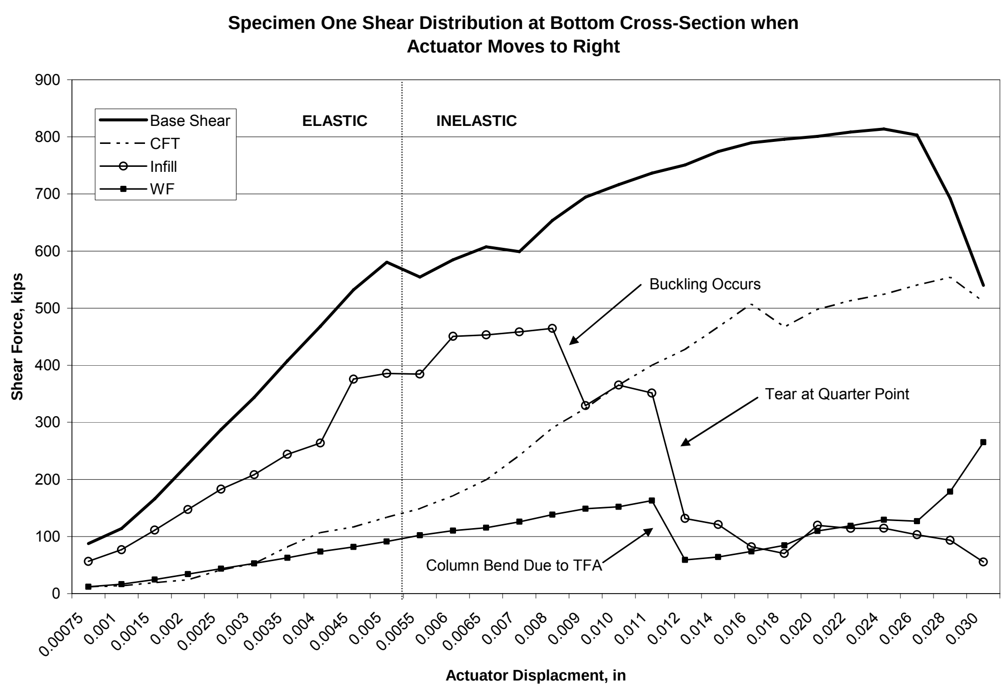

Figure 3.82: Specimen One Shear Distribution for Bottom Cross-Section when Actuator Moves to Right

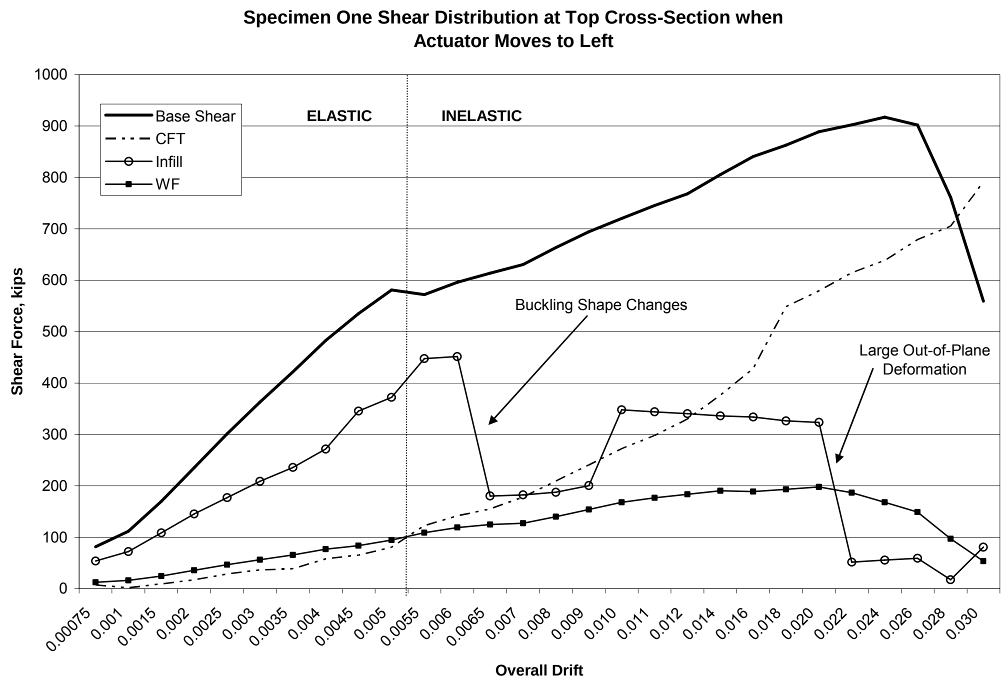

Figure 3.83: Specimen One Shear Distribution for Top Cross-Section when Actuator Moves to Left

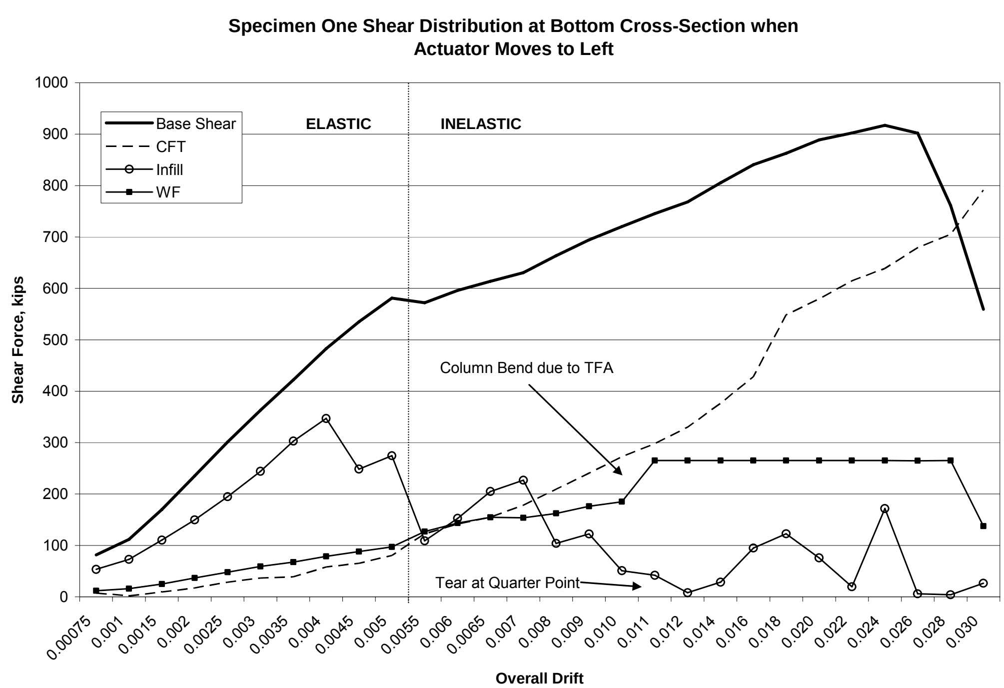

Figure 3.84: Specimen One Shear Distribution for Bottom Cross-Section when Actuator Moves to Left

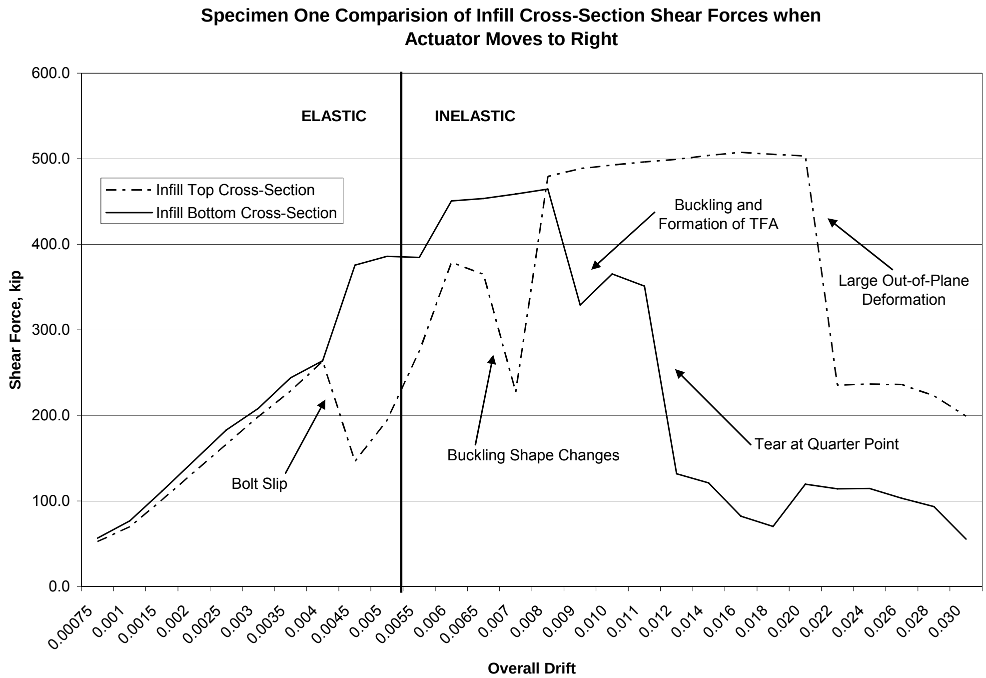

Figure 3.85: Specimen One Infill Comparison when Actuator Moves to Right

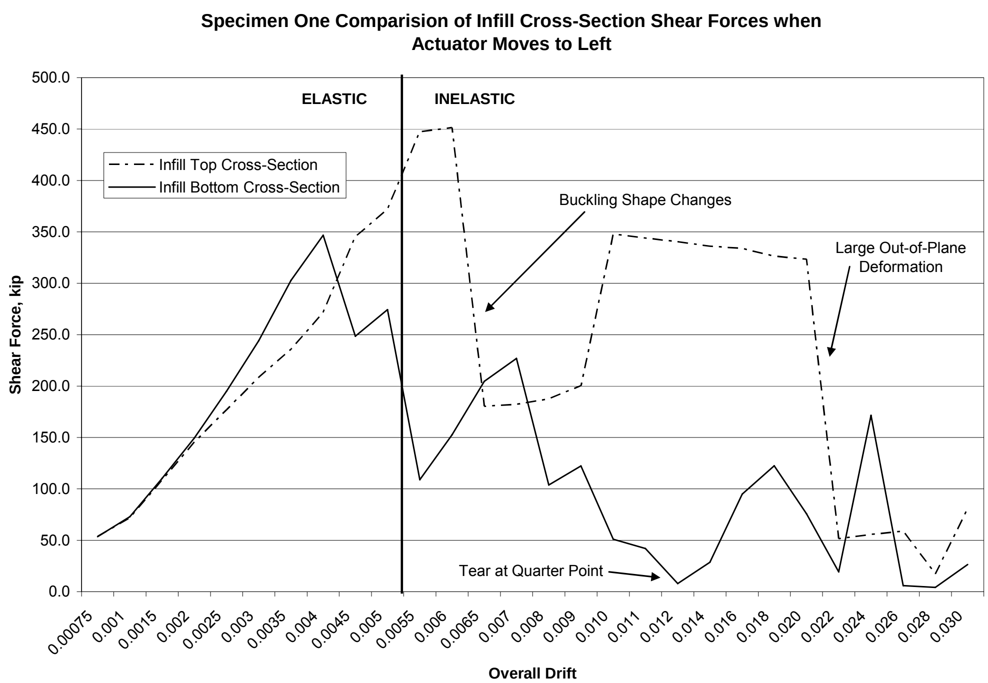

Figure 3.86: Specimen One Infill Comparison when Actuator Moves to Left

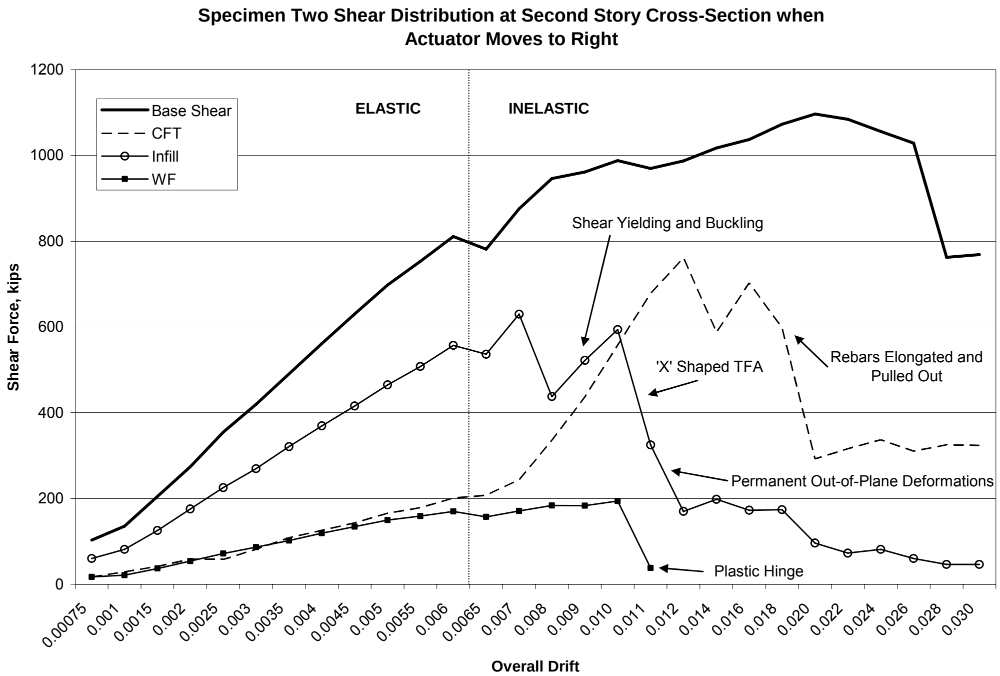

Figure 3.87: Specimen Two Shear Distribution for Second Story when Actuator Moves to Right

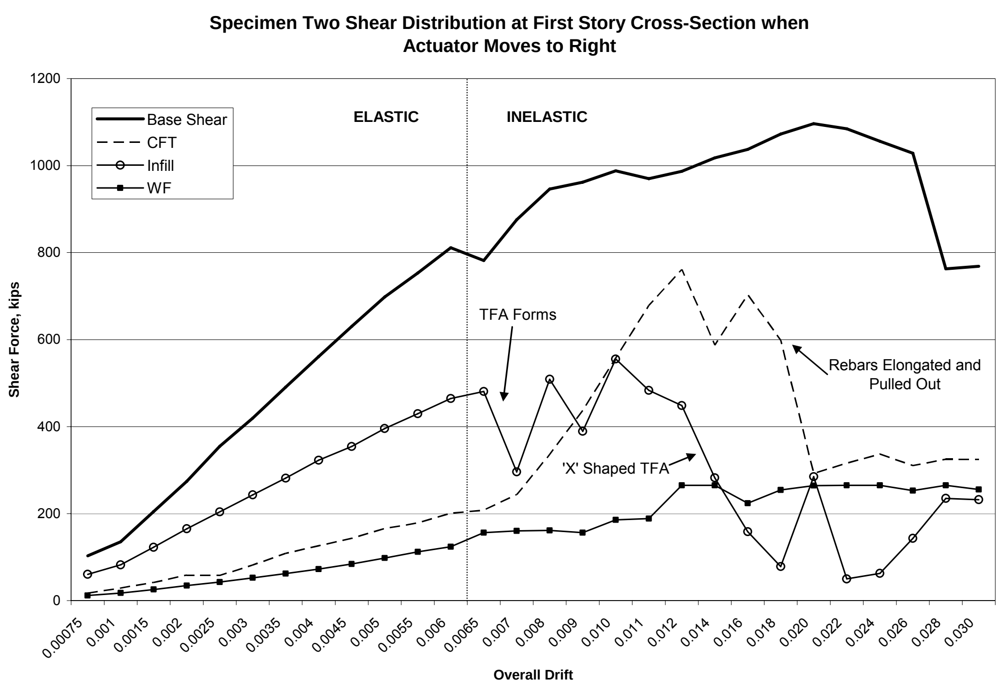

Figure 3.88: Specimen Two Shear Distribution for First Story when Actuator Moves to Right

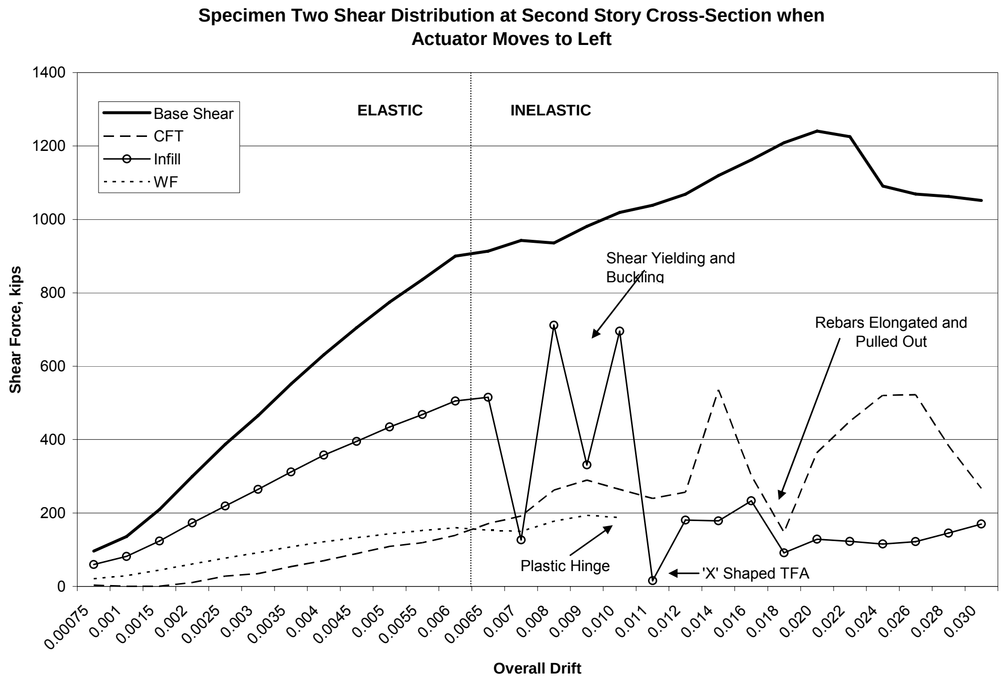

Figure 3.89: Specimen Two Shear Distribution for Second Story when Actuator Moves to Left

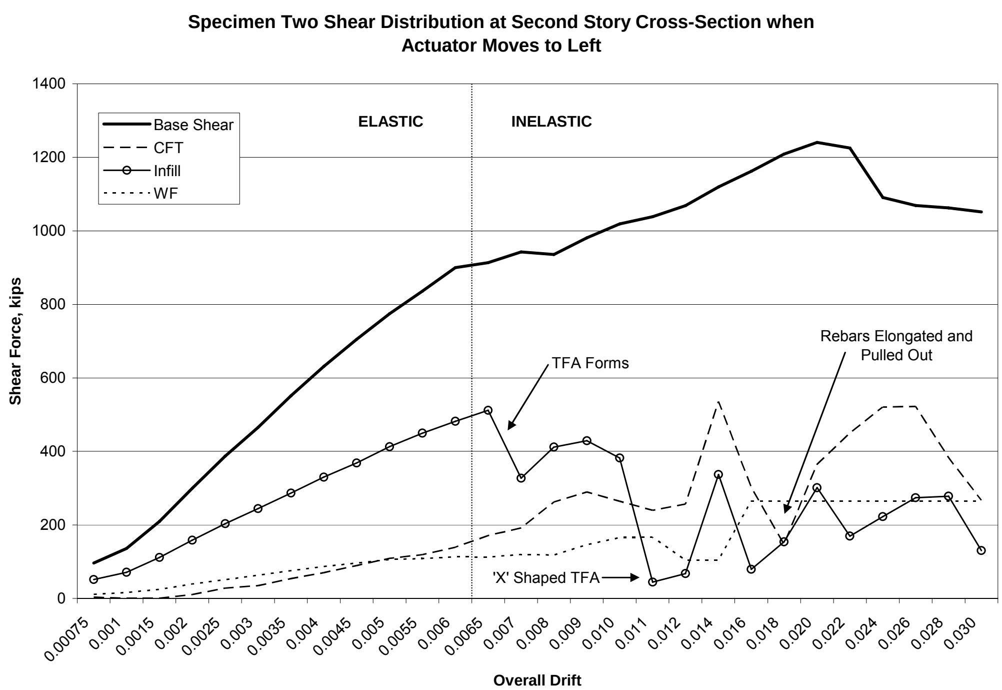

Figure 3.90: Specimen Two Shear Distribution for First Story when Actuator Moves to Left

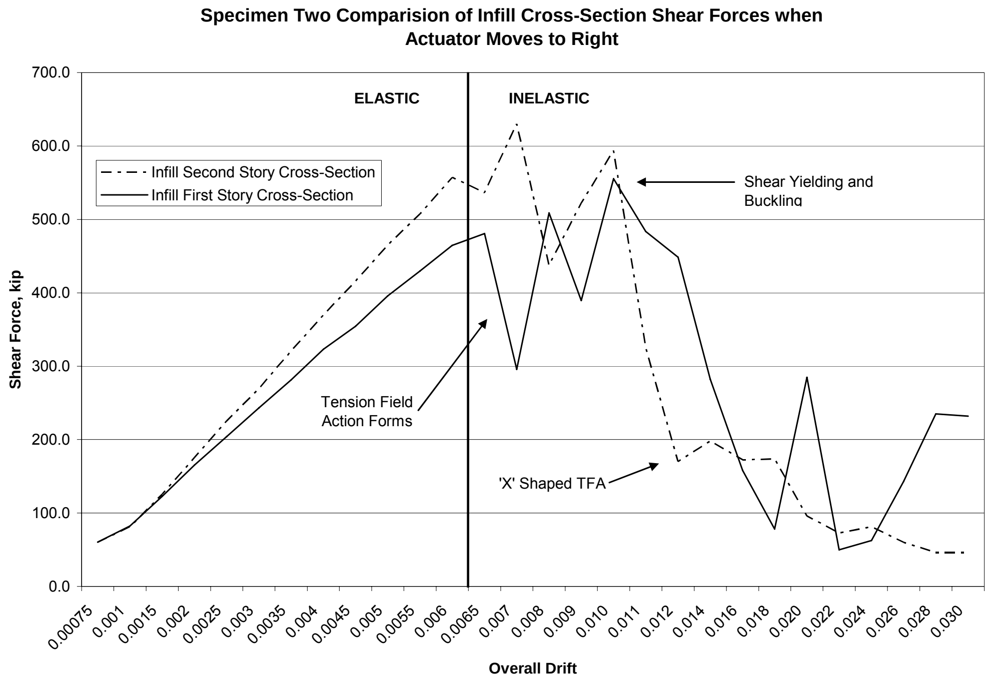

Figure 3.91: Specimen Two Infill Comparison when Actuator Moves to Right

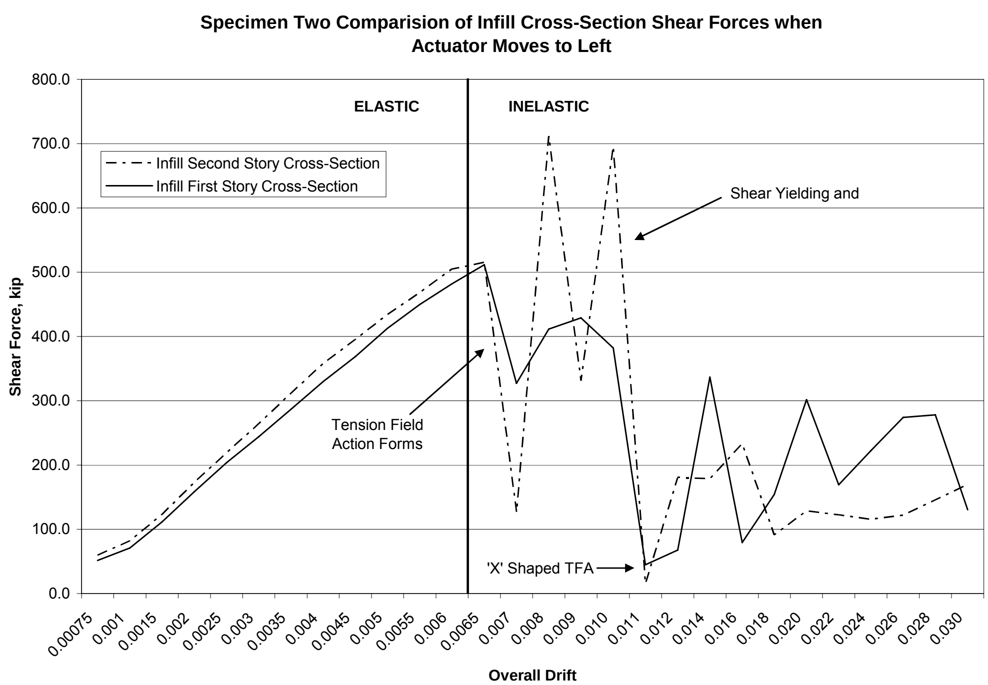

Figure 3.92: Specimen Two Infill Comparison when Actuator Moves to Left

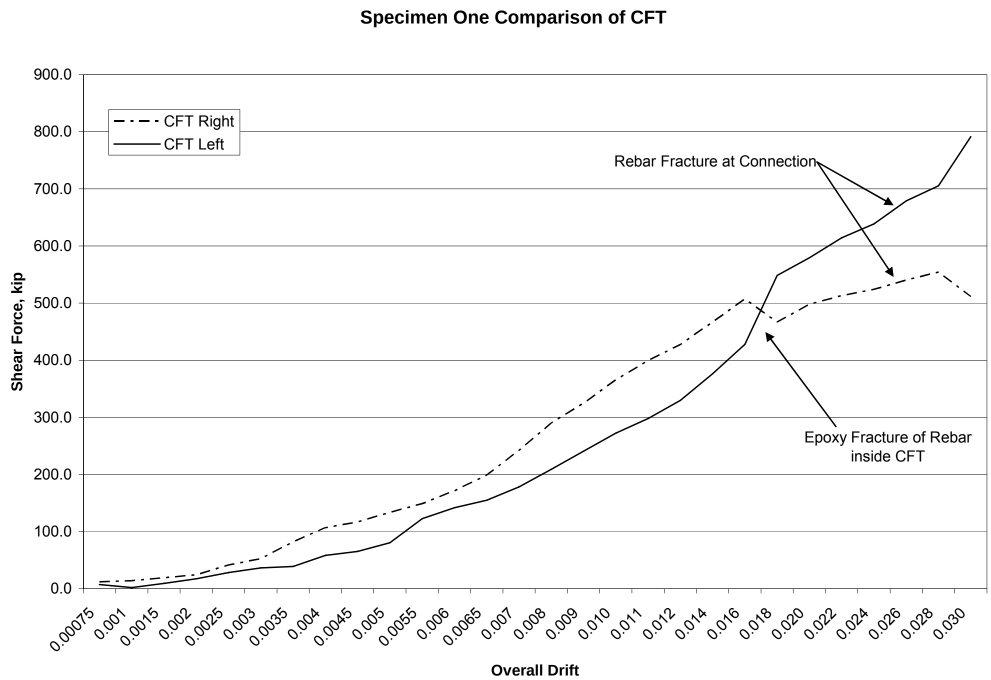

Figure 3.93: Specimen One CFT Comparison

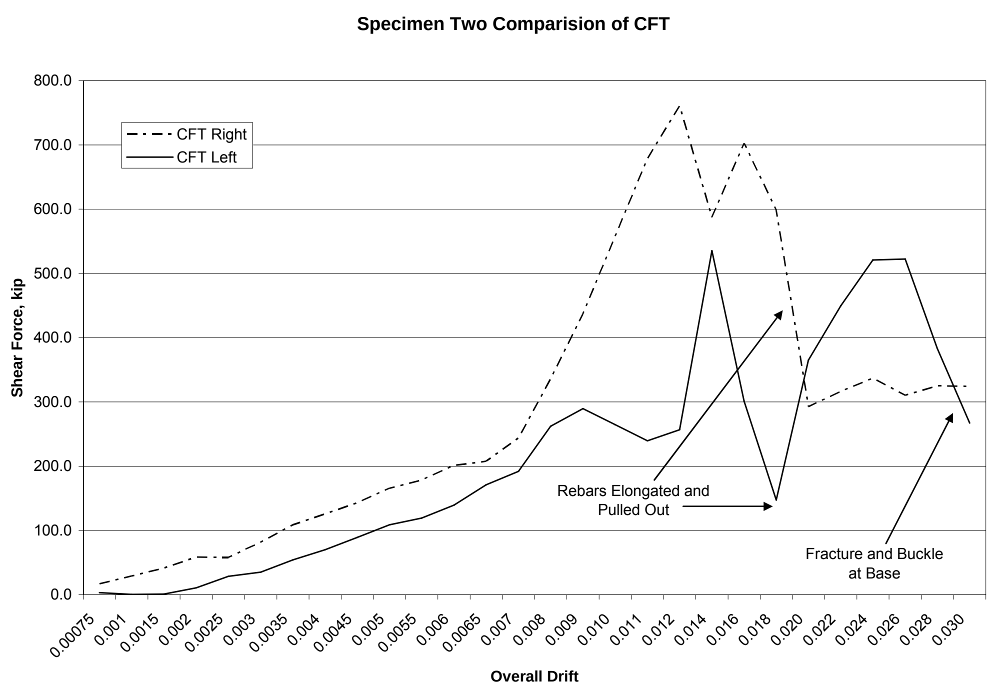

Figure 3.94: Specimen Two CFT Comparison

Table 3.10: Comparison of Experimental vs. Analytical Shear Wall Capacity

Shear Capacity of Steel Wall	Specimen One	Specimen Two
AISC Specifications for Plate Girder	283 kips	590 kips
AISC Specifications for Special Steel Plate Walls	425 kips	649 kips
Experimental Results (V_{BASE} - V_{CFT} – V_{WF})	356 kips	540 kips
Experimental Results (V_{infill} max at yield)	448 kips	630 kips

APPENDIX B: SAMPLE CALCULATIONS AND EQUATIONS

Shear Calculations for CFT
*All equations according to Appendix D, Mechanics of Materials, Gere

Steel Tube:

$$G = \frac{E}{2(1+\nu)} = \frac{29000ksi}{2(1+0.3)} = 11153.8ksi$$

$$A = \pi rt = \pi(11.843in)\left(\tfrac{5}{16}in\right) = 11.63in^2$$

$$\bar{y} = \frac{r\sin\beta}{\beta} = \frac{11.843in\sin\left(\frac{\pi}{2}\right)}{\frac{\pi}{2}} = 7.54in$$

$$I = \frac{\pi d^3 t}{8} = \frac{\pi(23.6875in)^3\left(\tfrac{5}{16}in\right)}{8} = 1631.1in^4$$

$$Q = A\bar{y} = 11.63in^2(7.54in) = 87.7in^3$$

$$V = \frac{\tau Ib}{Q} = \frac{1631.1in^4(2)\left(\tfrac{5}{16}in\right)}{87.7in^3}\tau = 11.63\tau$$

Concrete Infill:

$$G = \frac{E}{2(1+\nu)} = \frac{57\sqrt{3000}ksi}{2(1+0.2)} = 1300.8ksi$$

$$A = \frac{\pi r^2}{2} = \frac{\pi(11.6875in)^2}{2} = 214.57in^2$$

$$\bar{y} = \frac{4r}{3\pi} = \frac{4(11.6875)}{3\pi} = 4.96in$$

$$I = \frac{\pi r^4}{8} = \frac{\pi(11.6875in)^4}{8} = 14654.7in^4$$

$$Q = A\bar{y} = 214.57in^2(4.96in) = 1064.3in^3$$

$$V = \frac{\tau Ib}{Q} = \frac{14654.7in^4(23.375in)}{1064.3in^3}\tau = 321.9\tau$$

AISC Code – Plate Girder

Specimen One

A_w = 81 in * 0.25 in = 20.25 in^2
a = 10' = 120"
h = 81"
t_w = 0.25"

$$a/h = \frac{120"}{81"} = 1.481 \geq \left[\frac{260}{h/t_w}\right]^2 = \left[\frac{260}{81"/0.25"}\right]^2 = 0.6434$$

$$\therefore k_v = 5$$

$$1.10\sqrt{\frac{k_v E}{F_y}} = 1.10\sqrt{\frac{5(29{,}000ksi)}{36ksi}} = 69.81$$

$$1.37\sqrt{\frac{k_v E}{F_y}} = 1.37\sqrt{\frac{5(29{,}000ksi)}{36ksi}} = 86.95 \leq \frac{h}{t_w} = \frac{81"}{0.25"} = 324$$

$$\therefore C_v = \frac{1.51Ek_v}{\left(h/t_w\right)^2 F_y} = \frac{1.51(29{,}000ksi)(5)}{\left(81"/0.25"\right)^2(36ksi)} = 0.05794$$

$$V_n = 0.6F_y A_w\left(C_v + \frac{1-C_v}{1.15\sqrt{1+\left(a/h\right)^2}}\right) = 0.6(45ksi)(20.25in^2)\left(0.05794 + \frac{1-0.05794}{1.15\sqrt{1+\left(120"/81"\right)^2}}\right) =$$

$$V_n = 282.3kip$$

Specimen Two

A_w = 81 in * 0.375 in = 30.375 in^2
a = 6'8" = 80"
h = 81"
t_w = 0.375"

$$a/h = \frac{80''}{81''} = 0.9877 \le \left[\frac{260}{h/t_w}\right]^2 = \left[\frac{260}{81''/0.375''}\right]^2 = 1.4489$$

$$\therefore k_v = 5 + \frac{5}{\left(a/h\right)^2} = 5 + \frac{5}{\left(80''/81''\right)^2} = 10.13$$

$$1.10\sqrt{\frac{k_v E}{F_y}} = 1.10\sqrt{\frac{10.13(29{,}000ksi)}{36ksi}} = 99.37$$

$$1.37\sqrt{\frac{k_v E}{F_y}} = 1.37\sqrt{\frac{10.13(29{,}000ksi)}{36ksi}} = 123.76 \le \frac{h}{t_w} = \frac{81''}{0.375''} = 216$$

$$\therefore C_v = \frac{1.51Ek_v}{\left(h/t_w\right)^2 F_y} = \frac{1.51(29{,}000ksi)(10.13)}{\left(81''/0.375''\right)^2(36ksi)} = 0.2641$$

$$V_n = 0.6F_y A_w\left(C_v + \frac{1-C_v}{1.15\sqrt{1+\left(a/h\right)^2}}\right) = 0.6(45ksi)(30.375in^2)\left(0.2641 + \frac{1-0.2641}{1.15\sqrt{1+\left(80''/81''\right)^2}}\right) =$$

$$V_n = 590.0kip$$

AISC Code – SPSW

Specimen one

2 CFT's
t_w = .25 in
h = 10' = 120"
A_b = 25.3 in^2
A_c = 452.4 in^2
I_c = 16286 in^4
L_{cf} = 8'6" = 102"

$$\tan^4\alpha = \frac{1+\dfrac{0.25''(102'')}{2(452.4in^2)}}{1+0.25''(120'')\left[\dfrac{1}{25.3in^2}+\dfrac{(120'')^3}{360(16{,}286in^4)(102'')}\right]}$$

$$\alpha = 39.36°$$

$$V_n = 0.42F_y t_w L_{cf}\sin 2\alpha$$
$$V_n = 0.42(45ksi)(0.25'')(102'')\sin(2)(39.36°) = 472.6kips$$
$$\phi V_n = 0.9(472.6kips) = 425.4kips$$

2 W 18x86's
t_w = .25 in
h = 10' = 120"
A_b = 25.3 in^2
A_c = 25.3 in^2
I_c = 1530 in^4
L = 8'6" = 102"

$$\tan^4\alpha = \frac{1+\dfrac{0.25''(102'')}{2(25.3in^2)}}{1+0.25''(120'')\left[\dfrac{1}{25.3in^2}+\dfrac{(120'')^3}{360(1530in^4)(102'')}\right]}$$

$$\alpha = 39.83°$$

$$V_n = 0.42F_y t_w L_{cf}\sin 2\alpha$$
$$V_n = 0.42(45ksi)(0.25'')(102'')\sin(2)(39.83°) = 474.1kips$$
$$\phi V_n = 0.9(474.1kips) = 426.7kips$$

Specimen Two

2 CFT's
t_w = 0.375 in
h = 6'8" = 80"
A_b = 25.3 in^2
A_c = 452.4 in^2
I_c = 16286 in^4
L = 8'6" = 102"

$$\tan^4\alpha = \frac{1+\dfrac{0.375''(102'')}{2(452.4in^2)}}{1+0.375''(80'')\left[\dfrac{1}{25.3in^2}+\dfrac{(80'')^3}{360(16{,}286in^4)(102'')}\right]}$$
$$\alpha = 39.64°$$

$$V_n = 0.42F_y t_w L_{cf}\sin 2\alpha$$
$$V_n = 0.42(45ksi)(0.375'')(102'')\sin(2)(39.64°) = 710.3kips$$
$$\phi V_n = 0.9(710.3kips) = 639.3kips$$

2 W 18x86's
t_w = 0.375 in
h = 6'8" = 80"
A_b = 25.3 in^2
A_c = 25.3 in^2
I_c = 1530 in^4
L = 8'6" = 102"

$$\tan^4\alpha = \frac{1+\dfrac{0.375''(102'')}{2(25.3in^2)}}{1+0.375''(80'')\left[\dfrac{1}{25.3in^2}+\dfrac{(80'')^3}{360(1530in^4)(102'')}\right]}$$
$$\alpha = 42.59°$$

$$V_n = 0.42F_y t_w L_{cf}\sin 2\alpha$$
$$V_n = 0.42(45ksi)(0.375'')(102'')\sin(2)(42.59°) = 720.4kips$$
$$\phi V_n = 0.9(720.4kips) = 648.3kips$$

PART 4: **CONCLUSION**

4.1 Conclusions

Since the introduction of steel plate shear walls as an alternative to reinforced concrete shear walls for lateral load resisting systems, a significant amount of research has been conducted to investigate the behavior. In order to develop practical methods for design, it is important to fully understand and predict the behavior of a system. Past research has supplied important factors for consideration in steel plate shear wall design. Along with this knowledge covering traditional steel plate shear wall designs, new analysis has been completed focusing on the innovative design which integrates a concrete filled tube (CFT) column and the use of thin steel infill plates.

Steel plate shear walls have proved to be an excellent lateral load resisting system continuously performing in a stable and ductile manner. While the system is favorable, there are several areas of concern. Special attention is needed at the column base to prevent a premature failure due to buckling which has been the failure mode in numerous past experiments. Additional demands are placed on the frame elements after tension field action forms in the steel panels, so it is important to design beams and columns for these added internal forces. Connections have not shown to significantly affect the system capacity, but moment connections may be used to create a redundant system. Experimental results also show no significant difference in the use of welded or bolted connections for inserting the infill panels. Modeling techniques have been developed to a reasonable level of accuracy, so that engineers can implement this design. By accounting for the special considerations developed through experimentation and the modeling techniques suggested by researchers, steel plate shear walls can be practically applied by design engineers.

Expanding the concept of a steel plate shear wall, Magnusson Klemencic Associates developed the innovative design studied. Both specimens studied showed ductile behavior and high energy dissipation. Energy dissipation was evenly distributed throughout the specimen. First story columns were subjected to high axial forces in the elastic region transferring to high bending moments in the inelastic region. Coupling beams in both specimens were subjected to high bending moments early in loading with a sudden increase in axial forces after yielding of the specimen. Angle of inclination for the specimens was studied and showed that the angle at which tension field forces act will decrease as the ratio of height to width decreases. Infill panels resisted the majority of the applied lateral load in the elastic region and then maintained strength with gradual decreasing shear capacity. After yielding, the CFT maintained the integrity of the system and continued to resist higher shear forces. Results from the experimental analysis were compared with the AISC seismic provisions and it was determined that, though conservative, the suggested AISC formulas produces reasonable results.

WORKS CITED

AISC. (2005). “Seismic Provisions for Structural Steel Buildings.” *American Institute of Steel Construction*, Chicago.

Alinia, M. M. and Dastfan, M. (2007). “Cyclic Behavior, Deformability and Rigidity of Stiffened Steel Shear Panels.” *Journal of Constructional Steel Research.* 63(4), 554-563.

ATC-24. (1992). “Guidelines for Cyclic Seismic Testing of Component of Steel Structures.” *Applied Technology Council,* Redwood City, CA.

Behbahanifard, M. and Grondin, G.Y. (2001). “Cyclic Behavior of Three-Story Unstiffened Steel Plate Shear Wall.” *Proceedings,* 29th CSCE Annual Conference, May, Victoria, British Columbia. A8.

Behbahanifard, M., Grondin, G.Y., and Elwi, A.E. (2003). “Experimental and Numerical Investigation of Steel Plate Shear Walls.” *Structural Engineering Report No. 254,* Dept. of Civil Engineering, University of Alberta, Edmonton, Alta., Canada.

Berman, J. W. and Bruneau, M. (2004). “Steel Plate Shear Walls are not Plate Girders.” *Engineering Journal.* 41(3), 95-106.

Berman, J., and Bruneau, M. (2005). “Experimental Investigation of Light-Gauge Steel Plate Shear Walls.” *Journal of Structural Engineering.* 131(2), 259-267.

Bruneau, M., Berman, J., Lopez-Garcia, D., and Vian, D. (2007). “A Review of Steel Plate Shear Wall Design Requirements and Research.” *Journal of Structural Engineering.* 133(1), 27-34.

Caccese, V., Elgaaly, M., and Chen, R. (1993). “Experimental Study of Thin Steel-Plate Shear Walls Under Cyclic Load.” *Journal of Structural Engineering.* 119(2), 573-587.

Chen, S. J., and Jhang, C. (2006). “Cyclic Behavior of Low Yield Point Steel Shear Walls.” *Thin-Walled Structures*. 44, 730-738.

CAN/CSA S16-01. (2001). “Limit States Design of Steel Structures.” *Canadian Standard Association*, Toronto, Canada.

Driver, R. G. (1997). “Seismic Behavior of Steel Plate Shear Walls.” Ph.D. Dissertation, Dept. of Civil Engineering, University of Alberta, Edmonton, Alberta, Canada.

Driver, R. G., Kulak, G. L., Kennedy, D. J. L., and Elwi, A. E. (1997). "Seismic Behaviour of Steel Plate Shear Walls." *Structural Engineering Report No. 215.* Dept. of Civil Engineering, University of Alberta, Edmonton, Alta., Canada.

Driver, R. G., Kulak, G. L., Kennedy, D.J., and Elwi, A. E. (1998). "Cyclic Test of a Four-Story Steel Plate Shear Wall." *Journal of Structural Engineering.* 124(2), 112-130.

Elgaaly, M. and Caccese, V. (1990). "Steel Plate Shear Walls." *Proceedings,* National Steel Construction Conference, Kansas City.

Elgaaly, M., Caccese, V., and Du, C. (1993). "Postbuckling Behavior of Steel-Plate Shear Walls under Cyclic Loading." *Journal of Structural Engineering.* 119(2), 588-605.

Elgaaly, M. (1998). "Thin Steel Plate Shear Walls Behavior and Analysis." *Thin-Walled Structures.* 32(1-3), 151-180.

Hitaka, T. and Matsui, C. (2003). "Experimental Study on Shear Walls with Slits." *Journal of Structural Engineering.* 129(5), 586-595.

Kulak, G.L., Kennedy, D.J.L., Driver, R.G., and Medhekar, M. (2000). "Behavior and Design of Steel Plate Shear Walls." *Proceedings,* North American Steel Construction Conference, AISC. 11(1-20).

Kulak, G. L., Kennedy, D. J. L., Driver, R. G., and Medhekar, M. (2001). "Steel Plate Shear Walls – An Overview." *Engineering Journal.* 38(1), 50-62.

Lubell, A. S., Prion, H. G. L., Ventura, C. E., and Rezai, M. (2000). "Unstiffened Steel Plate Shear Wall Performance under Cyclic Loading." *Journal of Structural Engineering.* 126(4), 453-460.

Nakashima, M. (1995). "Strain-Hardening Behavior of Shear Panels Made of Low-Yield Steel. I: Test." *Journal of Structural Engineering.* 121(12), 1742-1749.

Park, H., Kwack, J., Jeon, S., Kim, W., and Choi, I. (2007). "Framed Steel Plate Wall Behavior under Cyclic Lateral Loading." *Journal of Structural Engineering.* 133(3), 378-388.

Rezai, M., Ventura, C.E., Prion, H.G.L., and Lubell, A.S. (1998). "Unstiffened Steel Plate Shear Walls: Shake Table Testing." *Proceedings,* 6th U.S. National Conference on Earthquake Engineering, May, Seattle, Washington.

Rezai, M. (1999). “Seismic Behavior of Steel Plate Shear Walls by Shake Table Testing.” Ph.D. Dissertation, Dept. of Civil Engineering, University of British Columbia.

Roberts, T. M. and Sabouri-Ghomi, S. (1992). “Hysteretic Characteristics of Unstiffened Perforated Steel Plate Shear Panels.” *Thin-Walled Struct.* 14(2), 139-151.

Schumacher, A., Grondin, G.Y., and Kulak, G.L. (1997). “Connection of Infill Panels in Steel Plate Shear Walls.” *Structural Engineering Report No. 217,* Dept. Civil Engineering, University of Alberta, Edmonton, Alta., Canada.

Sabelli, R. and Bruneau, M. (2007). “Design Guide 20: Steel Plate Shear Walls.” American Institute of Steel Construction, Inc.

Schumacher, A., Grondin, G.Y., and Kulak, G.L. (1999). “Connection of Infill Panels in Steel Plate Shear Walls.” *Canadian Journal of Civil Engineering.* 26(5): 549-563.

Shishkin, J.J., Driver, R. G. and Grondin, G. Y. (2005). “Analysis of Steel Plate Shear Walls using the Modified Strip Model.’ *Structural Engineering Report No. 261,* Dept. of Civil Engineering, University of Alberta, Edmonton, Alta., Canada.

Takahashi, Y., Takeda, T., Takemoto, T., and Takagi, M. (1973), “Experimental Study on Thin Steel Shear Walls and Particular Bracing under Alternative Horizontal Load” *Preliminary Report,* IABSE, Symp. On Resistance and Ultimate Deformability of Structures Acted on by Well-defined Repeated Loads, Lisbon, Portugal.

Timler, P.A. and Kulak, G.L. (1983). “Experimental Study of Steel Plate Shear Walls.” *Structural Engineering Report No. 114*, Department of Civil Engineering, University of Alberta, Edmonton, Alta., Canada.

Thorburn, L. J., Kulak, G. L., and Montgomery, C. L. (1983). “Analysis of Steel Plate Shear Walls.” *Structural Engineering Report No. 107*, Dept. of Civil Engineering, University of Alberta, Edmonton, Alta., Canada.

Tromposch, E. W., and Kulak, G. L. (1987). “Cyclic and Static Behavior of Thin Panel Steel Plate Shear Walls.” *Structural Engineering Report No. 145*, Dept. of Civil Engineering, University of Alberta, Edmonton, Alta., Canada.

Xue, M. and Lu, L. W. (1994). “Interaction of Infilled Steel Shear Wall Panels with Surrounding Frame Members.” *Proceeding*, Structural Stability Research Council Annual Technical Session, Bethlehem, Pennsylvania. 339-354.

Yamaguchi, T.; Takeuchi, T.; Nagao, T.; Suzuki, T.; Nakata, Y.; Ikebe, T.; Minami, A. (1998). “Seismic Control Devices Using Low-Yeild-Point Steel.” *Nippon Steel Technical Report No. 77.*

Zhao, Q. (2006). “Experimental and Analytical Studies of Cyclic Behavior of Steel and Composite Shear Wall Systems.” Ph.D. Dissertation, Dept. of Civil Engineering, University of California, Berkley.

Zhao, Q. and Astaneh-Asl, A. (2003). “Cyclic Behavior of Steel and Composite Shear Wall Systems.” *Proceedings*, Conference on Behavior of Steel Structures in Seismic Areas, June, Naples, Italy. 231-238.

Zhao, Q. and Astaneh-Asl, A. (2004). “Cyclic Behavior of an Innovative Steel Shear Wall System.” *Proceedings,* 13th World Conference on Earthquake Engineering, August, Vancouver. 2576.

WORKS REFERENCED

Alinia, M. M., and Dastfan, M. (2006). “Behavior of Thin Steel Plate Shear Walls Regarding Frame Members.” *Journal of Constructional Steel Research.* 62(7), 730-738.

Alinia, M. M. and Dastfan, M. (2007). “Cyclic Behavior, Deformability and Rigidity of Stiffened Steel Shear Panels.” *Journal of Constructional Steel Research.* 63(4), 554-563.

Astaneh-Asl, A. (2000). “Steel Plate Shear Walls.” *Proceedings,* U.S. – Japan Partnership for Advanced Steel Structures, U.S. – Japan Workshop on Seismic Fracture issues in Steel Structures, February 2000, San Fransico.

Astaneh-Asl, A. (2001). “Seismic Behavior and Design of Steel Shear Walls.” Paper Distributed and presented at the 2001 SEOANC Seminar, Structural Engineers Assoc. of Northern California, November 7, 2001, San Francisco.

Astaneh-Asl, A. and Zhao, Q. (2002). “Cyclic Behavior of Steel Shear Wall Systems.” *Proceedings,* Annual Stability Conference, Structural Stability Research Council, April, Seattle.

Baldelli, Jr, J. A. (1983). “Steel Shear Walls for Existing Buildings.” *Engineering Journal.* 20(2), 70-77.

Berman, J. W., and Bruneau, M. (2003). “Plastic Analysis and Design of Steel Plate Shear Walls.” *Journal of Structural Engineering.* 129(11), 1448-1456.

Berman, J. W., Celik, O. C., and Bruneau, M. (2005). “Comparing Hysteretic Behavior of Light-Gauge Steel Plate Shear Walls and Braced Frames.” *Engineering Structures*. 27(3), 475-485.

Berman, J. W., Vian, D., and Bruneau, M. (2005). “Steel Shear Walls – From Research to Codification.” *Proceedings*, ASCE 2005 Structures Congress, New York, New York. 1789-1798.

Bruneau, M. and Bhagwagar, T. (2002). “Seismic Retrofit of Flexible Steel Frames using Thin Infill Panels.” *Engineering Structures.* 24(4), 443-453.

Bruneau, M., Berman, J., Garcia, D. L., and Vian, D. (2005). “A Review of Steel Plate Shear Wall Design Requirements and Research.” *Proceedings,* NASCC Annual Conference, April, Montreal, Quebec. 27, 1-8.

Bruneau, M. (2005). “Seismic Retrofit of Steel Structure.” *Proceedings,* 1st Canadian Conference on Effective Design of Structures, July, Hamilton, Ontario. 49-66.

Bruneau, M., Berman, J., Lopez-Garcia, D., and Vian, D. (2005). “Steel Plate Shear Wall Buildings: Design Requirements and Research.” *Proceedings,* North American Steel Construction Conference, April, Montreal, Canada. CD-ROM paper #075.

Caccese, V. (1990). “Cyclic Testing of 1:4 Scale Models of Thin Steel Plate Shear Walls.” *Proceedings,* 4th U.S. National Conference on Earthquake Engineering, May, Palm Springs, California. 565.

De Matteis, G., Mazzolani, F. M., and Panico, S. (2003). “Pure Aluminum Shear Panels as Passive Control System for Seismic Protection of Steel Moment Resisting Frames.” *Proceedings*, Conference on Behavior of Steel Structures in Seismic Areas, June, Naples, Italy. 599-608.

De Matteis, G. and Mistakidis, E. S. (2003). “Seismic Retrofitting of Moment Resisting Frames using Low Yield Steel Panels as Shear Walls.” *Proceedings*, Conference on Behavior of Steel Structures in Seismic Areas, June, Naples, Italy. 677-682.

Driver, R.G., Kulak, G. L., Kennedy, D.J.L. and Elwi, A.E., (1996) “Seismic Performance of Steel Plate shear Walls Based on a Large-Scale Multi-Storey Test”, *Proceedings on CD-ROM,* 11th World Conference on earthquake Engineering, Mexico, Paper No. 1876. 8pp.

Driver, R. G., Kulak, G. L., Kennedy, D.J.L., and Elwi, A.E. (1997). “Finite Element Modeling of Steel Plate Shear Walls.” *Proceedings,* Annual Technical Session and Meeting, Structural Stability Research Council, June, Toronto, Ontario. 253-264 + 689-691.

Driver, R. G., Kulak, Elwi, A. E. and G. L., Kennedy, D. J. L., (1998). “FE and Simplified Models of Steel Plate Shear Wall.” *Journal of Structural Engineering.* 124(2), 121-130.

Driver, R. G., Grondin, G. Y., Behbahanifard, M. R., and Hussain, M. A. (2001). “Recent Developments and Future Directions in Steel Plate Shear Wall Research.” *Proceedings,* 12th North American Steel Construction Conference, AISC, May, Ft. Lauderdale, FL. 5-1-5-23.

Driver, R.G. and Grondin, G.Y. (2001). “Steel Plate Shear Walls: Now Performing on the Main Stage.” *Modern Steel Construction.* 41(9), 48-58.

Elgaaly, M., Caccese, V., and Du, C. (1990). "Steel Plate Shear Walls Post-Buckling Behavior under Cyclic Loads." *Proceedings,* 4th U.S. National Conference on Earthquake Engineering, May, Palm Springs, California. 895-904.

Elgaaly, M., Liu, Y., and Caccese, V. (1995). "Thin Plate Shear Walls, Research to Practice." *Proceedings,* Conference NSF, April. 82-93.

Elgaaly, M. and Liu, Y. (1997). "Analysis of Thin-Steel-Plate Shear Walls." *Journal of Structural Engineering.* 123(11), 1487-1496.

Elgaaly, M. (2000). "Post-Buckling Behavior of Thin Steel Plates using Computational Models." *Advances in Engineering Software.* 31(8), 511-517.

Featherston, C.A. (1999). "The Use of Finite Element Analysis in the Examination of Instability in Flat Plates and Curved Panels under Compression and Shear." *International Journal of Non-Linear Mechanics.* 2000(35), 515-529.

Gere, James M. (2004). *Mechanics of Materials.* Brooks and Cole.

Gilmor, M. I. (2002). "Canadian Requirements for Seismic Design of Ductile Steel Structures." *Proceedings,* NASCC Annual Conference, April, Seattle. 30.

Kharrazi, M. H. K., Ventura, C. E., Prion, H. G. L., Sabouri-Ghomi, S. (2004). "Bending and Shear Analysis and Design of Ductile Steel Plate Walls." *Proceedings,* 13th World Conference on Earthquake Engineering, August, Vancouver, British Columbia. 77.

Kulak, G. L. (1984). "Behavior of Steel Plate Shear Walls." *Proceedings,* Canadian Structural Engineering Conference, Toronto. 29.

Kulak, G. L. (1986). "Behavior of Unstiffened Steel Plate Shear Walls." *Proceedings,* Pacific Structural Steel Conference, August, New Zealand. 43-57.

Lange, J., and Naujoks, B. (2006). "Behavior of Cold-Formed Steel Shear Walls under Horizontal and Vertical Loads." *Thin-Walled Structures.* 44, 1214-1222.

Lubell, A. S., (1997). "Performance of unstiffened steel plate shear walls under cyclic quasi-static loading", *M.A.Sc. Thesis*, Department of Civil Engineering, University of British Columbia, Vancouver, BC, Canada.

Monnier, A. B and Harasimowicz, A. P. (2007). "Shear Strength." *Modern Steel Construction*. January 2007, 22.

Montgomery, C. J. (2001). “Discussion of ‘Unstiffened Steel Plate Shear Wall Performance under Cyclic Loading’.” *Journal of Structural Engineering.* 127(8), 973-975.

Nakashima, M., Akazawa, T., and Tsuji, B. (1995). “Strain-Hardening Behavior of Shear Panels Made of Low-Yield Steel. II: Model.” *Journal of Structural Engineering.* 121(12), 1750-1757.

Rezai, K. M. (1997). “Vibration Testing of an Unstiffened Steel Plate Shear Wall Frame.” Proceedings, CSCE Annual Conference: Second Symposium on Applied Mechanics Structures: Seismic Engineering, May, Sherbrooke, Quebec. 299-308.

Rezai, M., Ventura, C. E., and Prion, H. G. L. (2000). “Numerical Investigation of This Unstiffened Steel Plate Shear Walls.” *Proceedings,* 12th World Conference on Earthquake Engineering.

Roberts, T. M. (1995). “Seismic Resistance of Steel Plate Shear Walls.” *Engineering Structures.* 17(5), 344-351.

Sabouri-Ghomi, S. and Roberts, T. M. (1991). “Nonlinear Dynamic Analysis of Thin Steel Plate Shear Walls.” *Computers & Structures.* 39(1-2), 121-127.

Sabouri-Ghomi, S. and Roberts, T. M. (1992). “Nonlinear Dynamic Analysis of Steel Plate Shear Walls Including Shear and Bending Deformations.” *Engineering Structures.* 14(5), 309-317.

Sabouri-Ghomi, S. (2005). “Discussion of ‘Plastic Analysis and Design of Steel Plate Shear Walls’ by Jeffrey Berman and Michel Bruneau.” *Journal of Structural Engineering.* 131(4), 695-697.

Sabouri-Ghomi, S., Ventura, C. E., and Kharrazi, M. H. K. (2005). “Shear Analysis and Design of Ductile Steel Plate Walls.” *Journal of Structural Engineering.* 131(6), 878-889.

Scibilia, N. and Sacco, M. M. (2003). “Design of Steel Plate Shear Walls in High-Rise Buildings.” *Proceedings*, Conference on Behavior of Steel Structures in Seismic Areas, June, Naples, Italy. 197-202.

Seilie, I. F. and Hooper, J. D. (2005). “Steel Plate Shear Walls: Practical Design and Construction.” *Modern Steel Construction*. 45(4), 37-43.

Shishkin, J. J. (2005). “Analysis of Steel Plate Shear Walls using Conventional Engineering Software.” *Proceedings,* 33rd CSCE Annual Conference General

Conference and International History Symposium, June, Toronto. GC-251-1-GC-251-10.

Sugii, K., and Yamada, M. (1996) " Steel Panel Shear Walls with and Without Concrete Covering", *Proceedings on CD-Rom*, 11th World Conference on Earthquake Engrg., Acapulco, Mexico, Paper No. 403.

Timler, P. A., Ventura, C. E., Prion, H., and Anjam, R. (1998). "Experimental and Analytical Studies of Steel Plate Shear Walls as Applied to the Design of Tall Buildings." *Structural Design of Tall Buildings.* 7(3), 233-249.

Torii, S., Teramoto, H., Kihara, H., and Kitamura, H. (1996). "The Response Control Design of High-Rise Building with Low-Yield Steel Wall." *Proceeding,* 11th World Conference on Earthquake Engineering*.* Paper No. 97.

Troy, R. G. and Richard, R. M. (1988). "Steel Plate Shear Wall Designs." *Strucural. Engineering Review.* 1: 35-39.

Vian, D. and Bruneau, M. (2004). "Testing of Special LYS Steel Plate Shear Walls." *Proceedings,* 13th World Conference on Earthquake Engineering, August, Vancouver. 978.

Wagner, H. (1931). "Flat Steel Metal Girder with Very Thin Metal Web: Part 1 – General Theories and Assumptions." *Technical Memorandum No. 604*, Nat. Advisory Committee for Aeronautics, Washington, D.C.

Yamada, M. and Yamakaji, T. (2000). "Steel Panel Shear Wall – Analysis on the Center Core Steel Panel Shear Wall System." *Proceedings,* 3rd International Conference STESSA: Behavior of Steel Structures in Seismic Areas, August, Montreal, Canada. 541-550.

VITA

Rebecca Anne Lind was born in Chicago, Illinois on September 6th. At the age of five, her family moved to Signal Mountain, Tennessee a suburb to Chattanooga. Her primary education was completed at Signal Mountain Elementary and Signal Mountain Middle School, before attending Girls Preparatory School for the remainder of her education. She has completed both her Undergraduate and Graduate degrees at the University of Tennessee at Knoxville. After graduation with her M.S. in Civil Engineering, she continues to pursue her interest in structural engineering as a design engineer.